2020

Mechanotransduction: Cellular dynamic mechanical behavior quantification and control

Keyvan Mollaeian
Iowa State University

Mechanotransduction: Cellular dynamic mechanical behavior quantification and control

by

Keyvan Mollaeian

A dissertation submitted to the graduate faculty

in partial fulfillment of the requirements for the degree of

DOCTOR OF PHILOSOPHY

Major: Mechanical Engineering

Program of Study Committee:
Juan Ren, Major Professor
Pranav Shrotriya
Ian Schneider
Meng Lu
Sarah A. Bentil

The student author, whose presentation of the scholarship herein was approved by the program of study committee, is solely responsible for the content of this dissertation. The Graduate College will ensure this dissertation is globally accessible and will not permit alterations after a degree is conferred.

Iowa State University

Ames, Iowa

2020

TABLE OF CONTENTS

Page

LIST OF TABLES

LIST OF FIGURES

ACKNOWLEDGMENTS

I would like to take this opportunity to acknowledge those who helped me throughout my doctoral studies over the years. First, I would like to thank my advisor, Dr. Juan Ren, for her guidance, encouragement and her inspiring words to motivate me throughout my graduate study. I would like to thank my success to my parents. Their support and encouragement has always been the main reason of my success not only for this dissertation but for my whole life. I would like to thank my beloved, Fatemeh Amini, who supported me throughout my PhD. Special thanks to my older brothers and sisters, Dr.Hossein Ghaednia, Dr. Aida Mollaeian, Dr. Hamed Ghaednia, Dr. Khazar Mollaeian and Dr. Hamid Ghaednia, whom their continuous support made this dissertation possible. I

I also thank my committee members Dr. Pranav Shrotriya, Dr. Ian Schneider, Dr. Meng Lu, Dr. Sarah A. Bentil for their efforts and contributions to this work.

ABSTRACT

Living cells sense and induce mechanical forces within their extracellular environment. Recent studies suggest that these mechanical cues activate signaling pathways and reform the structure of the cells. However, understanding of how these mechanical forces are transmitted to the cells and how the intracellular biochemical reactions change the mechanical behavior of the cells remains unclear. In addition, creating a microenvironment where the cell mechanics can be controlled is a challenge. In this dissertation, a set of experimental and computational approaches for investigation of cell biomechanics in a variety of physiological conditions were developed. In addition, novel methods for changing the microenvironment of the cells and controlling the mechanical behavior of the cells were presented. Firstly, the nanoscale poroelasticity of human mammary basal/claudin low carcinoma cell (MDA-MB-231) was investigated using indentation-based atomic force microscopy. The cell poroelastic behavior (i.e., the diffusion coefficient) was quantified at different indenting velocities (0.2, 2, 10, 20, 100, 200 μm/s) and indentation depths (635, 965, and 1313 nm) by fitting the force-relaxation curves using a poroelastic model. Cell treated with cytoskeleton inhibitors are measured to investigate the effect of the cytoskeletal components on the cell poroelasticity. Our results demonstrated that MDA-MB-231 cells behaved less poroelastic (i.e., with lower diffusion coefficient) at higher indenting velocities due to the local stiffening up and dramatic pore size reduction caused by faster force load and was more pronounced when the local cytoplasm porous structure was stretched by higher indentation. Furthermore, inhibition of cytoskeletal components resulted in pronounced poroelastic relaxation when compared with the control, and affected the nonlinearity of cell poroelasticity at different depth range inside of the cell. Then, the effect of substrate mechanics with different stiffness on the nonlinear biomechanical behavior of living cells was investigated using AFM. the actin filament (F-actin) cytoskeleton of the cells was fluorescently stained to investigate the adaptation of F-actin cytoskeleton structure to the substrate mechanics.

It was found that living cells sense and adapt to substrate mechanics: the cellular Young's modulus, shear modulus, apparent viscosity, and their nonlinearities (mechanical property vs. measurement depth relation) were adapted to the substrates' nonlinear mechanics. Moreover, the positive correlation between the cellular poroelasticity and the indentation remained the same despite the substrate stiffness nonlinearity, but was indeed more pronounced for the cells seeded on the softer substrates. Comparison of the F-actin cytoskeleton morphology confirmed that the substrate affects the cell mechanics by regulating the intracellular structure. Next, the effect of the substrate morphology on the biomechanical behavior of living cells was thoroughly investigated using indentation-based atomic force microscopy. The results showed that the cellular biomechanical behavior was affected by the substrate morphology significantly. The elasticity and viscosity of the cells on the patterned substrates were much lower compared to those of the ones cultured on flat. The poroelastic diffusion coefficient of the cells was higher on the patterned substrates. In addition, fluorescence images confirmed that cell mechanical behavior and morphology can be controlled using substrates with properly designed topography. Finally, to investigate the cell uptake of NPs, a dynamic cell culture substrate was designed in two steps: 1. the polyaniline polymer (PANI) was deposited on the cell culture petri dish, and 2. the PANI substrate was coated by PDMS with base to curing agent ratio of 10:3 (PDMS/PANI). The substrates were characterized using Fourier Transform Infrared (FTIR) and Atomic Force Microscopy (AFM). It was found that the PDMS/PANI substrate expansion was positively correlated with the applied voltage to the PANI. In addition, the PDMS/PANI substrate was implemented for NPs delivery. Our results showed that the uptake of NPs by the cells cultured on PDMS/PANI substrate increases by expansion of the substrates. Moreover, our results suggest that the PDMS/PANI substrate is a promising device that can be used for controlling intra- and extracellular behavior of the cells.

CHAPTER 1. INTRODUCTION

Structure of living cells are subject to different external and internal biomechanical stimulation throughout the human body(Rodriguez et al. (2013)). Their dynamic mechanical and chemical properties change in response to the biomechanical stimulations (Moeendarbary and Harris (2014)). For example, gene transcripts, intracellular organelle transport, and signaling pathways affect the cell cycling and elongation (Niclas et al. (1996); Coller et al. (2000); Elledge (1996)). In addition, crawling and contraction of cells are driven by extracellular induced forces (Moore et al. (2010)). The irregularity of the cell mechanics results in pathological diseases such as osteoporosis, glaucoma, and asthma (Affonce and Lutchen (2006); Klein-Nulend et al. (2003); Tan et al. (2006)). Therefore, studying the cell biomechanics is crucial for an in-depth understanding of the cellular behavior and response to different physiological conditions.

The interior of a living cell consists of organelles, macromolecules and cytoskeleton bathed within intracellular fluid (i.e., cytosol). The main components of the cytoskeleton, actin filaments, microtubules and myosin, play an important role in maintaining the cellular integrity (Moeendarbary and Harris (2014)). Actin filaments are the semiflexible structure with the persistent length of $\sim$20 μm that regulate the cellular processes such as cell shape and migration (Moeendarbary and Harris (2014); Gittes et al. (1993)). In addition, the mechanical behavior of anchorage dependent cells mainly depend on the meshwork of the actins below the apical plasma membrane (Salbreux et al. (2012)). As the internally induced-stresses by myosin creates 3-4 pN force that results in contractility of actin filaments and stress fibers (Finer et al. (1994); Kumar et al. (2006)). Moreover, microtubules are stiff structure with the persistence length of millimeters that are mostly concentrated near the nucleus envelope (Lodish et al. (2000); de Forges et al. (2012)). The compression of microtubules balances the stress distributed by actin-myosin network within the cytoskeleton (Ingber (2003, 1993)).

In addition to internal biomechanical stimulation, the cells sense and respond to their surrounding environment through cell-cell, cell-cytosol, and cell-ECM interface (Rodriguez et al. (2013)). In addition, the external force stimuli transmitted to the interior of the cells via focal adhesions or macro/micro molecules in the membrane such a glycocalyx, primary cilia, and ion channels, which further activate signaling pathways and regulates the cell function (Jaalouk and Lammerding (2009); Janmey and McCulloch (2007); Vogel and Sheetz (2006)). For instance, the underlying substrate mechanics affects the differentiation and apoptosis of the cells (Engler et al. (2006); Discher et al. (2005)). The cell migration is directed by the substrate stiffness toward stiffer substrates (Discher et al. (2005)). Therefore, research on cell biomechanics provides new avenues for understanding the role of mechanics in disease.

In the following section, we summarize three common experimental approaches including optical tweezer, particle tracking microrheology, and atomic force microscopy.

1.1 Experimental approaches

A variety of experimental techniques have been employed to investigate the mechanical behavior of living cells. Design of these mechanical approaches were based on the size, type, and characteristics of the targeted biological structure (Moeendarbary and Harris (2014)). In general, there are two categories for cell mechanical measurement: those that measure cell response to an applied force stimuli such as otical tweezer, flow rheometry, and AFM, and those that measure the cell response on deformable substrates such as traction force microscopy (TFM), particles tracking microrheology (PTM), and micropost arrays. The force range and limitation of some of these techniques are listed in Table 1.1 (Rodriguez et al. (2013)). In the next section, we will briefly discuss three common mechanical measurements.

1.1.1 Optical tweezer

Optical tweezer is a technique that employs optical trapping to control the cell (Block (1992); Svoboda and Block (1994)). In this method, the infrared laser passes through an object with

Table 1.1 Capability and limitation of several experimental techniques

Experimental Technique	**Force Stimulation**	**Force Sensing**	**Spatial Sensitivity**
AFM	10–10^7 pN	$10 - 10^5$ pN	$1 - 10^5$ nm
Optical Tweezers	0.01-10^3 pN	1-100 pN	10-10^5 nm
Magnetic Tweezers	0.01-10^4 pN	1-10^3 pN	0.1-100 μm
Traction force microscopy	-	1-10^6 pN	-
Micropost arrays	-	1-100 nN	1-10^3 μm

different refractive index and changes its path which further results in momentum change (Lim et al. (2006a)). The change in momentum generates a force that traps the object such as cell, intra- and extracellular particles (Neuman and Block (2004)). Extensive studies on cell mechanics have been performed using optical tweezer owning to its pico-newton resolution and high accuracy. Henon et al. (1999) reported the shear modulus of the human erythrocyte membrane by trapping the silica beads bounded to cell membrane using optical tweezer (Henon et al. (1999)). Koch et al. (2002) investigated the dynamics protein-DNA interaction by unzipping a single DNA double helix using optical tweezers (Koch et al. (2002)). Guck et al. (2005) investigated the optical deformability of fibroblast cells using optical tweezer combined with microfluidic delivery and found that the optical deformability of the cells increased during cancer progression. Although this approach provides valuable information on cell mechanics in subcellular level, the applied force stimuli is limited and higher optical forces can damage the cell surface (Moeendarbary and Harris (2014)).

1.1.2 Particle Tracking Microrheology (PTM)

This method is used to measure the viscoelastic behavior of the materials including living cells (Tseng et al. (2002)). In this method the fluorescent beads are injected to the cytoplasm of the cells (Wirtz (2009)). The viscoelastic measurements was obtained by the analysis of the beads movement inside the cytoplasm (Wirtz (2009)). In addition, this technique is one of the few methods that allows the quantification of the mechanical behavior of the cells embedded in 3D matrix (Baker et al. (2009)). The cell behavior in PTM measurement consists of two regimes: 1. Elastic response at short time (0.1-10 s) and 2. Viscous behavior at longer time scale (greater than 10-20 s) (Wirtz

(2009)). For instance Tseng et al. (2004) investigated the stiffness of the cell components and found that nucleus was stiffer compared to the cytoplasm of the cell (Tseng et al. (2004)). Panorchan et al. (2006) reported the decreased stiffness of the human endothelial cell embedded within the 3D matrix compared to the cells cultured on the top of the matrix using PTM (Panorchan et al. (2006)). Daniels et al. (2006) noted the highly viscous behavior of the cytoplasm of developing Caenorhabditis elegans embryos compared to the differentiated cells using PTM (Daniels et al. (2006)). One of the most important advantage of this method compared to the other techniques such as optical tweezer and AFM is the non-direct contact with the cell membrane. However, one of the limitation of PTM is the limited allowed particle concentration (Savin and Doyle (2005)). In addition, In PTM measurements, the noise is also assumed to be uniform.

1.1.3 Atomic Force Microscopy (AFM)

Atomic force microscopy (AFM) has been widely implemented for imaging and mapping the mechanical properties of a variety of materials such as biological and soft samples due to its physiological friendly environment and pico-newton resolution (Kalcioglu et al. (2012); Mollaeian et al. (2018a); Müller and Dufrene (2010)). The main part of the AFM is a cantilever with a tip attached to its free end (probe), and the fix end is driven up and down by piezoelectric in a controlled way, as the sample is moved under the micron-size tip. In this technique, the interaction of the probe-sample deforms the cantilever beam, and the deflection of the laser light on top of the free end is monitored and recorded using photo-detector. The acquired information from AFM can be used to estimate topography and mechanical properties of the samples including stiffness, sample height, Adhesion, dissipation (Butt et al. (2005)).

The AFM has been widely used for studies of cell mechanics and rheology (Moeendarbary et al. (2013); Yamane et al. (2000); Liu et al. (2018b); Weafer et al. (2015)). For instance, Mathur et al. (2000) reported that Young's modulus of human umbilical vein endothelial cells near the nucleus and the edges were 2.97$\pm$0.79 kPa, and 1.27$\pm$0.36 kPa, respectively, using AFM (Mathur et al. (2000). Yamane et al. (2000) noted the uniform Young's modulus of 200-700 kPa when imaging

the fixed astrocytes using AFM (Yamane et al. (2000)). In addition, several AFM measurement techniques such as creep indentation (constant load) and stress-relaxation (constant displacement) have been implemented to study the viscoelastic and poroelastic behavior of the cells. While creep indentation determines the cell response to constant stress, stress-relaxation process measures the cellular behavior in response to constant strain (Leipzig and Athanasiou (2005); Moeendarbary et al. (2013); Mollaeian et al. (2018a)). Specifically, in the stress-relaxation process, the probe is rested in the sample after indenting the cell and the intracellular fluid redistributes within the cell to equilibrate the internal cell pressure, which further results in the reduction of the probe-sample interaction force (Charras et al. (2005); Keren et al. (2009); Mollaeian et al. (2018b)). For example, Nia et al. (2011) reported that the cartilage behaves poroelastic during stress-relaxation process using AFM (Nia et al. (2011)). Ketene et al. (2012) found that apparent viscosity obtained from AFM stress-relaxation for the late-stage MOSE cells were lower than the early stages ones' (Ketene et al. (2012)).

As previously shown, AFM is a superior technique compared to others since the measurements can be performed in variety of physiological conditions in nano- and micro-scale level with its pico-newton resolution and it does not have the limitations of the aforementioned techniques.

1.2 Modelling approaches

Modelling approaches have been implemented to interpret the mechanical measurements on the cells. For instance, liquid drop models were developed for micropipette aspiration measurements of the cell where the cell is assumed to be homogeneous (Tran-Son-Tay et al. (1991); Yeung and Evans (1989); Hochmuth et al. (1993); Drury and Dembo (1999)). Hertzian and Sneddon models were implemented on AFM measurement of the cells by assuming that the contact is repulsive (Liu (2006); Butt et al. (2005)). In addition, models such as Maxwell and Zener models were developed to describe the time-dependent behavior of the cells (Darling et al. (2006); Moreno-Flores et al. (2010)). The power law structural damping models were also commonly used for the magnetic twisting cytometry and AFM measurements to study the frequency-dependent behavior

of cells (Ren et al. (2015); Hochmuth et al. (1993)). However, as cytoplasm consists of a porous elastic meshwork bathed in intracellular fluid, i.e., cytosol, these models are not adequate enough to describe the biphasic nature of the cytoplasm (Mollaeian et al. (2018a); Moeendarbary et al. (2013)). Therefore, poroelastic model was developed to account for the fluid flow and viscoelatic solid network of cytoskeleton (Moeendarbary et al. (2013)). The Poroelastic model was used to interpret the AFM measurements of the cells. In this section, we will briefly review two models that were implemented in this manuscript to interpret the cell stress-relaxation measurements.

1.2.1 Thin-layer Hertzian model

The thin-layer Hertzian model has been implemented widely to study the cell response to applied constant strain by AFM (i.e., stress-repaxation process), and can be written as (Darling et al. (2007)):

$$F(t) = \frac{4E\sqrt{r}}{3(1-\nu^2)}\delta(t)^{\frac{3}{2}} f(X) \tag{1.1}$$

$F(t)$ is the probe-sample interaction force. r and ν represents the tip radius and poisson ratio of the sample, respectively. E and $\delta(t)$ also denote the Young's modulus of the cell and indentation depth, respectively. In addition, $f(x)$ is given as:

$$f(x) = \left[\ 1 - \frac{2\alpha_0}{\pi}X + \frac{4\alpha_0^2}{\pi^2}X^2 - \frac{8}{\pi^3}(\alpha_0^3 + \frac{4\pi^2}{15}\beta_0)X^3 + \frac{16\alpha_0}{\pi^4}(\alpha_0^3 + \frac{3\pi^2}{5}\beta_0)X^4\ \right] \tag{1.2}$$

where $X = \frac{\sqrt{r\delta(t)}}{h}$ is the geometrical correction factor. h is the height of the cell. α_0 and β_0 are defined as:

$$\alpha_0 = -\frac{1.2867 - 1.4678\nu + 1.3442\nu^2}{1-\nu} \tag{1.3}$$

$$\beta_0 = -\frac{0.6387 - 1.0277\nu + 1.5164\nu^2}{1-\nu} \tag{1.4}$$

When the indentation is less than 10% of the cell height, $f(x)$ can be considered as one. Therefore, the modified Hertzian model can be rewritten as:

$$F(t) = \frac{4E\sqrt{r}}{3(1-\nu^2)}\delta(t)^{\frac{3}{2}} \tag{1.5}$$

In addition, it has beeen shown that shear modulus, G, and Young's modulus, E of the cell are linearly related as:

$$E = 2G(1+\nu) \tag{1.6}$$

Solving the Eq.(1.5) in Laplace domain by taking Eq.(1.6) into account yields the following expression(Darling et al. (2006)):

$$F(t) = \frac{4\sqrt{r}}{3(1-\nu)} E_r \delta_0^{\frac{3}{2}} [1 + (\frac{\tau_\sigma - \tau_\epsilon}{\tau_\epsilon}) e^{-\frac{\tau}{\tau_\epsilon}}] \tag{1.7}$$

where E_r is the relaxed modulus, and τ_σ and τ_ϵ are relaxation load and deformation time constants, respectively. Moreover, E_r, τ_σ, and τ_ϵ can be estimated by fitting Eq.(1.7) to force-time data acquired from the AFM stress-relaxation measurements. In addition, the viscoelastic reponse of the cells as a spring-dashpot in parallel with a spring can be estimated as:

$$\eta = E_r(\tau_\sigma - \tau_\varepsilon) \tag{1.8}$$

$$k_1 = E_r \tag{1.9}$$

$$k_2 = E_r(\frac{\tau_\sigma - \tau_\epsilon}{\tau_\epsilon}) \tag{1.10}$$

where η is the apparent viscosity. k_1 and k_2 are Kelvin spring constants.

1.2.2 Biot poroelastic approach

The poroelastic approach has been implemented to describe biphasic nature of porous materials consist of porous elastic solid network bathed with fluid. The theory of poroelasticity was first introduced by Biot (Biot (1941)), and then implemented for studies of the cell biomechanics by moeendarbary et al (2013) (Moeendarbary et al. (2013)). Here, we consider the cell as isotropic material that is fully saturated with fluid to simplify the Biot poroelastic formulation. if we consider part of the cell as a cube, the total stress, σ, and infinitesimal strain, ϵ can be written as:

$$\sigma = \begin{bmatrix} \sigma_x & \tau_{xy} & \tau_{xz} \\ \tau_{xy} & \sigma_y & \tau_{yz} \\ \tau_{xz} & \tau_{yz} & \sigma_z \end{bmatrix}, \qquad \epsilon = \begin{bmatrix} \epsilon_x & \gamma_{xy} & \gamma_{xz} \\ \gamma_{xy} & \epsilon_y & \gamma_{yz} \\ \gamma_{xz} & \gamma_{yz} & \epsilon_z \end{bmatrix}$$

The relationship between stress and strain is given by the constitutive equation as:

$$\begin{aligned} \sigma_x &= 2G(\epsilon_x + \frac{\nu\theta}{1-2\nu}) - p, \\ \sigma_y &= 2G(\epsilon_y + \frac{\nu\theta}{1-2\nu}) - p, \\ \sigma_z &= 2G(\epsilon_z + \frac{\nu\theta}{1-2\nu}) - p, \\ \tau_{yz} &= G\gamma_{yz}, \\ \tau_{xz} &= G\gamma_{xz}, \\ \tau_{xy} &= G\gamma_{xy}. \end{aligned} \tag{1.11}$$

where p is the pore fluid pressure. θ is the variation in fluid content. In addition, the equilibrium equation in terms of stress elements is:

$$\begin{aligned} \frac{\partial\sigma_x}{\partial x} + \frac{\partial\tau_{xy}}{\partial y} + \frac{\partial\tau_{xz}}{\partial z} &= 0, \\ \frac{\partial\tau_{xz}}{\partial x} + \frac{\partial\sigma_y}{\partial y} + \frac{\partial\tau_{yz}}{\partial z} &= 0, \\ \frac{\partial\tau_{xy}}{\partial x} + \frac{\partial\tau_{yz}}{\partial y} + \frac{\partial\sigma_z}{\partial z} &= 0. \end{aligned} \tag{1.12}$$

Therefore, the Navier equation is drived by substituting Eqs.(1.11) for the stresses of the Eqs.(1.12):

$$\begin{aligned} G\nabla^2 u_x + \frac{G}{1-2\nu}\frac{\partial\theta}{\partial x} - \frac{\partial p}{\partial x} &= 0, \\ G\nabla^2 u_y + \frac{G}{1-2\nu}\frac{\partial\theta}{\partial y} - \frac{\partial p}{\partial y} &= 0, \\ G\nabla^2 u_z + \frac{G}{1-2\nu}\frac{\partial\theta}{\partial z} - \frac{\partial p}{\partial z} &= 0. \end{aligned} \tag{1.13}$$

u_x, u_y, and u_z represent the displacement elements. In addition, the Eqs.(1.13) can be expressed in the matrix form as follows:

$$G\nabla^2\mathbf{u} + \frac{G}{1-2\nu}\nabla^2(\mathbf{div}\,\mathbf{u}) - \nabla p = 0 \tag{1.14}$$

Fluid flow through porous medium can be described by Darcy's law as $q = -K\nabla p$, where q and K are the flow rate through porous medium and hydraulic permeability. In addition, by considering mass conservation, the continuity equation written as (Cheng (2016)):

$$\mathbf{div}\, q = -\frac{\partial \theta}{\partial t} \tag{1.15}$$

Substituting Darcy's equation into Eq.(1.15) yields:

$$\frac{\partial \theta}{\partial t} - K\nabla^2 p = 0 \tag{1.16}$$

Therefore, combination of Eqs. 1-14 and 1-16 results in:

$$\frac{\partial \theta}{\partial t} - \frac{2G(1-\nu)}{1-2\nu}\nabla^2 \theta K = 0 \tag{1.17}$$

where,

$$D = \frac{2G(1-\nu)}{1-2\nu}K \tag{1.18}$$

D is the diffusion coefficient of the cell.

The aforementioned experimental and modelling approaches have been implemented to study the the effect of extracellular environment on the mechanical behavior of the cells (Moeendarbary et al. (2013)). However, Although the cytoplasm of a living cell is heterogeneous, the cytoplasm poroelasticity quantified in previous work was limited to the specific measurement specifications and physical conditions (e.g., indenter size, approach velocity, and indentation depth). Particularly, due to the biphasic nature of living cells, the cell deformation rate (i.e., the AFM probe approach velocity) affects the measured cell stiffness significantly (Moeendarbary et al. (2013); Cheng (2016)), and the deformation/indentation depth range determines the layers of the cells triggered and measured during the mechanical quantification (Kasas et al. (2005); Fuhrmann et al. (2011)). Therefore, to address these issues, a suit of indentation-based Atomic Force Microscopy (AFM) approaches are presented to study the viscoelastic and poroelastic behavior the cells at different measurements and physiological conditions. In addition, novel biocompatible substrate is proposed to improve the drug delivery of the nanoparticles. The rest of the dissertation proposal is organized as follows:

In Chapter 2, the contribution of external force conditions to cellular rheology of human mammary basal/claudin low carcinoma cell at nanometer scale is investigated using AFM. Specifically, the cells is probed under forces with different approach velocities and magnitudes, and the poroelasticity diffusion coefficient Elasticity are then quantified for each condition by fitting the force-relaxation curve using an empirical poroelastic model. Furthermore, the effect of internal cell structural property on determining the cell rheology and the nonlinearity of cell poroelasticity is studied. particularly, cell treated with cytoskeleton inhibitors (latrunculin B, blebbistatin, and nocodazole) are measured to investigate the effect of the cytoskeletal components on the cell poroelasticity. Our results shows that the MDA-MB-231 cells behave less poroelastic at higher indenting velocities due to the local stiffening up and dramatic pore size reduction caused by faster force load, and the cytoplasm is nonlinear in terms of poroelasticity. The poroelastic relaxation is more pronounced when the local cytoplasm porous structure is stretched by higher indentation. Furthermore, inhibition of cytoskeletal components results in pronounced poroelastic relaxation when compared with the control, and affects the nonlinearity of cell poroelasticity at different depth range inside of the cell. Our results indicate that the cytoplasm porous geometry is more dominant than the cell Young's modulus in terms of affecting cell poroelasticity.

In Chapter 3, the effects of substrate's mechanics on the nonlinear mechanical behavior of living cells is investigated using AFM force indentation measurements. Two different cell lines are studied: an epithelial cell line (Madin–Darby canine kidney (MDCK) and a fibroblast cell line (NIH/3T3)). Specifically, for each cell type, the cells are cultured on substrates with different stiffness (Polydimethylsiloxane (PDMS) with the base-to-curing agent ratios of 10:0.5, 10:1, and 10:3, and the polystyrene cell culture dish), and the relation between the substrate mechanics and cell nonlinear mechanical behavior (stiffness, viscosity, and poroelasticity) is investigated by indenting the cells at different depths. Moreover, the cells are fluorescently stained to study the actin filament (F-actin) morphology change caused by the four substrates. Our results shows that living cells sense and adapt to substrate mechanics: the cellular Young's modulus, shear modulus, apparent viscosity, and their nonlinearities (mechanical property vs. measurement depth

relation) are adapted to the substrates' nonlinear mechanics. Moreover, the cellular poroelasticity is positively correlated with the indentation for the cells cultured on the four substrates but is indeed more pronounced for the cells seeded on the softer substrates. The results are validated by the Comparison of the F-actin cytoskeleton morphology.

In Chapter 4, the effect of the substrate morphology on the biomechanical behavior of living cells is thoroughly investigated using indentation-based atomic force microscopy. Specifically, mechanical characterization is performed on Madin-Darby canine kidney (MDCK) cells cultured on PDMS substrates of the same base/curing agent ratio with different patterns (flat, ridges (1D) and elevated disks (2D) with 80 nm height and 0.5 μm pitch size), and the relationship between the substrate's texture and cell mechanical behavior (elasticity E, shear modulus G, viscoelasticity η, and poroelasticity D) at different indentation depths is presented. Furthermore, the actin filament (F-actin) morphology change caused by different substrate patterns is also investigated. The results shows that the cellular biomechanical behavior was affected by the substrate morphology significantly. The elasticity and viscosity of the cells on the patterned Polydimethylsiloxane (PDMS) substrates are much lower compared to those of the ones cultured on flat PDMS. The poroelastic diffusion coefficient of the cells is higher on the patterned PDMS substrates, specifically on the substrate with 2D pitches. In addition, fluorescence images showes that the substrate topography directly affects the cell cytoskeleton morphology. Therefore, our results suggests that cell mechanical behavior and morphology can be controlled using substrates with properly designed topography.

In Chapter 5, a novel and biocompatible cell culture dish is proposed to modulate the cellular uptake of NPs. Specifically, the cell culture petri-dish is functionalized by depositing polyaniline (PANI) which was synthesized via in-situ polymerization. Then the functionalized petri-dish is coated by Polydimethylsiloxane (PDMS) with the base-to-curing agent ratio of 10:3. The relation between the electrical and mechanical properties of the substrates is investigated using Atomic Force Microscopy (AFM). To understand how the substrate affects the cellular uptake, the Fluorescent Silica NPs are injected to the medium containing Madin–Darby canine kidney (MDCK) to study

the change of cellular uptake caused by substrate motion. Our results show that stretching the confluent cells cultured on the substrates increases the efficacy of the nanoparticle's internalization by the cells, and the fabricated PDMS/PANI substrate is a promising tool for controlling the cell mechanical behavior and drug delivery.

Our conclusions are presented in Chapter 6.

1.3 References

Affonce, D. A. and Lutchen, K. R. (2006). New perspectives on the mechanical basis for airway hyperreactivity and airway hypersensitivity in asthma. *Journal of applied physiology*, 101(6):1710–1719.

Baker, E. L., Bonnecaze, R. T., and Zaman, M. H. (2009). Extracellular matrix stiffness and architecture govern intracellular rheology in cancer. *Biophysical journal*, 97(4):1013–1021.

Biot, M. A. (1941). General theory of three-dimensional consolidation. *Journal of applied physics*, 12(2):155–164.

Block, S. M. (1992). Making light work with optical tweezers. *Nature*, 360(6403):493–495.

Butt, H.-J., Cappella, B., and Kappl, M. (2005). Force measurements with the atomic force microscope: Technique, interpretation and applications. *Surface science reports*, 59(1):1–152.

Charras, G. T., Yarrow, J. C., Horton, M. A., Mahadevan, L., and Mitchison, T. (2005). Non-equilibration of hydrostatic pressure in blebbing cells. *Nature*, 435(7040):365–369.

Cheng, A. H.-D. (2016). *Poroelasticity*, volume 27. Springer.

Coller, H. A., Grandori, C., Tamayo, P., Colbert, T., Lander, E. S., Eisenman, R. N., and Golub, T. R. (2000). Expression analysis with oligonucleotide microarrays reveals that myc regulates genes involved in growth, cell cycle, signaling, and adhesion. *Proceedings of the National Academy of Sciences*, 97(7):3260–3265.

Daniels, B. R., Masi, B. C., and Wirtz, D. (2006). Probing single-cell micromechanics in vivo: the microrheology of c. elegans developing embryos. *Biophysical journal*, 90(12):4712–4719.

Darling, E., Zauscher, S., and Guilak, F. (2006). Viscoelastic properties of zonal articular chondrocytes measured by atomic force microscopy. *Osteoarthritis and cartilage*, 14(6):571–579.

Darling, E. M., Zauscher, S., Block, J. A., and Guilak, F. (2007). A thin-layer model for viscoelastic, stress-relaxation testing of cells using atomic force microscopy: do cell properties reflect metastatic potential? *Biophysical journal*, 92(5):1784–1791.

de Forges, H., Bouissou, A., and Perez, F. (2012). Interplay between microtubule dynamics and intracellular organization. *The international journal of biochemistry & cell biology*, 44(2):266–274.

Discher, D. E., Janmey, P., and Wang, Y.-l. (2005). Tissue cells feel and respond to the stiffness of their substrate. *Science*, 310(5751):1139–1143.

Drury, J. L. and Dembo, M. (1999). Hydrodynamics of micropipette aspiration. *Biophysical Journal*, 76(1):110–128.

Elledge, S. J. (1996). Cell cycle checkpoints: preventing an identity crisis. *Science*, 274(5293):1664.

Engler, A. J., Sen, S., Sweeney, H. L., and Discher, D. E. (2006). Matrix elasticity directs stem cell lineage specification. *Cell*, 126(4):677–689.

Finer, J. T., Simmons, R. M., and Spudich, J. A. (1994). Single myosin molecule mechanics: piconewton forces and nanometre steps. *Nature*, 368(6467):113–119.

Fuhrmann, A., Staunton, J., Nandakumar, V., Banyai, N., Davies, P., and Ros, R. (2011). Afm stiffness nanotomography of normal, metaplastic and dysplastic human esophageal cells. *Physical biology*, 8(1):015007.

Gittes, F., Mickey, B., Nettleton, J., and Howard, J. (1993). Flexural rigidity of microtubules and actin filaments measured from thermal fluctuations in shape. *The Journal of cell biology*, 120(4):923–934.

Henon, S., Lenormand, G., Richert, A., and Gallet, F. (1999). A new determination of the shear modulus of the human erythrocyte membrane using optical tweezers. *Biophysical journal*, 76(2):1145–1151.

Hochmuth, R., Ting-Beall, H., Beaty, B., Needham, D., and Tran-Son-Tay, R. (1993). Viscosity of passive human neutrophils undergoing small deformations. *Biophysical journal*, 64(5):1596–1601.

Ingber, D. E. (1993). Cellular tensegrity: defining new rules of biological design that govern the cytoskeleton. *Journal of cell science*, 104(3):613–627.

Ingber, D. E. (2003). Tensegrity i. cell structure and hierarchical systems biology. *Journal of cell science*, 116(7):1157–1173.

Jaalouk, D. E. and Lammerding, J. (2009). Mechanotransduction gone awry. *Nature reviews Molecular cell biology*, 10(1):63–73.

Janmey, P. A. and McCulloch, C. A. (2007). Cell mechanics: integrating cell responses to mechanical stimuli. *Annu. Rev. Biomed. Eng.*, 9:1–34.

Kalcioglu, Z. I., Mahmoodian, R., Hu, Y., Suo, Z., and Van Vliet, K. J. (2012). From macro- to microscale poroelastic characterization of polymeric hydrogels via indentation. *Soft Matter*, 8(12):3393–3398.

Kasas, S., Wang, X., Hirling, H., Marsault, R., Huni, B., Yersin, A., Regazzi, R., Grenningloh, G., Riederer, B., Forro, L., et al. (2005). Superficial and deep changes of cellular mechanical properties following cytoskeleton disassembly. *Cytoskeleton*, 62(2):124–132.

Keren, K., Yam, P. T., Kinkhabwala, A., Mogilner, A., and Theriot, J. A. (2009). Intracellular fluid flow in rapidly moving cells. *Nature cell biology*, 11(10):1219–1224.

Ketene, A. N., Schmelz, E. M., Roberts, P. C., and Agah, M. (2012). The effects of cancer progression on the viscoelasticity of ovarian cell cytoskeleton structures. *Nanomedicine: Nanotechnology, Biology and Medicine*, 8(1):93–102.

Klein-Nulend, J., Bacabac, R., Veldhuijzen, J., and Van Loon, J. (2003). Microgravity and bone cell mechanosensitivity. *Advances in Space Research*, 32(8):1551–1559.

Koch, S. J., Shundrovsky, A., Jantzen, B. C., and Wang, M. D. (2002). Probing protein-dna interactions by unzipping a single dna double helix. *Biophysical Journal*, 83(2):1098–1105.

Kumar, S., Maxwell, I. Z., Heisterkamp, A., Polte, T. R., Lele, T. P., Salanga, M., Mazur, E., and Ingber, D. E. (2006). Viscoelastic retraction of single living stress fibers and its impact on cell shape, cytoskeletal organization, and extracellular matrix mechanics. *Biophysical journal*, 90(10):3762–3773.

Leipzig, N. D. and Athanasiou, K. A. (2005). Unconfined creep compression of chondrocytes. *Journal of biomechanics*, 38(1):77–85.

Lim, C., Zhou, E., Li, A., Vedula, S., and Fu, H. (2006). Experimental techniques for single cell and single molecule biomechanics. *Materials Science and Engineering: C*, 26(8):1278–1288.

Liu, K.-K. (2006). Deformation behaviour of soft particles: a review. *Journal of Physics D: Applied Physics*, 39(11):R189.

Liu, Y., Mollaeian, K., and Ren, J. (2018). An image recognition-based approach to actin cytoskeleton quantification. *Electronics*, 7(12):443.

Lodish, H., Berk, A., Zipursky, S. L., Matsudaira, P., Baltimore, D., and Darnell, J. (2000). Molecular cell biology 4th edition. *National Center for Biotechnology Information, Bookshelf*.

Mathur, A. B., Truskey, G. A., and Reichert, W. M. (2000). Atomic force and total internal reflection fluorescence microscopy for the study of force transmission in endothelial cells. *Biophysical journal*, 78(4):1725–1735.

Moeendarbary, E. and Harris, A. R. (2014). Cell mechanics: principles, practices, and prospects. *Wiley Interdisciplinary Reviews: Systems Biology and Medicine*, 6(5):371–388.

Moeendarbary, E., Valon, L., Fritzsche, M., Harris, A. R., Moulding, D. A., Thrasher, A. J., Stride, E., Mahadevan, L., and Charras, G. T. (2013). The cytoplasm of living cells behaves as a poroelastic material. *Nature materials*, 12(3):253–261.

Mollaeian, K., Liu, Y., Bi, S., and Ren, J. (2018a). Atomic force microscopy study revealed velocity-dependence and nonlinearity of nanoscale poroelasticity of eukaryotic cells. *Journal of the mechanical behavior of biomedical materials*, 78:65–73.

Mollaeian, K., Liu, Y., Bi, S., Wang, Y., Ren, J., and Lu, M. (2018b). Nonlinear cellular mechanical behavior adaptation to substrate mechanics identified by atomic force microscope. *International journal of molecular sciences*, 19(11):3461.

Moore, S. W., Roca-Cusachs, P., and Sheetz, M. P. (2010). Stretchy proteins on stretchy substrates: the important elements of integrin-mediated rigidity sensing. *Developmental cell*, 19(2):194–206.

Moreno-Flores, S., Benitez, R., dM Vivanco, M., and Toca-Herrera, J. L. (2010). Stress relaxation and creep on living cells with the atomic force microscope: a means to calculate elastic moduli and viscosities of cell components. *Nanotechnology*, 21(44):445101.

Müller, D. J. and Dufrene, Y. F. (2010). Atomic force microscopy as a multifunctional molecular toolbox in nanobiotechnology. In *Nanoscience And Technology: A Collection of Reviews from Nature Journals*, pages 269–277. World Scientific.

Neuman, K. C. and Block, S. M. (2004). Optical trapping. *Review of scientific instruments*, 75(9):2787–2809.

Nia, H. T., Han, L., Li, Y., Ortiz, C., and Grodzinsky, A. (2011). Poroelasticity of cartilage at the nanoscale. *Biophysical journal*, 101(9):2304–2313.

Niclas, J., Allan, V. J., and Vale, R. D. (1996). Cell cycle regulation of dynein association with membranes modulates microtubule-based organelle transport. *Journal of Cell Biology*, 133(3):585–594.

Panorchan, P., Lee, J. S., Kole, T. P., Tseng, Y., and Wirtz, D. (2006). Microrheology and rock signaling of human endothelial cells embedded in a 3d matrix. *Biophysical journal*, 91(9):3499–3507.

Ren, J., Huang, H., Liu, Y., Zheng, X., and Zou, Q. (2015). An atomic force microscope study revealed two mechanisms in the effect of anticancer drugs on rate-dependent young's modulus of human prostate cancer cells. *PloS one*, 10(5):e0126107.

Rodriguez, M. L., McGarry, P. J., and Sniadecki, N. J. (2013). Review on cell mechanics: experimental and modeling approaches. *Applied Mechanics Reviews*, 65(6).

Salbreux, G., Charras, G., and Paluch, E. (2012). Actin cortex mechanics and cellular morphogenesis. *Trends in cell biology*, 22(10):536–545.

Savin, T. and Doyle, P. S. (2005). Static and dynamic errors in particle tracking microrheology. *Biophysical journal*, 88(1):623–638.

Svoboda, K. and Block, S. M. (1994). Biological applications of optical forces. *Annual review of biophysics and biomolecular structure*, 23(1):247–285.

Tan, J., Kalapesi, F., and Coroneo, M. (2006). Mechanosensitivity and the eye: cells coping with the pressure. *British journal of ophthalmology*, 90(3):383–388.

Tran-Son-Tay, R., Needham, D., Yeung, A., and Hochmuth, R. (1991). Time-dependent recovery of passive neutrophils after large deformation. *Biophysical journal*, 60(4):856–866.

Tseng, Y., Kole, T. P., and Wirtz, D. (2002). Micromechanical mapping of live cells by multiple-particle-tracking microrheology. *Biophysical journal*, 83(6):3162–3176.

Tseng, Y., Lee, J. S., Kole, T. P., Jiang, I., and Wirtz, D. (2004). Micro-organization and viscoelasticity of the interphase nucleus revealed by particle nanotracking. *Journal of cell science*, 117(10):2159–2167.

Vogel, V. and Sheetz, M. (2006). Local force and geometry sensing regulate cell functions. *Nature reviews Molecular cell biology*, 7(4):265–275.

Weafer, P., Reynolds, N., Jarvis, S., and McGarry, J. (2015). Single cell active force generation under dynamic loading–part i: Afm experiments. *Acta biomaterialia*, 27:236–250.

Wirtz, D. (2009). Particle-tracking microrheology of living cells: principles and applications. *Annual review of biophysics*, 38:301–326.

Yamane, Y., Shiga, H., Haga, H., Kawabata, K., Abe, K., and Ito, E. (2000). Quantitative analyses of topography and elasticity of living and fixed astrocytes. *Microscopy*, 49(3):463–471.

Yeung, A. and Evans, E. (1989). Cortical shell-liquid core model for passive flow of liquid-like spherical cells into micropipets. *Biophysical journal*, 56(1):139–149.

CHAPTER 2. ATOMIC FORCE MICROSCOPY STUDY REVEALED VELOCITY DEPENDENCE AND NONLINEARITY OF NANOSCALE POROELASTICITY OF EUKARYOTIC CELLS

This manuscript has been published by *Journal of the Mechanical Behavior of Biomedical Materials*.

Keyvan Mollaeian [1], Yi Liu[1], Siyu Bi[1], and Juan Ren[1]*

[1] Department of Mechanical Engineering, Iowa State University, Ames, Iowa, 50011, USA

Correspondence: juanren@iastate.edu; Tel.: +1-515-294-1805

2.1 Abstract

Intracellular network deformation of the cell plays an important role in cellular shape formation. Recent studies suggest that cell reshaping and deformation due to external forces involve cellular volume, pore size, elasticity, and intracellular filaments polymerization degree change. This cell behavior can be described by poroelastic models due to the porous structure of the cytoplasm. In this study, the nanoscale poroelasticity of human mammary basal/claudin low carcinoma cell (MDA-MB-231) was investigated using indentation-based atomic force microscopy. The effects of cell deformation (i.e., indentation) velocity and depth on the poroelasticity of MDA-MB-231 cells were studied. Specifically, the cell poroelastic behavior (i.e., the diffusion coefficient) was quantified at different indenting velocities (0.2, 2, 10, 20, 100, 200 μm/s) and indentation depths (635, 965, and 1313 nm) by fitting the force-relaxation curves using a poroelastic model. Cell treated with cytoskeleton inhibitors (latrunculin B, blebbistatin, and nocodazole) were measured to investigate the effect of the cytoskeletal components on the cell poroelasticity. It was found that in general the MDA-MB-231 cells behaved less poroelastic (i.e., with lower diffusion coefficient) at higher indenting velocities due to the local stiffening up and dramatic pore size reduction caused

by faster force load, and the cytoplasm is nonlinear in terms of poroelasticity. The poroelastic relaxation was more pronounced when the local cytoplasm porous structure was stretched by higher indentation. Furthermore, inhibition of cytoskeletal components resulted in pronounced poroelastic relaxation when compared with the control, and affected the nonlinearity of cell poroelasticity at different depth range inside of the cell. The comparison between the diffusion coefficient variation and the Young's modulus change under each indentation/treatment condition suggested that the cytoplasm porous geometry is more dominant than the cell Young's modulus in terms of affecting cell poroelasticity.

2.2 Introduction

Nowadays, attention toward cell rheology is growing due to the sensitivity of cell shape and deformation to external and internal biomechanical stimulation. For example, internal induced-forces due to biochemical interaction, intracellular organelle transport Niclas et al. (1996), transcriptional change of genes Coller et al. (2000), and signaling pathways Elledge (1996) proceed to elongation of the cells and cell cycling. Mutation of the genes, adapted pathways, and chemical interactions in different cell lines such as cancerous cells lead to significant cell rheological behavior change Moeendarbary and Harris (2014); Maloney et al. (2010); Sun et al. (2012); Brandao et al. (2003). Moreover, integrin-mediated focal adhesion Balaban et al. (2001); Plotnikov et al. (2012), ion channels Hayakawa et al. (2008), and cytoskeleton of the cell Mitrossilis et al. (2009); Colombelli et al. (2009); Hayakawa et al. (2011) are responsive to extracellular forces applied on the cell. As cytoplasm forms the largest part of a cell by volume, its biomechanical property plays a key role in cell rheology by dictating the cell deformation magnitude and cell shape change rate. Therefore, investigating the biomechanical behavior of the cytoplasm is crucial in achieving in-depth understanding of cell rheology. Furthermore, as it is widely found that living cells probe, react, and adapt to external mechanical stimulation Moeendarbary et al. (2013); Schillers et al. (2010), studying the mechanical properties of cytoplasm also promotes the modeling and quantification of the transduction of external mechanical stimulation into intracellular mechanical changes Zhu

et al. (2016); Charras et al. (2005, 2009).

Classical mechanical models have been implemented to biomechanics investigation of cell cytoplasm. The cortical shell–liquid core models (e.g., the Newtonian liquid drop model Tran-Son-Tay et al. (1991); Yeung and Evans (1989), the compound Newtonian liquid drop model Dong et al. (1990); Hochmuth et al. (1993), the shear thinning liquid drop model Drury and Dembo (1999, 2001), and the Maxwell liquid drop model Sung et al. (1988)) were developed to describe the rheology of cytoplasm in micropipette aspiration by assuming the homogeneity of the cell layer structure Lim et al. (2006b); Evans and Kukan (1984); Yeung and Evans (1989). To study the mechanics of cytoskeleton, solid models, such as the Hertzian model and the Sneddon model can be used to describe the contact mechanics between an elastic indenter and living cells by assuming the latter as an elastic isotropic body, and the contact is purely repulsive Liu (2006); Butt et al. (2005); Ghaednia et al. (2015b); Jackson et al. (2015); Ghaednia et al. (2016). Due to the existence of attractive forces (e.g, van der Waals forces) when the indenters are brought into close proximity with the cells, the Johnson-Kendall-Roberts (JKR) Chu et al. (2005) and the Derjaguin-Muller-Toporov (DMT) Gao and Yao (2004) models were then used to incorporate the effect of adhesion in Hertzian contact by taking the thermodynamic work of adhesion into account Johnson et al. (1971); Derjaguin et al. (1975); Wu (1982). The power-law structural damping model Hildebrandt (1969); Fredberg and Stamenovic (1989); Maksym et al. (2000); Fabry et al. (2001); Kardel et al. (2017); Ghaednia et al. (2015a) was used for studying the viscoelasticity and the dynamic behavior of adherent cells Ren et al. (2013). However, these models are not adequate enough to describe the biomechanical behavior of both the liquid flow (e.g., the cytosol) and the viscoelastic network (e.g., the cytoskeleton) —the biphasic nature of the cytoplasm. Therefore, a poroelastic model was implemented to study the biomechanics of cytoplasm, in which the cytoplasm was considered as a biphasic material consisting of a porous elastic solid meshwork (cytoskeleton, organelles, macromolecules) bathed in an interstitial fluid (cytosol) Oster (1989); Gu et al. (1997); Bachrach et al. (1995); Guilak and Mow (2000); Moeendarbary et al. (2013). In the poroelastic model, the response of cells to external force load depends only on the poroelastic diffusion coefficient, D, which is determined by E the elastic

modulus, ξ the pore size of the cytoskeleton meshwork, and μ the viscosity of the cytosol Moeendarbary et al. (2013); Charras et al. (2009, 2008). According to the coarse graining of the physical parameters in the poroelastic model, cellular rheology results from the effects of the interstitial fluid Keren et al. (2009), the related cell volume changes Moeendarbary et al. (2013); CHENG (2014), macromolecular crowding and the cytoskeletal network Moeendarbary et al. (2013); Schillers et al. (2010), this is consistent with the observed rheological properties of the cell that the internal cell pressure equilibrates by redistribution of intracellular fluids in response to localized deformation Charras et al. (2005); Keren et al. (2009); Rosenbluth et al. (2008); Charras et al. (2009); Zicha et al. (2003).

Poroelasticity studies of eukaryotic cells have been performed on atomic force microscopy (AFM) because of AFM's unique capability of applying force stimuli and then, measuring the sample response at specific locations in a physiologically friendly environment with piconewton force and nanometer spatial resolutions Giridharagopal et al. (2012); Yan et al. (2017); Efremov et al. (2017). Weafer et al. (2015) investigated the force generation of the cells under an applied constant cyclic loading and unloading nominal strain rate at a frequency of 1 Hz, and it was found that the compression force was recovered and reached equilibrium at the end of the last cycle. Weafer et al. (2015). Hu el al. (2010) reported that interaction force between the AFM tip and the hydrogels was decreased during relaxation of the tip on the sample which led to deformation of the hydrogels Hu et al. (2010). Tavakoli Nia et al. (2011) noted the poroelastic behavior of cartilage during relaxation experiment using AFM Nia et al. (2011). It has been noted that the mechanical response of fluid-filled materials, like cells, depends on the time and length scales of the measurements and the mechanical deformation of the materials changes during the entire experimental time span Kalcioglu et al. (2012). Moeendarbary et al. (2013) investigated the poroelastic behavior of the cell using micro bead when the approach velocity was 10 μm/s, and it was found that the components of the cells including actin, microtubules, myosin, and internediate filaments affect the diffusion coefficient of the cell Moeendarbary et al. (2013). However, since the cytoplasm of a living cell is highly heterogeneous and consists of a multi-layer structured viscoelastic cytoskeleton (i.e.,

velocity dependent), the cytoplasm poroelasticity quantified in previous work was limited to the specific measurement specifications and physical conditions (e.g., indenter size, approach velocity, and indentation depth). Particularly, due to the biphasic nature of living cells, the cell deformation rate (i.e., the AFM probe approach velocity) affects the measured cell stiffness significantly Moeendarbary et al. (2013); CHENG (2014), and the deformation/indentation depth range determined the layers of the cells triggered and measured during the mechanical quantification Kasas et al. (2005); Fuhrmann et al. (2011). Thus, to achieve in-depth understanding of the cell rheological behavior, study the poroelastic behavior of cytoplasm under different external excitation conditions is necessary.

In this study, we investigated the contribution of external force conditions to cellular rheology of human mammary basal/claudin low carcinoma cell at nanometer scale using AFM. Specifically, the cells were probed under forces with different approach velocities and magnitudes, and the poroelasticity diffusion coefficient was then quantified for each condition by fitting the force-relaxation curve using an empirical poroelastic model. Furthermore, to study the effect of internal cell structural property on determining the cell rheology and the nonlinearity of cell poroelasticity, we examined the importance of cytoskeleton in affecting cell poroelasticity.

2.3 Materials and Methods

2.3.1 Chemicals

The human mammary basel/claudin low carcinoma cell line (MDA-MB-231) and Leibovitz's L-15 Medium (L-15) were purchased from American Type Culture Collection (ATCC, Rockville, MD, USA). Dubecco's Modified Eagles Medium (DMEM) and Dimethyl sulfoxide (DMSO) were purchased from Sigma Aldrich (St. Louis, MO, USA). Fetal bovine serum and penicillin-streptomycin were obtained from Gibco (Grand Island, New York, USA). Latrunculin B and blebbistatin were purchased from Millipore sigma (Billerica, Massachusetts, USA). Nocodazole was purchased from Acros organics (New Jersey, USA).

2.3.2 Cell culture and treatment

MDA-MB-231 cells were cultured in the following cell growth medium: DMEM containing 10% fetal bovine serum (FBS) and 1% penicillin-steptomycin (pen-strep). The cells were subcultured at a density of 2.0×10^4 cells/ml on 35 mm cell culture dishes (Falcon, Durham, NC, USA) and maintained at 37 °C in 5% CO_2 incubator 24 hours prior to the AFM measurement. For the AFM poroelasticity measurements, the existing medium in the dishes was replaced by L-15 with the same concentration of FBS and pen-strep to remove dead and loosely attached cells, and to maintain the health of the cells during the experiment.

2.3.3 Cytoskeleton treatments

To investigate the contribution of cytoskeleton components on cell poroelasticity, the cells were treated with latrunculin B (750 nM to depolymerize F-actin), nocodazole (5 μM to depolymerize microtubules), and blebbistatin (100 μM to inhibit myosin II ATPase) separately in the aforementioned cell growth medium and incubated 30 min prior to the AFM measurements Moeendarbary et al. (2013). Then, the cell growth medium was replaced by L-15 with 10% FBS, 1% pen-strep, and the same drug concentration such that the drug effect was present during all measurements. Stock solutions were made by dissolving each drug in DMSO. Then, the aforementioned stock concentrations were prepared by adding the medium dropwise into the solution Mikulich et al. (2012). The DMSO concentration during the treatments and AFM measurement was 0.05%. To study the effects of the treatments on cell poroelasticity, the untreated cells were exposed to the same DMSO concentration, and used as control.

2.3.4 Atomic Force Microscopy (AFM) measurement

AFM measurement was performed at room temperature in aforementioned medium on a Bruker BioScope Resolve AFM system (Santa Barbara, CA, USA), which was integrated with an inverted optical microscope (Olympus, IX73, Japan). MLCT-BIO-DC-C (Bruker, Camarillo, CA) probe was used to measure the cells, and the spring constant of 0.03 N/m was acquired using thermal

tune approach Hutter and Bechhoefer (1993). During the experiment, the AFM probe (guided by the optical microscope camera) was in contact with the cells at locations away from the top of the cells to avoid the nucleus effect. As an example, the AFM topography image of one cell measured during the experiment is shown in Fig. 2.1, where the measurement location on the cell and the cross-section are also shown. All of the AFM drive voltage and sensor data were acquired using an NI PCIe-6353 DAQ board (National Instrument, Austin, TX, USA) with Matlab Simulink Desktop Real-Time system (Mathworks, MA, USA).

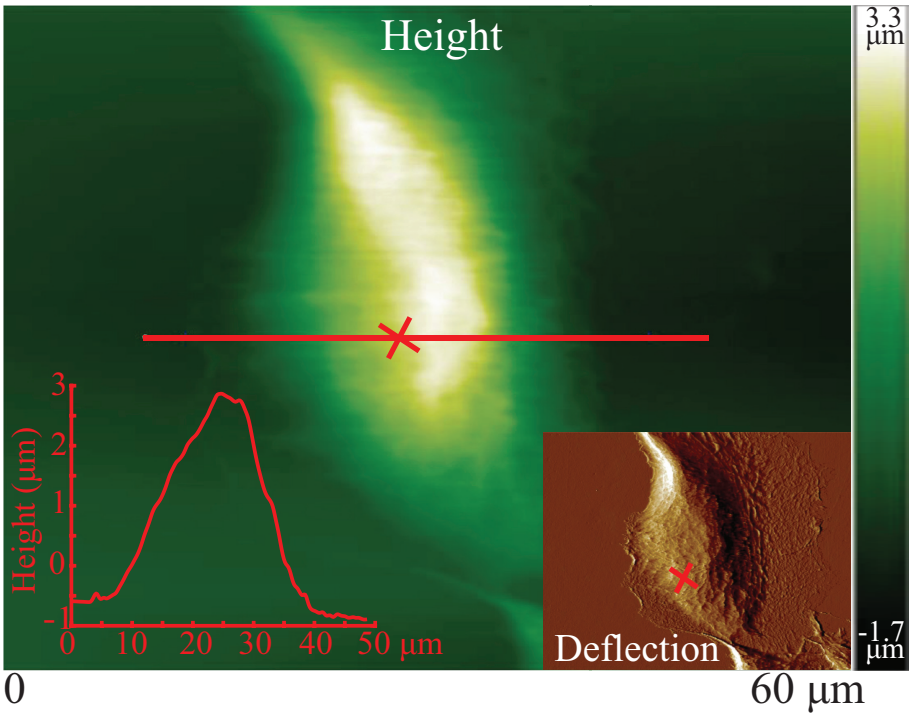

Figure 2.1 AFM topography image of a MDA-MB-231 cell, where the red cross denotes the poroelasticity measurement.

As the cell poroelasticity is caused by intracellular fluid redistribution to equilibrate the intracellular pressure, to experimentally quantify the cell poroelastic behavior, the local cell internal pressure needs to be suddenly disturbed to trigger the intracellular fluid redistribution. Therefore, rapid AFM indentation was chosen in this study to disturb the cells, and the effects of both the

loading speed and amplitude were studied. To investigate the effect of indenting speed (i.e., AFM probe approaching velocity) on poroelasticity of MDA-MB-231 cells, the AFM probe was brought into contact with the cells at six different speeds (0.2, 2.0, 10.0, 20.0, 100.0, and 200.0$\sim \mu m/s$) until reaching a target indentation of 960$\sim$nm (as illustrated in Fig. 2.2 (I-II)), and then the AFM z-piezo displacement was maintained constant at the corresponding value for 1 sec to acquire the force relaxation data (Fig. 2.2 (II-III)). To investigate the effect of indentation depth on the poroelastic behavior of MDA-MB-231 cell, the approaching speed of the probe was kept at 10$\sim \mu m/s$ until the desired indentations were reached (635, 965, and 1313$\sim nm$). A proportional-integral (PI) feedback control loop was implemented to control the AFM piezo displacement. For each desired indenting velocity and indentation depth, the force measurement was performed on at least six different cells using the same AFM probe.

2.3.5 Nanomechanical quantification of MDA-MB-231 cell

Indentation depth was calculated by subtracting the cantilever deflection, $d(t)$, from the displacement of the AFM z-piezo displacement Ren et al. (2015), $z(t)$ i.e.,

$$\delta(t) = z(t) - d(t). \tag{2.1}$$

Since the AFM probe used had a conical shape, the Young's Modulus of MDA-MB-231 cells was quantified using the Sneddon model Sneddon (1965), i.e.,

$$F(t) = \frac{2}{\pi}\tan(\alpha)\frac{E}{1-\nu^2}\delta^2(t). \tag{2.2}$$

where α and ν are the tip opening angle and the Poisson ratio of the cell, respectively. Additionally, the Poisson's ratio $\nu = 0.3$ Moeendarbary et al. (2013); Charras et al. (2001) was used for elasticity measurements.

2.3.6 Cellular poroelasticity measurement

As the cell size (>30 μm) was more than three orders of magnitude larger than the AFM tip radius (25 nm), the probe-cell interaction could be approximated as a poroelastic half-space

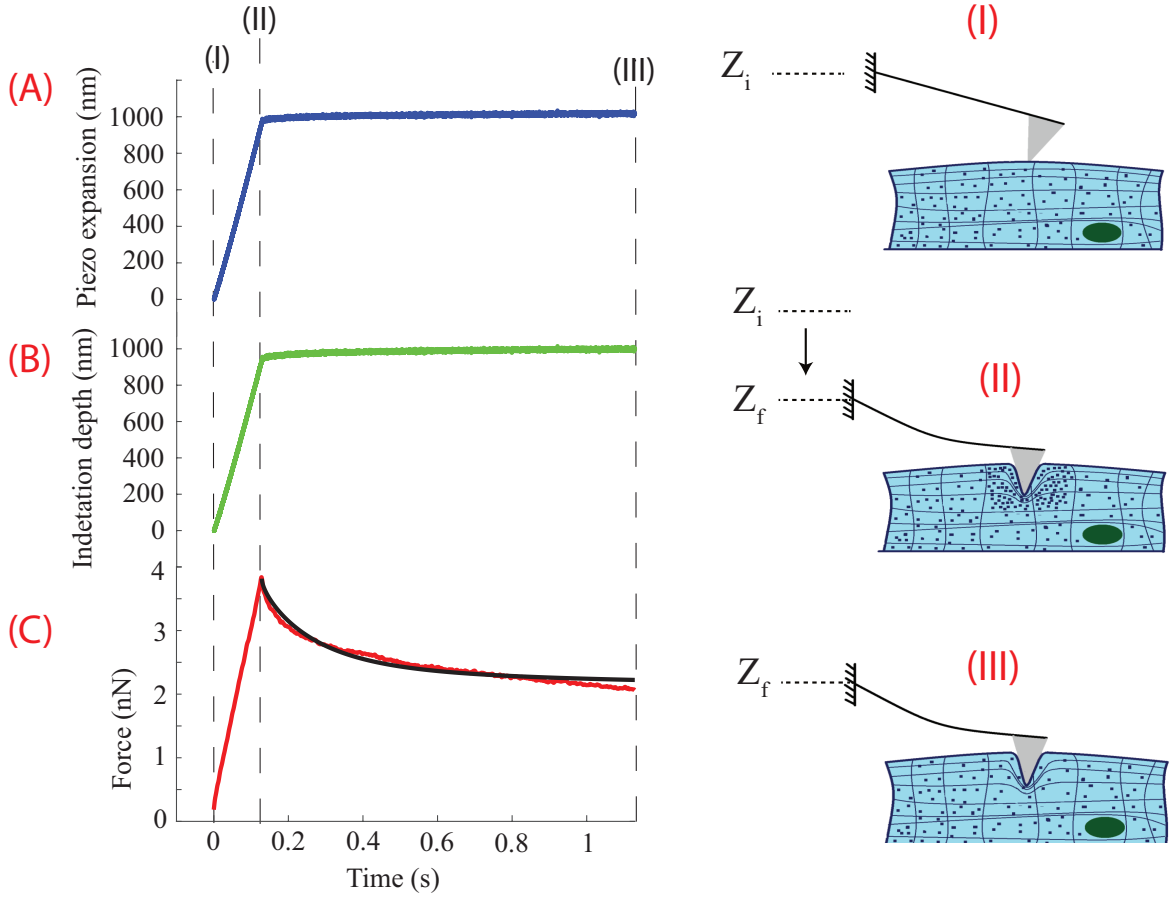

Figure 2.2 (A,B,C) The AFM piezo displacement, the indentation depth, and the probe-sample interaction force during the poroelasticity measurement: I) At the beginning of the measurement the AFM tip was in contact with the surface of the cell with zero velocity. II) Indenting: the AFM probe indented the cell at a constant velocity until the desired indentation was reached. Multiple layers and the intracellular fluid of the cell were compressed during this loading process. III) Relaxation: the AFM probe rested on the cell, and the intracellular fluid redistributed to equilibrate the cell internal pressure, while the AFM z-piezo displacement was maintained at a constant since the end of the indenting process. The force-relaxation curve (the black solid curve in (C)) was then fitted using the poroelastic model.

indented by a conical indenter, and the following empirical poroelastic model obtained by finite-element-analysis was used for analyzing the cell poroelasticity Hu et al. (2010):

$$\frac{F(t)-F_f}{F_i-F_f} = 0.493e^{-0.822\sqrt{\frac{Dt}{a^2}}} + 0.507e^{-1.348\frac{Dt}{a^2}}. \tag{2.3}$$

where F_i and F_f are the initial and final forces in the relaxation portion of the force-time curve, respectively. D is the diffusion coefficient. The probe-cell contact size, a, can be quantified using the indentation depth as:

$$a = \frac{2}{\pi}\bar{\delta}\tan(\alpha). \tag{2.4}$$

where $\bar{\delta}$ is the indentation depth at the beginning of the force-relaxation process (i.e., the indentation caused by the displacement of the AFM piezo), and α is the half opening angle of the conical shaped AFM probe.

2.3.7 Curve fitting and statistical analysis

Relaxation portions of collected force-time curves from AFM were fitted by the poroelastic model (Eq. (2.3)) using Matlab. Each force-relaxation curve was fitted and the RMS fitting error was included in the results to demonstrate the measurement consistency.

2.4 Results and discussion

2.4.1 Poroelastic behavior of living cells

First, the experiment results validated the chosen empirical poroelasticity model and demonstrated that living cells exhibited poroelastic behavior. As shown in Fig. 2.3, the probe-cell interaction force started to decrease once the probe was rested on the cell surface following the indenting process, and went through a rapid exponential decay during the 1 sec relaxation measurement. This observation is consistent with the previous studies on other cell types Moeendarbary et al. (2013); Wu et al. (1998). Indeed, the poroelasticity model (Eq. (2.3)) fitted the force-relaxation curve well with the relative RMS fitting error ranging between $2.5-14\%$. These indicate that the force decrease during the relaxation corresponds to cellular poroelastic behavior. As can be seen in

Figs. 2.3 (C) and (F), the force reduced by at least 50% on average for all of the measurements but the indentation increase was less than 6 %, indicating that the force-relaxation data were collected under approximately constant applied intracellular strain. Therefore, the force relaxation (i.e., the force decrease) was primarily caused by intracellular fluid (e.g., cytosol) redistribution within the cytoplasm. Although the probe was rested in the cell following the indenting process, the applied compression on the cell caused the intracellular liquid to move out of the probe-cell contact region through the porous structured cytoskeleton to equilibrate, and consequently, a reduction of the probe-cell interaction force.

To further study how the measurement conditions affect cell poroelasticity, we measured the force–relaxation curve under different indenting velocities and indentation depths.

2.4.2 Effect of indenting velocity on poroelasticity of the cell

Six different indenting velocities (0.2, 2.0, 10.0, 20.0, 100.0, and 200.0 μm/s) were tested with the same targeted AFM indentation depth of 960 nm, and the force relaxation measurement was performed on at least six different cells for each velocity, respectively. The measured force relaxation curves were then fitted using Eq. 2.3, yielded a relative RMS fitting error in the range of $2.5-14\%$ for all of the measurements. The results indicated that the cell poroelastic relaxation was more significant at higher indenting velocities. Specifically, as shown in Figs. 2.3 (C) and (F), the indentation increase and the force reduction were over 4% and 40%, with respect to their initial values (i.e., the indentation and force at the beginning of the relaxation), respectively, when the indenting velocity was higher than 10 μm/s. However, the indentation remained almost unchanged (with about 1% increase), and the force only decreased at most 23% for indenting velocities at 0.2 and 2 μm/s, indicating the probe-cell interaction was closer to equilibrium at the beginning of the one sec relaxation process-the end of the indenting process. In another word, the poroelastic relaxation phenomenon was more pronounced when the indenting velocity was higher than 10 μm/s. This is also confirmed by the normalized force-relaxation curve. The fitted force relaxation curves for different indenting velocities were normalized as $(F(t)-F_f)/(F_i-F_f)$ as shown in Fig. 2.3

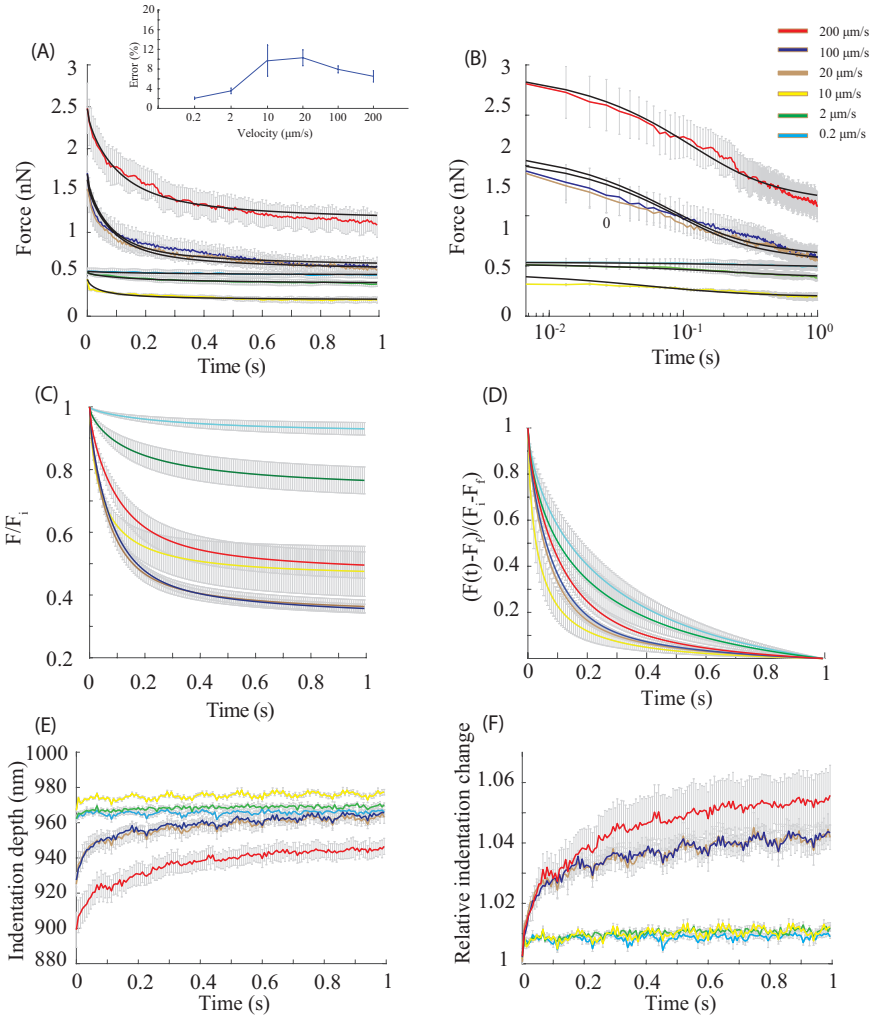

Figure 2.3 A) Force-relaxation curve for indenting velocities of (0.2, 2, 10, 20, 100, and 200 μm/s when the targeted indentation depth was 960 nm. The mean value of the fitted curves for each velocity was shown as solid lines. The error bars denote the raw force data for each indenting velocity. B) Log-Log plots of A). C)Relative force reduction during the relaxation process of the poroelastic fitted results in A). D)Normalized force reduction curve for different indenting velocities when the indentation depth was 960 nm. At the same time instant, lower normalized value denotes faster poroelastic relaxation. E) Indentation change during the relaxation process: the indentation depth gradually increased when the probe was resting on the cell following the rapid indenting process. F) Relative indentation change $\delta/\bar{\delta}$ during the relaxation process.

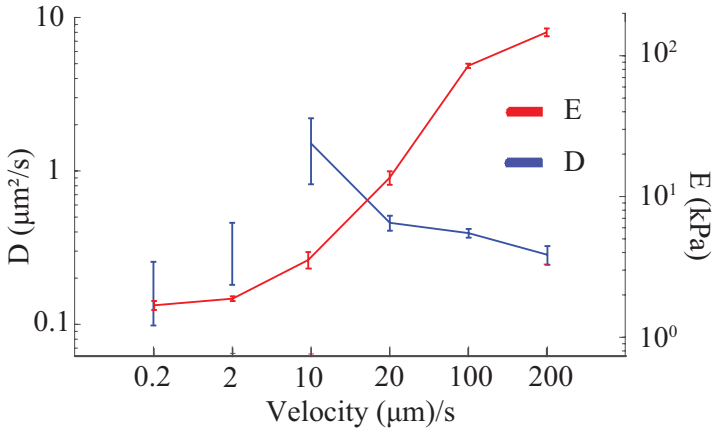

Figure 2.4 Changes of cell oroelasticity and elasticity in response to change in indenting velocity.

(D). The normalized force relaxation curves for the indenting velocities of 0.2 and 2μm/s are above those for the higher velocities, especially after 0.2 s. Since higher normalized force values indicate less active intracellular fluid redistribution, the intracellular pressure was closer to equilibrium at the beginning of the relaxation process (i.e., at the end of the indenting process) when the cells were indented at 0.2 and 2μm/sec.

This observation can be explained using the empirical poroelastic model (Eq. (2.3)). According to Eq. (2.3), the poroelastic relaxation becomes more significant if the indenting velocity v is faster than the fluid efflux Moeendarbary et al. (2013); Ibata et al. (2011), i.e., $v > \bar{\delta}/t_p$, where t_p is the timescale of the intracellular fluid movement and $t_p \sim a^2/D$. As the quantified diffusion coefficient (by fitting the force-relaxation curve using Eq. (2.3)) for the targeted indentation $\bar{\delta} \sim 960$ nm is in the range of 0.2-1.5 μm^2/s (see Fig. 2.4), the indenting velocity for poroelastic relaxation measurement needs to satisfy $v >$7 μm/s. This condition indicates that the intracellular fluid efflux can be negligible for all $v >$7 μm/s velocities during the indenting process and contributes to the force reduction observed during the force relaxation process. Otherwise, significant intracellular fluid efflux can occur to equilibrate the inner pressure of the cell during the indenting process when $v <$7 μm/s, and no much force reduction will be observed during the relaxation process. Therefore, the force relaxation immediately following rapid AFM indentation observed in this study was

indeed caused by intracellular fluid efflux, and became more significant once the indenting velocity is faster than the fluid efflux rate. In particular, for the indenting velocities lower than 7 μm/s, the intracellular fluid flew out of the probe-cell contact region to equilibrate the pore pressure during the approaching process and soon reached equilibrium (steady-state), which resulted in barely changed force and indentation, i.e., the cell behavior was more elastic other than poroelastic, during the relaxation measurement. On the contrary, the intracellular fluid was not able to respond fast enough during rapid indentation (v >7 μm/s), and then the efflux started to occur once the probe was rested on the cell to equilibrate the intracellular pressure, causing a significant reduction of the probe-cell interaction force. It is worth to note that by using nanometer-sized AFM probes the quantified diffusion coefficient in this study was smaller than those reported (in the range of 1-100 μm^2/s) by using micro-beads on AFM Moeendarbary et al. (2013).

To further study the relation between the cytoskeleton elasticity (i.e., Young's modulus) and cell poroelasticity, we fitted the force-indentation curve with the Sneddon contact model (Eq. (2.2)) to quantify the Young's modulus, E, under different indenting velocities. The fitting results yielded E increasing from 1.5 kPa to 147 kPa monotonically with the indenting velocity increase as shown in Fig. 2.4. This monotonic E vs. v trend is consistent with previous results CHENG (2014) that as the cytoskeleton is highly viscoelastic and faster indenting velocities can increase the polymerization degree of the local actin, which further leads to local stiffening of the cytoskeleton Rotsch and Radmacher (2000); Moeendarbary et al. (2013). As a result, the increased actin polymerization and cytoskeleton stiffening may decrease the cytoskeleton pore size significantly, and further slows down the intracellular fluid efflux during the force relaxation process. This analysis can be confirmed by Fig. 2.3 (C), where the force reduction is smaller for higher indenting velocities during poroelastic relaxation for all v >7 μm/s (note that the cases for v <7 μm/s are excluded since fluid efflux happened even before the relaxation process started as discussed earlier). The trend of the quantified diffusion coefficient D (see Figs. 2.4) is also consistent with the above discussion, where D has an inverse relation with E for all v >7 μm/s, as a higher value of D corresponds to more rapid fluid efflux. Note that this inverse relation between D and E doesn't conflict with the

general recognized scaling law of diffusion coefficient: $D \sim E\eta^2/\mu$, where η is the pore radius of the cytoskeleton mesh work, and μ is the viscosity of the intracellular fluid (i.e., cytosol). Although a higher approach velocity resulted in an increase of E, but the local cytoskeleton stiffening and actin polymerization caused the pore size η to decrease, and led to an overall smaller D. This indicates that change in η were more dominant than that of E in affecting the cytoplasm poroelasticity, and thereby, the cell rheology. As it is known that living cells are highly heterogeneous, and the cell shows high nonlinearity in terms of mechanical responses to external force excitation Schillers et al. (2010); Fernández et al. (2006), next we investigated the nonlinearity of cell poroelasticity.

2.4.3 Effect of indentation depth on poroelasticity of the cell

It has been studied that the structure heterogeneity may affect the mechanical behavior of living cells, e.g., stiffness and viscoelasticity Kasas et al. (2005); Fuhrmann et al. (2011). Thus, we investigated the cell poroelasticity measured under three different indentation depths (635, 965, and 1313 nm) at the indenting velocity of 10 μm/s.

As can be seen in Fig. 2.5, the cells showed poroelastic behavior at all indentation depths measured when the indenting velocity was 10 μm/s. The poroelastic model fitted the force-relaxation curve well with a RMS fitting error less that 5% (Fig. 2.5 (A)), and the force reduction was more that 30% during the one sec relaxation process for all three indentation depths (Fig. 2.5 (B)) while the indentation remained nearly unchanged (Fig. 2.5 (E) and (F)). Moreover, the cell poroelasticity was indentation depth-dependent. The normalized force $((F(t) - F_f)/(F_i - F_f))$ curves collapse onto one master curve for all three indentation depth at time >0.6 sec (see Fig. 2.5 (D)); however, they are completely different for $t < 0.6$ sec showing that the indentation depth affected the cell poroelastic relaxation during short time scale. This indicates that although the indenting velocity was kept the same, the change of indentation depth altered the cell's initial response of the relaxation process. Due to the multilayered structure of the cytoplasm, as the indentation depth increases, more layers of the cytoplasm (especially the cytoskeleton) could be excited and deformed during the indentation, and the measured cell mechanical response (poroelasticity and elasticity)

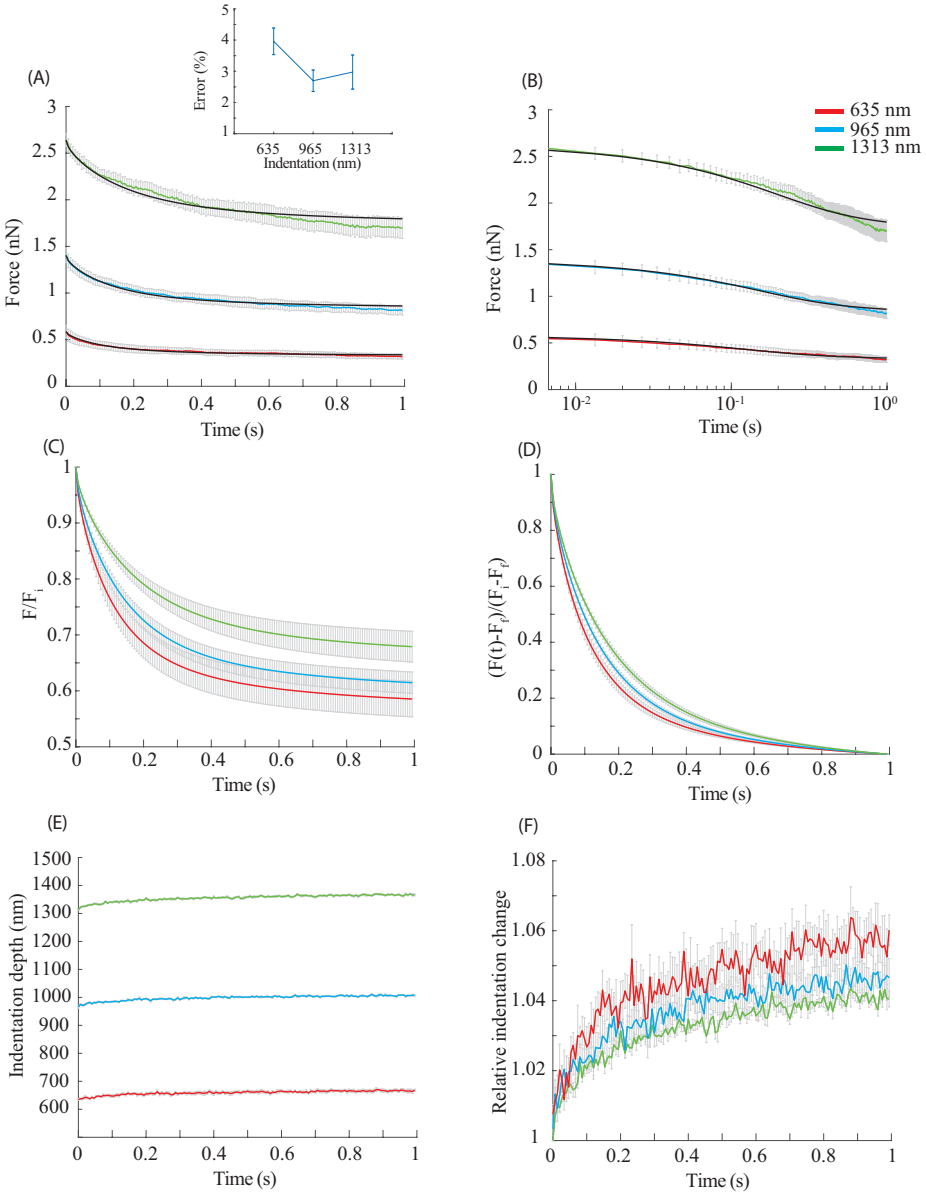

Figure 2.5 A) Force-relaxation curve for different indentation depths (635, 965, and 1313 nm) when the indenting velocity was 10 μm/s. The mean value of the fitted curves for each velocity was shown as solid thick lines. The error bars denote the raw force data for each indenting velocity. B) Log-Log plot of A). C) Relative force reduction during the relaxation process of the poroelastic fitted results in A). D)Normalized force reduction curve for different indentation depths when the indenting velocity was 10 μm/s. At the same time instant, higher normalized value denotes slower intracellular fluid efflux. E) Indentation change during the relaxation process: the indentation depth gradually increased when the probe was resting on the cell following the rapid indenting process. F) Relative indentation change $\delta/\bar{\delta}$ during the relaxation process.

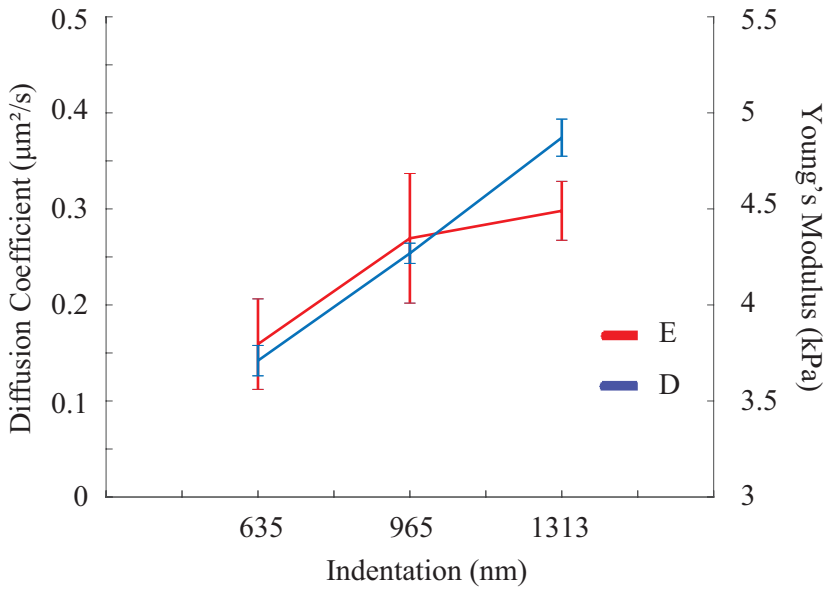

Figure 2.6 Changes of the cell poroelasticity and elasticity in response to change in indentation depth at indenting velocity of 10 μm/s.

changed accordingly. In particular, mainly the superficial layer of the cell (e.g., actin filament and cortical myosin II) deformed when the indentation depth was small Schillers et al. (2010). At deeper indentations, more layers of the cytoplasm (e.g., bulky cytosol) may also be deformed along with the superficial layer. Therefore, distinct force-relaxation curves were observed at the beginning of the relaxation process, and then the force-relaxation curves collapsed together towards the end of the relaxation process, denoting that the intracellular pressure was close to equilibrium due to fluid efflux.

Different diffusion coefficient D and different Young's modulus E were obtained for the three measured indentation depths, respectively. A monotonic relation was observed between E and the indentation depth, and E increased by 30%, (see Fig 2.6). This monotonic relation is consistent with previous findings that mammalian cells are not homogeneous in terms of elasticity Schillers et al. (2010); Fernández et al. (2006). Particularly, the measured Young's modulus was determined by the elastic properties of both the superficial layer and the underneath second layer for deep indentation, and the latter had higher stiffness than the former Schillers et al. (2010). In addition,

stress stiffening of the cytoskeleton could also contribute to the the Young's modulus increase for much deeper indentation. The elevated E for larger indentation depths indicated significant changes of the cytoskeleton structure, such as filament entanglement reinforcement Moeendarbary et al. (2013); Schillers et al. (2010). These structural changes together with the local cytoskeleton network stretching by deeper indentations could lead to significant increase of the cytoplasmic pore size η, which directly resulted in an increase of the diffusion coefficient. As confirmed by the results shown in Fig. 2.6, the diffusion coefficient D increased by 164% when the indentation depth increased from 635 to 1313 nm. This finding together with the aforementioned diffusion coefficient scaling law suggests that η was more dominant than E in affecting the cytoplasm poroelasticity.

2.4.4 Effect of cell cytoskeleton on cell poroelasticity

It has been reported that the components of cell cytoskeleton (e.g., actin filaments, microtubules, and myosin) affect the biomechanical behavior of the living cell Rotsch and Radmacher (2000); Schillers et al. (2010). Therefore, to understand the contribution of cytoskeleton on cell poroelasticity, the effects of actin filaments, microtubules, and myosin II on cell poroelasticity under different indentation depths (635, 965, and 1313 nm) at the indenting velocity of 10 μm/s were investigated. The cells were treated with nocodazole (to depolymerize microtubules), latrunculin B (to depolymerize F-actin), and blebbistatin (to inhibit myosin II).

As can be seen in Fig. 2.7, nonlinearity of cell poroelasticity was more pronounced on the cells treated by the three drugs. Specifically, the diffusion coefficient of the cells treated with 5 μM nocodazole increased from 0.11 to 0.45 $\mu m^2/s$ (increased by 309%) when the indentation was increased from 635 to 1313 nm, comparing with the control (0.14 to 0.37 $\mu m^2/s$, a 164% increase). Depolymerization of the microtubules did not affect the measured D and E significantly when the indentation was relatively small (635 nm). This result agrees with the previous finding that microtubules had no significant effect on cell poroelasticity when the indentation was small (less than 800 nm) Moeendarbary et al. (2013). However, the effect of microtubule depolymerization became more and more significant as the indentation depth increased–resulted in a 22% increase in

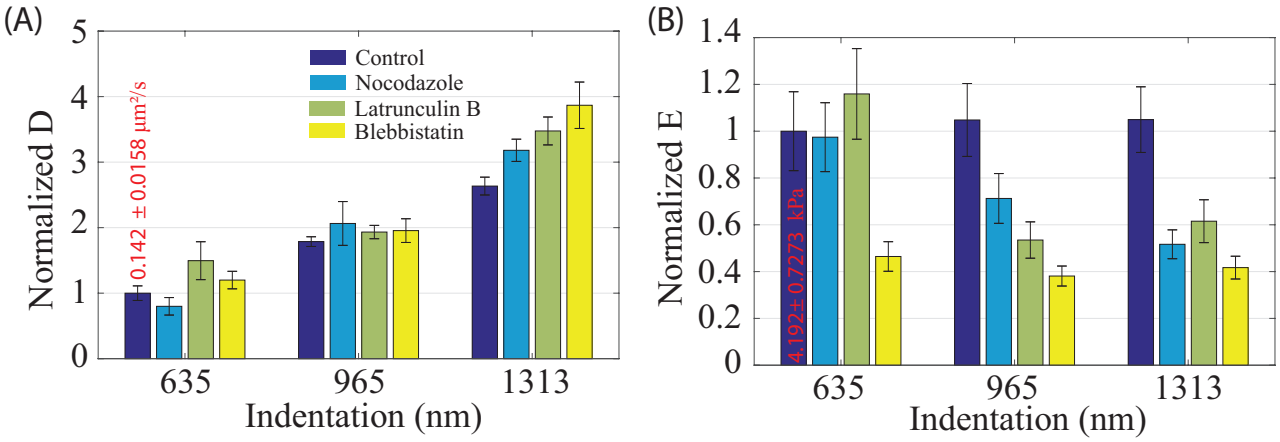

Figure 2.7 Effect of microtubules depolymerization, F-actin depolymerization, and myosin inhibition on A) the diffusion coefficient and B) the Young's modulus under different indentation depth at the indenting velocity of 10 μm/s.

the diffusion coefficient and a 51 % decrease in the Young's modulus compared with the control at the indentation of 1313 nm. This observation revealed that microtubulues are more concentrated at deeper layers of the cytoskeleton (i.e., underneath the superficial layer), and thus its effect on cell mechanics can only be observed when the indentation depth is deep enough. Since depolymerization of the microtubules directly weakens the strength (i.e., stiffness) of the cytoskeleton, and results in an increase of the pore size, therefore, the diffusion coefficient was increased at all measured indentation depths compared with the control, and the opposite trend was observed for the Young's modulus. Furthermore, the deeper the indentation was, the more significant the microtubules effect was, thus, the changes of the diffusion coefficient and the Young's modulus were more significant. Note that due to the limited indentation depths used in previous studies, the effect of microtobulues on cell poroelasticity has never been reported before. Depolymerization of F-actin resulted in an overall increased diffusion coefficient and significantly decreased Young's modulus for all indentation depths measured (with respect to the control at each indentation) and treatment of cells with blebbistatin resulted in more significant increases in both the diffusion coefficient and the Young's modulus. These changes of the Young's modulus and the diffusion coefficient of the perturbed cells are consistent with previous studies Moeendarbary et al. (2013); Rotsch and Radmacher (2000);

Schillers et al. (2010) as depolymerization of F-actin and inhibition of myosin II activity contribute to reduction of cytoskeleton stiffness and increase of the cytoplasmic pore size. The change of the diffusion coefficient under these two treatments was quite notable at the indentation of 635 nm (50% for latrunculin B and 20% for blebbistatin) and became more significant as the indentation increased (at least 248% for both drugs at 1313 nm indentation). This indicates that depolymerization of F-actin and inhibition of myosin II can cause structural changes at both the superficial and the deeper layers of the cell cytoskeleton, and these structural changes are more significant as the indentation depth increases.

Beside the drug treatment effects, nonlinearity of the diffusion coefficient (i.e., the indentation depth-dependence) of the treated cells was also resulted from the stretching of the cytoskeleton network as discussed earlier. It is worth to note that the diffusion coefficient and the Young's modulus of the control are close to those of the cells measured in the L-15 medium without DMSO at the same velocity and the indentations (see Fig. 2.6), therefore, the change of cell poroelasticity of the treated cells was indeed caused by the cytoskeleton treatments other than DMSO. Taken together, these results revealed that F-actin and myosin II play a fundamental role in modulating cellular rheology, and myosin II plays a more dominant role in affecting the cytoplasm elasticity (i.e., Young's modulus). Moreover, the opposite trends of the diffusion coefficient and the Young's modulus changes confirmed that the cytoplasmic pore size dominates over elasticity in determining cell rheology.

2.5 Conclusion

In this study, the nanoscale cell poroelasticity was investigated using AFM indentation approach. Velocity-dependence and the nonlinearity of MDA-MB-231 cell poroelastic behavior was quantified by quantifying the diffusion coefficient through fitting the force-relaxation curves with the poroelastic model. Moreover, the effects of actin filaments, microtubules, and myosin II on the cell elastic and poroelastic behavior was studied. It was found that the cell had poor poroelastic behavior when the indenting velocity was lower than 10 μm/s due to intracellular fluid redistribu-

tion within the cell during indentation. Lower diffusion coefficient for faster indenting velocities confirmed poor poroelastic behavior of the cell due to local stiffening of the cell at faster velocity. Deeper indentation led to higher diffusion coefficient and more efficient poroelastic relaxation of the cell due to the increases of the cytoplasmic pore size and cell stiffness. Inhibition of the aforementioned cytoskeletal components resulted in significant increase of the diffusion coefficient and dramatic decrease of the Young's modulus compared with the control. Differences of the three cytoskeleton inhibition treatments in affecting the nonlinearity of cell poroelasticity revealed that F-actin and myosin II affects cytoskeleton structure at both the superficial and the deeper layers, while microtubule is mainly affects the cell mechanical behavior at the deeper layers of the cytoskeleton.

2.6 Acknowledgment

This work was supported by the National Science Foundation (NSF) [CMMI-1634592], and Iowa State University. The authors also thank Dr. Ian Schneider for providing MDA-MB-231 cells.

2.7 References

Bachrach, N. M., Valhmu, W. B., Stazzone, E., Ratcliffe, A., Lai, W. M., and Mow, V. C. (1995). Changes in proteoglycan synthesis of chondrocytes in articular cartilage are associated with the time-dependent changes in their mechanical environment. *Journal of biomechanics*, 28(12):1561–1569.

Balaban, N. Q., Schwarz, U. S., Riveline, D., Goichberg, P., Tzur, G., Sabanay, I., Mahalu, D., Safran, S., Bershadsky, A., Addadi, L., et al. (2001). Force and focal adhesion assembly: a close relationship studied using elastic micropatterned substrates. *Nature cell biology*, 3(5):466–472.

Brandao, M., Fontes, A., Barjas-Castro, M., Barbosa, L., Costa, F., Cesar, C., and Saad, S. (2003). Optical tweezers for measuring red blood cell elasticity: application to the study of drug response in sickle cell disease. *European journal of haematology*, 70(4):207–211.

Butt, H.-J., Cappella, B., and Kappl, M. (2005). Force measurements with the atomic force microscope: Technique, interpretation and applications. *Surface science reports*, 59(1):1–152.

Charras, G., Lehenkari, P. P., and Horton, M. (2001). Atomic force microscopy can be used to mechanically stimulate osteoblasts and evaluate cellular strain distributions. *Ultramicroscopy*, 86(1):85–95.

Charras, G. T., Coughlin, M., Mitchison, T. J., and Mahadevan, L. (2008). Life and times of a cellular bleb. *Biophysical journal*, 94(5):1836–1853.

Charras, G. T., Mitchison, T. J., and Mahadevan, L. (2009). Animal cell hydraulics. *Journal of Cell Science*, 122(18):3233–3241.

Charras, G. T., Yarrow, J. C., Horton, M. A., Mahadevan, L., and Mitchison, T. (2005). Non-equilibration of hydrostatic pressure in blebbing cells. *Nature*, 435(7040):365–369.

CHENG, A. H.-D. (2014). Fundamentals of poroelasticity. *Analysis and Design Methods: Comprehensive Rock Engineering: Principles, Practice and Projects*, 113.

Chu, Y.-S., Dufour, S., Thiery, J. P., Perez, E., and Pincet, F. (2005). Johnson-kendall-roberts theory applied to living cells. *Physical review letters*, 94(2):028102.

Coller, H. A., Grandori, C., Tamayo, P., Colbert, T., Lander, E. S., Eisenman, R. N., and Golub, T. R. (2000). Expression analysis with oligonucleotide microarrays reveals that myc regulates genes involved in growth, cell cycle, signaling, and adhesion. *Proceedings of the National Academy of Sciences*, 97(7):3260–3265.

Colombelli, J., Besser, A., Kress, H., Reynaud, E. G., Girard, P., Caussinus, E., Haselmann, U., Small, J. V., Schwarz, U. S., and Stelzer, E. H. (2009). Mechanosensing in actin stress fibers revealed by a close correlation between force and protein localization. *Journal of cell science*, 122(10):1665–1679.

Derjaguin, B. V., Muller, V. M., and Toporov, Y. P. (1975). Effect of contact deformations on the adhesion of particles. *Journal of Colloid and interface science*, 53(2):314–326.

Dong, C., Skalak, R., and Sung, K. (1990). Cytoplasmic rheology of passive neutrophils. *Biorheology*, 28(6):557–567.

Drury, J. L. and Dembo, M. (1999). Hydrodynamics of micropipette aspiration. *Biophysical Journal*, 76(1):110–128.

Drury, J. L. and Dembo, M. (2001). Aspiration of human neutrophils: effects of shear thinning and cortical dissipation. *Biophysical Journal*, 81(6):3166–3177.

Efremov, Y. M., Wang, W.-H., Hardy, S. D., Geahlen, R. L., and Raman, A. (2017). Measuring nanoscale viscoelastic parameters of cells directly from afm force-displacement curves. *Scientific Reports*, 7(1):1541.

Elledge, S. J. (1996). Cell cycle checkpoints: preventing an identity crisis. *Science*, 274(5293):1664.

Evans, E. and Kukan, B. (1984). Passive material behavior of granulocytes based on large deformation and recovery after deformation tests. *Blood*, 64(5):1028–1035.

Fabry, B., Maksym, G. N., Butler, J. P., Glogauer, M., Navajas, D., and Fredberg, J. J. (2001). Scaling the microrheology of living cells. *Physical review letters*, 87(14):148102.

Fernández, P., Pullarkat, P. A., and Ott, A. (2006). A master relation defines the nonlinear viscoelasticity of single fibroblasts. *Biophysical journal*, 90(10):3796–3805.

Fredberg, J. J. and Stamenovic, D. (1989). On the imperfect elasticity of lung tissue. *Journal of applied physiology*, 67(6):2408–2419.

Fuhrmann, A., Staunton, J., Nandakumar, V., Banyai, N., Davies, P., and Ros, R. (2011). Afm stiffness nanotomography of normal, metaplastic and dysplastic human esophageal cells. *Physical biology*, 8(1):015007.

Gao, H. and Yao, H. (2004). Shape insensitive optimal adhesion of nanoscale fibrillar structures. *Proceedings of the National Academy of Sciences of the United States of America*, 101(21):7851–7856.

Ghaednia, H., Cermik, O., and Marghitu, D. B. (2015a). Experimental and theoretical study of the oblique impact of a tennis ball with a racket. *Proceedings of the Institution of Mechanical Engineers, Part P: Journal of Sports Engineering and Technology*, 229(3):149–158.

Ghaednia, H., Marghitu, D. B., and Jackson, R. L. (2015b). Predicting the permanent deformation after the impact of a rod with a flat surface. *Journal of Tribology*, 137(1):011403.

Ghaednia, H., Pope, S. A., Jackson, R. L., and Marghitu, D. B. (2016). A comprehensive study of the elasto-plastic contact of a sphere and a flat. *Tribology International*, 93:78–90.

Giridharagopal, R., Rayermann, G. E., Shao, G., Moore, D. T., Reid, O. G., Tillack, A. F., Masiello, D. J., and Ginger, D. S. (2012). Submicrosecond time resolution atomic force microscopy for probing nanoscale dynamics. *Nano letters*, 12(2):893–898.

Gu, W., Lai, W., Hung, C., Liu, Z., and Mow, V. (1997). Analysis of transient swelling and electrical responses of an isolated cell to sudden osmotic loading. In *American Society of Mechanical Engineers, Bioengineering Division (Publication) BED*.

Guilak, F. and Mow, V. C. (2000). The mechanical environment of the chondrocyte: a biphasic finite element model of cell–matrix interactions in articular cartilage. *Journal of biomechanics*, 33(12):1663–1673.

Hayakawa, K., Tatsumi, H., and Sokabe, M. (2008). Actin stress fibers transmit and focus force to activate mechanosensitive channels. *J Cell Sci*, 121(4):496–503.

Hayakawa, K., Tatsumi, H., and Sokabe, M. (2011). Actin filaments function as a tension sensor by tension-dependent binding of cofilin to the filament. *J Cell Biol*, 195(5):721–727.

Hildebrandt, J. (1969). Comparison of mathematical models for cat lung and viscoelastic balloon derived by laplace transform methods from pressurevolume data. *Bulletin of Mathematical Biology*, 31(4):651–667.

Hochmuth, R., Ting-Beall, H., Beaty, B., Needham, D., and Tran-Son-Tay, R. (1993). Viscosity of passive human neutrophils undergoing small deformations. *Biophysical journal*, 64(5):1596–1601.

Hu, Y., Zhao, X., Vlassak, J. J., and Suo, Z. (2010). Using indentation to characterize the poroelasticity of gels. *Applied Physics Letters*, 96(12):121904.

Hutter, J. L. and Bechhoefer, J. (1993). Calibration of atomic-force microscope tips. *Review of Scientific Instruments*, 64(7):1868–1873.

Ibata, K., Takimoto, S., Morisaku, T., Miyawaki, A., and Yasui, M. (2011). Analysis of aquaporin-mediated diffusional water permeability by coherent anti-stokes raman scattering microscopy. *Biophysical journal*, 101(9):2277–2283.

Jackson, R. L., Ghaednia, H., and Pope, S. (2015). A solution of rigid–perfectly plastic deep spherical indentation based on slip-line theory. *Tribology Letters*, 58(3):47.

Johnson, K., Kendall, K., and Roberts, A. (1971). Surface energy and the contact of elastic solids. In *Proceedings of the Royal Society of London A: Mathematical, Physical and Engineering Sciences*, volume 324, pages 301–313. The Royal Society.

Kalcioglu, Z. I., Mahmoodian, R., Hu, Y., Suo, Z., and Van Vliet, K. J. (2012). From macro- to microscale poroelastic characterization of polymeric hydrogels via indentation. *Soft Matter*, 8(12):3393–3398.

Kardel, K., Ghaednia, H., Carrano, A. L., and Marghitu, D. B. (2017). Experimental and theoretical modeling of behavior of 3d-printed polymers under collision with a rigid rod. *Additive Manufacturing*, 14:87–94.

Kasas, S., Wang, X., Hirling, H., Marsault, R., Huni, B., Yersin, A., Regazzi, R., Grenningloh, G., Riederer, B., Forro, L., et al. (2005). Superficial and deep changes of cellular mechanical properties following cytoskeleton disassembly. *Cytoskeleton*, 62(2):124–132.

Keren, K., Yam, P. T., Kinkhabwala, A., Mogilner, A., and Theriot, J. A. (2009). Intracellular fluid flow in rapidly moving cells. *Nature cell biology*, 11(10):1219–1224.

Lim, C., Zhou, E., and Quek, S. (2006). Mechanical models for living cells–a review. *Journal of biomechanics*, 39(2):195–216.

Liu, K.-K. (2006). Deformation behaviour of soft particles: a review. *Journal of Physics D: Applied Physics*, 39(11):R189.

Maksym, G. N., Fabry, B., Butler, J. P., Navajas, D., Tschumperlin, D. J., Laporte, J. D., and Fredberg, J. J. (2000). Mechanical properties of cultured human airway smooth muscle cells from 0.05 to 0.4 hz. *Journal of Applied Physiology*, 89(4):1619–1632.

Maloney, J. M., Nikova, D., Lautenschläger, F., Clarke, E., Langer, R., Guck, J., and Van Vliet, K. J. (2010). Mesenchymal stem cell mechanics from the attached to the suspended state. *Biophysical journal*, 99(8):2479–2487.

Mikulich, A., Kavaliauskiene, S., and Juzenas, P. (2012). Blebbistatin, a myosin inhibitor, is phototoxic to human cancer cells under exposure to blue light. *Biochimica et Biophysica Acta (BBA)-General Subjects*, 1820(7):870–877.

Mitrossilis, D., Fouchard, J., Guiroy, A., Desprat, N., Rodriguez, N., Fabry, B., and Asnacios, A. (2009). Single-cell response to stiffness exhibits muscle-like behavior. *Proceedings of the National Academy of Sciences*, 106(43):18243–18248.

Moeendarbary, E. and Harris, A. R. (2014). Cell mechanics: principles, practices, and prospects. *Wiley Interdisciplinary Reviews: Systems Biology and Medicine*, 6(5):371–388.

Moeendarbary, E., Valon, L., Fritzsche, M., Harris, A. R., Moulding, D. A., Thrasher, A. J., Stride, E., Mahadevan, L., and Charras, G. T. (2013). The cytoplasm of living cells behaves as a poroelastic material. *Nature materials*, 12(3):253–261.

Nia, H. T., Han, L., Li, Y., Ortiz, C., and Grodzinsky, A. (2011). Poroelasticity of cartilage at the nanoscale. *Biophysical journal*, 101(9):2304–2313.

Niclas, J., Allan, V. J., and Vale, R. D. (1996). Cell cycle regulation of dynein association with membranes modulates microtubule-based organelle transport. *Journal of Cell Biology*, 133(3):585–594.

Oster, G. (1989). *Cell motility and tissue morphogenesis*. Academic Press, New York.

Plotnikov, S. V., Pasapera, A. M., Sabass, B., and Waterman, C. M. (2012). Force fluctuations within focal adhesions mediate ecm-rigidity sensing to guide directed cell migration. *Cell*, 151(7):1513–1527.

Ren, J., Huang, H., Liu, Y., Zheng, X., and Zou, Q. (2015). An atomic force microscope study revealed two mechanisms in the effect of anticancer drugs on rate-dependent young's modulus of human prostate cancer cells. *PloS one*, 10(5):e0126107.

Ren, J., Yu, S., Gao, N., and Zou, Q. (2013). Indentation quantification for in-liquid nanomechanical measurement of soft material using an atomic force microscope: Rate-dependent elastic modulus of live cells. *Physical Review E*, 88(5):052711.

Rosenbluth, M. J., Crow, A., Shaevitz, J. W., and Fletcher, D. A. (2008). Slow stress propagation in adherent cells. *Biophysical journal*, 95(12):6052–6059.

Rotsch, C. and Radmacher, M. (2000). Drug-induced changes of cytoskeletal structure and mechanics in fibroblasts: an atomic force microscopy study. *Biophysical journal*, 78(1):520–535.

Schillers, H., Wälte, M., Urbanova, K., and Oberleithner, H. (2010). Real-time monitoring of cell elasticity reveals oscillating myosin activity. *Biophysical journal*, 99(11):3639–3646.

Sneddon, I. N. (1965). The relation between load and penetration in the axisymmetric boussinesq problem for a punch of arbitrary profile. *International journal of engineering science*, 3(1):47–57.

Sun, Y., Villa-Diaz, L. G., Lam, R. H., Chen, W., Krebsbach, P. H., and Fu, J. (2012). Mechanics regulates fate decisions of human embryonic stem cells. *PLoS one*, 7(5):e37178.

Sung, K.-L. P., Schmid-Schb'nbein, G., and Chien, S. (1988). Passive deformation analysis of human leukocytes. *Journal of biomechanical engineering*, 110:27.

Tran-Son-Tay, R., Needham, D., Yeung, A., and Hochmuth, R. (1991). Time-dependent recovery of passive neutrophils after large deformation. *Biophysical journal*, 60(4):856–866.

Weafer, P., Reynolds, N., Jarvis, S., and McGarry, J. (2015). Single cell active force generation under dynamic loading–part i: Afm experiments. *Acta biomaterialia*, 27:236–250.

Wu, H., Kuhn, T., and Moy, V. (1998). Mechanical properties of l929 cells measured by atomic force microscopy: effects of anticytoskeletal drugs and membrane crosslinking. *Scanning*, 20(5):389–397.

Wu, S. (1982). *Polymer interface and adhesion*. M. Dekker.

Yan, B., Ren, J., Zheng, X., Liu, Y., and Zou, Q. (2017). High-speed broadband monitoring of cell viscoelasticity in real time shows myosin-dependent oscillations. *Biomechanics and Modeling in Mechanobiology*, pages 1–12.

Yeung, A. and Evans, E. (1989). Cortical shell-liquid core model for passive flow of liquid-like spherical cells into micropipets. *Biophysical journal*, 56(1):139–149.

Zhu, X., Siamantouras, E., Liu, K.-K., and Liu, X. (2016). Determination of work of adhesion of biological cell under afm bead indentation. *Journal of the mechanical behavior of biomedical materials*, 56:77–86.

Zicha, D., Dobbie, I. M., Holt, M. R., Monypenny, J., Soong, D. Y., Gray, C., and Dunn, G. A. (2003). Rapid actin transport during cell protrusion. *Science*, 300(5616):142–145.

CHAPTER 3. NONLINEAR CELLULAR MECHANICAL BEHAVIOR ADAPTATION TO SUBSTRATE MECHANICS IDENTIFIED BY ATOMIC FORCE MICROSCOPE

This manuscript has been published by *International Journal of Molecular Science*.

Keyvan Mollaeian [1], Yi Liu[1], Siyu Bi[1], Yifei Wang[2], Juan Ren[1]*, and Meng Lu[2]

[1] Department of Mechanical Engineering, Iowa State University, Ames, Iowa, 50011, USA

[2] Department of Electrical and Computer Engineering, Iowa State University, Ames, Iowa, 50011, USA

Correspondence: juanren@iastate.edu; Tel.: +1-515-294-1805

3.1 Abstract

Cell-substrate interaction plays an important role in intracellular behavior and function. Adherent cell mechanics is directly regulated by the substrate mechanics. However, previous studies on the effect of substrate mechanics only focused on the stiffness relation between the substrate and the cells, and how the substrate stiffness affects the time-scale and length-scale of the cell mechanics has not yet been studied. The absence of this information directly limits the in-depth understanding of the cellular mechanotransduction process. In this study, the effect of substrate mechanics on the nonlinear biomechanical behavior of living cells was investigated using indentation-based atomic force microscopy. The mechanical properties and their nonlinearities of the cells cultured on four substrates with distinct mechanical properties were thoroughly investigated. Furthermore, the actin filament (F-actin) cytoskeleton of the cells was fluorescently stained to investigate the adaptation of F-actin cytoskeleton structure to the substrate mechanics. It was found that living cells sense and adapt to substrate mechanics: the cellular Young's modulus, shear modulus, apparent viscosity, and their nonlinearities (mechanical property vs. measurement depth relation)

were adapted to the substrates' nonlinear mechanics. Moreover, the positive correlation between the cellular poroelasticity and the indentation remained the same regardless of the substrate stiffness nonlinearity, but was indeed more pronounced for the cells seeded on the softer substrates. Comparison of the F-actin cytoskeleton morphology confirmed that the substrate affects the cell mechanics by regulating the intracellular structure.

3.2 Introduction

Living cells are exquisitely sensitive to mechanical stimuli in their extracellular environment. Among many kinds of extracellular force stimuli, the stiffness of the underlying substrate where a cell attaches to is one of the most accessible (and widely studied) biomechanical factors in affecting cellular behavior Leipzig and Shoichet (2009); Yeung et al. (2005); Brandl et al. (2007). For instance, studies have shown that mesenchymal stem cells that attach to stiffer substrates commit to an osteogenic fate Kilian et al. (2010), whereas the cells express a neurogenic phenotype when are seeded on softer substrates Guilak et al. (2009). Also, the stiffness of the extracellular matrix (ECM) regulates the structure, motility, and proliferation of the cells Ulrich et al. (2009). Although extensive efforts have identified multiple signaling pathways, such as downstream signaling of $\alpha_v\beta_3$ and RPTP$_\alpha$ Jiang et al. (2006) and tyrosine phosphatase and kinase Giannone and Sheetz (2006), in the cellular rigidity sensing process, how the substrate mechanics affects the cellular mechanical properties at different depths still remains poorly understood. Questions such as which micro-/nano-scale cellular properties are more sensitive to the substrate mechanics and how the substrate stiffness affects the time-scale and length-scale of cellular mechanical responses have not yet been investigated. The absence of these studies directly limits in-depth understandings of cellular mechanotransduction process.

Previously, the effect of substrate mechanics on cellular mechanics has been mostly studied by quantifying the dependence of cellular stiffness (i.e., Young's modulus) on substrate rigidity at a certain indentation depth using atomic force microscope (AFM) owing to its ultra-high spatial and force resolutions and real-time data capturing capability Efremov et al. (2017); Xie and Ren

(2018). Studies have shown that cells are highly adaptive to the substrate stiffness: cell stiffness has a monotonically increasing relation with the substrate rigidity Discher et al. (2005); Rianna and Radmacher (2017); Tee et al. (2011). Wang et al. (2000) reported that normal NIH/3T3 cells reacted to the rigidity of the substrate with a decrease in the rate of DNA synthesis and an increase in the rate of apoptosis on flexible substrates Wang et al. (2000). Takai et al. (2005) found that the apparent elastic modulus of MC3T3-E1 cells were substrate dependent Takai et al. (2005). However, due to the biphasic nature and self-organization of living cells, stiffness alone is not adequate enough to represent the cellular mechanical and rheological behavior under various force measurement conditions Mollaeian et al. (2018a); Moeendarbary et al. (2013). Since cell rheology has been shown time/frequency dependent Mollaeian et al. (2018a); Moeendarbary et al. (2013); Nia et al. (2011), cellular viscosity should also be considered when studying the effect of substrate mechanics. Moreover, as the largest portion of the cell—cytoplasm—essentially consists of both the intracellular fluid (e.g., the cytosol) and the viscoelastic network (e.g., the cytoskeleton), the above two aspects cannot account for the ubiquitous biphasic nature of the cytoplasm Mollaeian et al. (2018a); Moeendarbary et al. (2013). Therefore, poroelasticity which links the biomechanical behavior of the cells to structural hierarchy, intracellular fluid flow (cytosol), related volume change, and biological parameters, must be quantitatively investigated as well Charras et al. (2005, 2009); Dembo and Harlow (1986). Poroelasticity describes the cell's ability to equilibrate the intracellular pressure under external loading force (i.e., localized deformation) through active intracellular fluid redistribution (efflux) Mollaeian et al. (2018a); Moeendarbary et al. (2013), and can be represented by the poroelastic diffusion coefficient, D, which depends on elastic modulus E, the pore size of the cytoskeleton meshwork ξ, and the viscosity of the cytosol μ Mollaeian et al. (2018a); Moeendarbary et al. (2013); Charras et al. (2008, 2009). Therefore, to investigate the time-scale and length-scale dependence of cell response to substrate mechanics, elasticity, viscoelasticity, and poroelasticity of the cells must be quantified simultaneously. Moreover, studies have reported that cellular mechanical behavior is nonlinear Mollaeian et al. (2018a); Moeendarbary et al. (2013)—ascribed to the multi-layered heterogeneity of living cells. Thus, the measured mechanical behavior entirely

depends on the deformation (e.g., the indentation in AFM measurements) scale of the cells, which determines the specific cell layers that are disturbed by the measurement. Therefore, the effect of substrate mechanics on the nonlinearity of cellular biomechanical behavior needs to be studied as well. However, such an important aspect has not been reported yet in previous studies.

In this study, we investigated the effects of substrate's mechanics on the nonlinear mechanical behavior of living cells using AFM force indentation measurements. As studies have shown that the cell-substrate relation in terms of mechanical properties may change significantly based on the cell type, two different cell lines were studied: an epithelial cell line (Madin-Darby canine kidney (MDCK) and a fibroblast cell line (NIH/3T3)). Specifically, for each cell type, the cells were cultured on substrates with different stiffness (Polydimethylsiloxane (PDMS) with the base-to-curing agent ratios of 10:0.5, 10:1, and 10:3, and the polystyrene cell culture dish), and the relation between the substrate mechanics and cell nonlinear mechanical behavior (stiffness, viscosity, and poroelasticity) was investigated by indenting the cells at different depths. Moreover, to understand how the substrate affects the cellular mechanics, the cells were fluorescently stained to study the actin filament (F-actin) morphology change caused by the four substrates.

3.3 Results and Discussion

Although, previous studies have shown the effect of the substrate stiffness on the stiffness of living cells Takai et al. (2005); Solon et al. (2007), more detailed results on how the substrate mechanics affects the cell rheology and its nonlinearity has not been reported. Thus, we investigated the effect of the four substrates with different stiffness (three PDMS substrates and polystyrene cell culture dish) on the elasticity, viscoelasticity, and poroelasticity of NIH/3T3 and MDCK cells. The cell Young's modulus, E, was quantified according to the Hertz contact model Sneddon (1965); Ghaednia et al. (2017) (Eq. 3.2) using the data obtained at the end of the indenting process. Then, cell viscoelastic and poroelastic behavior were quantified using the force and indentation data of the force-relaxation process (see Eqs. (3.7) and (3.9)).

3.3.1 Effect of substrate mechanics on the nonlinear elastic and viscoelastic behavior of the cells

The results clearly show that the cellular mechanical behavior (in terms of elasticity) is significantly different for each substrate, as shown in Fig. 3.1. To demonstrate the substrate mechanics effect, the nonlinear stiffness (i.e., Young's modulus) of the four substrates was also measured (20 μm/s, see Fig. 3.2). Comparing Figs. 3.1 and 3.2, it is clear that the mechanical behavior of both NIH/3T3 and MDCK cells adapts to the substrates mechanics closely, including both the stiffness and its nonlinearity. Note that since the substrate stiffness is at least three orders higher than the cells', and the indentation used was less than one quarter of the cell height, substrate effect could be ignored during the cell mechanics quantification. Thus, the quantified results in Fig. 3.1 indeed represent the biomechanical behavior of the measured cells.

Significant changes are shown for the elasticity (Young's modulus E, shear modulus G) and viscoelasticity (apparent viscosity η) of both types of cells seeded on the four substrates. In general, the cell elasticity and viscoelasticity are synchronized with the substrate stiffness closely, as shown in Fig. 3.1. At each indentation depth, E, G, and η are positively correlated with the substrate stiffness, except no clear trend is shown for MDCK cells at the lowest indentation depth. For the cells seeded on each of the four substrates, the nonlinearity of these three cellular mechanical parameters (E, G, and η) are consistent with the substrate stiffness nonlinearity as well. Specifically, as the stiffness of the 10:3 PDMS and the cell culture dish is monotonic with the indentation depth (see Fig. 3.2), E of NIH/3T3 and MDCK cells on 10:3 PDMS increased by 161% and 94%, respectively, when the indentation was increased from 650 to 1300 nm, and the increase was 253% and 360%, respectively, for the cells seeded on the culture dish. However, on the other two softer substrates which become softer as the indentation depth increases, the Young's modulus of NIH/3T3 and MDCK cells on 10:0.5 PDMS at the indentation depth of 1300 nm was at most 27 and 142 Pa, respectively—more than 70% reduction compared to the values at the 650 nm indentation. Also, E reduced at least 14% for both cell types on 10:1 PDMS when the indentation depth was doubled from 650 nm. Similar changes of nonlinearity of the shear modulus and apparent viscosity were also

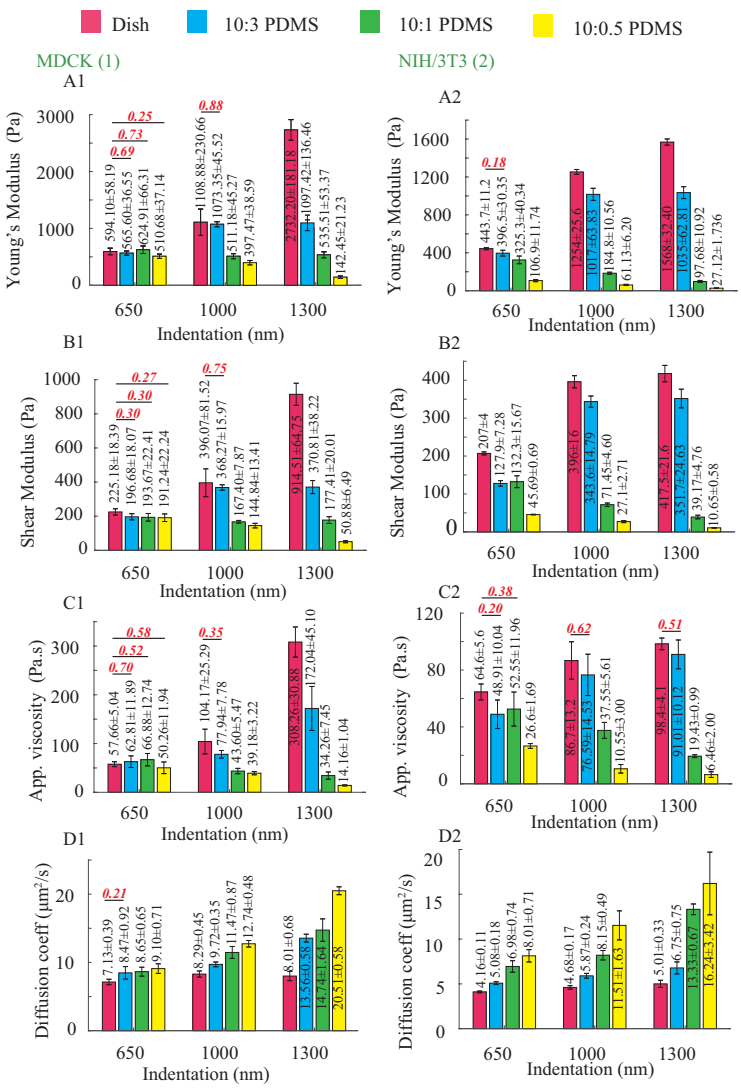

Figure 3.1 The nonlinear cellular (A1,A2) Young's modulus, (B1,B2) shear modulus, (C1,C2) apparent viscosity, and (D1,D2) diffusion coefficient of MDCK and NIH/3T3 cells seeded on different substrate, respectively, quantified at different indentation depths at the indenting velocity of 20 μm/s. The AFM measurements were performed on six different cells at each indentation depth and the error bars represent the standard errors. n=6. Student's t-test was performed to analyze the statistical difference: for each indentation, data were compared with respect to the ones measured on the dish (control) at the same indentation; and for each substrate, the data measured at the minimum indentation (650 nm) for that substrate were chosen as control. A p <0.05 was yielded for each comparison unless otherwise denoted in the figure (with p values in red bold italic font).

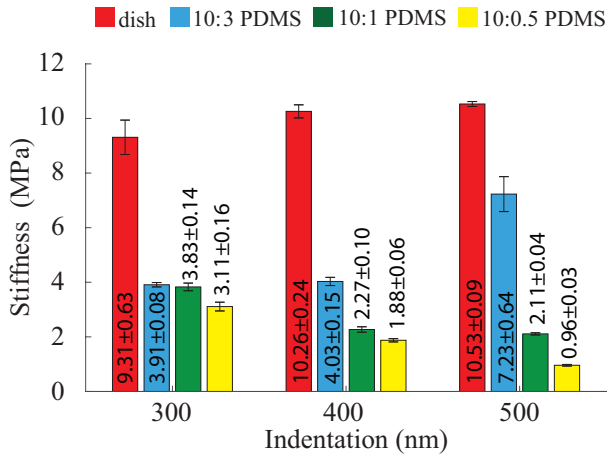

Figure 3.2 Stiffness nonlinearity of the four different substrates measured at the indenting velocity of 20 μm/s. The error bars represent the standard errors. n=6. Student's t-test was performed to analyze the statistical difference: for each indentation, data were compared with respect to the ones measured on the dish (control) at the same indentation; and for each substrate, the data measured at the minimum indentation (650 nm) for that substrate were chosen as control. A p <0.05 was yielded for each comparison unless otherwise denoted in the figure (with p values in red bold italic font).

observed for both cell types. As shown in Fig. 3.1, the shear modulus and the apparent viscosity of NIH/3T3 and MDCK cells are synchronized with the substrate stiffness at each indentation depth, respectively. Specifically, G and η for these two types of cells on the cell culture dish and 10:3 PDMS increased by at least 89% and 52%, respectively, when the indentation depth increased from 650 nm to 1300 nm. However, both of them decreased for both cell types on the softer substrates (i.e., 10:1 and 10:0.5 PDMSs).

The experiment results demonstrated that the adherent cells sense and adapt to substrate mechanics: the nonlinear cellular elasticity and viscosity are regulated by the substrate stiffness nonlinearity. However, previous studies only showed the dependence of the cellular elasticity to the substrate stiffness at a single measurement depth Solon et al. (2007). To explain the presented results on the adaptation of the cellular biomechanical behavior to the substrate's nonlinear mechanics, a systematic sketch to illustrate the cell-substrate contact mechanism was generated based on the previous studies on cell-substrate interaction and is presented in Fig. 3.3. Specifically, as

reported previously, in response to a stiffer substrate, stronger cell-substrate bonding is established (i.e., larger cell-substrate adhesion force) Wang et al. (2001); Ghibaudo et al. (2008); Saez et al. (2005), which further leads to the stiffening of the cells—higher E Solon et al. (2007). Thus, at each measured indentation depth, the cell Young's modulus is positively correlated with the substrate stiffness. By changing the elastomer base-to-curing agent ratio from 10:0.5 to 10:3, the cross-linking density of the PDMS substrates increased significantly Deuschle et al. (2010), which further stiffens the polymer network (see Fig. 3.2). For the harder substrates (10:3 PDMS and polystyrene cell culture dish), the highly cross-linked polymer network generates stronger resistance at deeper layers from the surface, thus a higher stiffness is yielded as the indentation depth increases Carrillo et al. (2005); Alisafaei et al. (2013); Deuschle et al. (2010). However, for the softer PDMSs (10:1 and 10:0.5), not only the stiffness at a certain indentation depth is lower, but also the polymer behaves softer at the deeper indentation Charitidis (2010); Wang et al. (2014). This is because low cross-linking degree makes the effect of higher order displacement gradients more pronounced due to higher molecular motion freedom at deeper indentations Alisafaei et al. (2013); Deuschle et al. (2010). As the indentation depth increases, the cell-substrate interface is pushed down further, thus the stiffness of the substrate at deeper layer is sensed and adapted by the cells (see Fig. 3.3). Therefore, similar Young's modulus nonlinearity was observed for the cells. Note that the results presented are not contradictory to the previous finding that the cell stiffness measured on glass coverslips at nanometer scale decreases with the indentation increase Pogoda et al. (2012). Indeed, the cell mechanical behavior quantified at micrometer scale is quite different as that measured at nanometer scale as the former leads to a "bulk" scale characterization and the latter is localized quantification. This difference can be directly seen from the quantified cell Young's modulus values: E is at the order of 10^2 Pa in this study and previous work where μm sized probes were used Schillers et al. (2010); Moeendarbary et al. (2013), however, E is at the order of kPa when nm sized probes were used Mollaeian et al. (2018a); Sirghi et al. (2008). In fact, our results agree with the previous studies on cell elasticity nonlinearity well: it has been reported that the Young's modulus

of cells seeded on glass coverslips increased as the indentation depth increased from 300 nm to 1000 nm Schillers et al. (2010).

At the same time, as the cell-substrate bonding strength is monotonically increasing with the substrate stiffness Discher et al. (2005), the softer the substrate is, the weaker the cell-substrate adhesion force is Park et al. (2011); Wang et al. (2001); Guo et al. (2006). This directly results in lower shear stress of the cytoskeleton and lower cell contractility Discher et al. (2005); Engler et al. (2004). Thus, the cells are prone to the higher degree of lateral expansion once they are indented at a certain depth Moeendarbary et al. (2013); Discher et al. (2005), which directly leads to the larger shear strain. Thus, it appears that the cells possess lower shear modulus, (G=shear stress/shear strain McNaught and McNaught (1997)) when their substrate is softer. Also, the higher degree of lateral expansion during indentation can cause significant expanded cytoskeleton network Moeendarbary et al. (2013); Burridge et al. (1988); Chen et al. (2004); Geiger et al. (2009); Yim et al. (2010), thus the intracellular fluid flow rate (i.e., shear rate Munson et al. (2014)) is increased. Together with the decreased cytoskeleton shear stress, the cell apparent viscosity, η=shear stress/shear rate Wells and Merrill (1961), is decreased. Therefore, the cell shear modulus and apparent viscosity are also positively correlated with the substrate stiffness and its nonlinearity.

3.3.2 Effect of substrate mechanics on the poroelastic behavior of the cells

As can be seen in Fig. 3.1, at each measured indentation, the diffusion coefficient, D, is negatively correlated with the substrate stiffness for both NIH/3T3 and MDCK cells. Specifically, for all of the three measured indentation depths, the stiffer the substrate is, the lower the poroelastic diffusion coefficient is. As aforementioned, the cells are subject to larger shear strain on softer substrates due to weakened cell-substrate bonding. This indicates that the cell structure (e.g., the cytoskeleton) is more expanded on softer substrates, which directly results in larger pore radius, ξ, of the cytoskeleton network (Fig. 3.3). Thus, larger D is quantified for the cells seeded on the softer substrates at each indentation, although the Young's modulus of these cells are lower than those seeded on the harder substrates. Note that this observation is not contradictory to

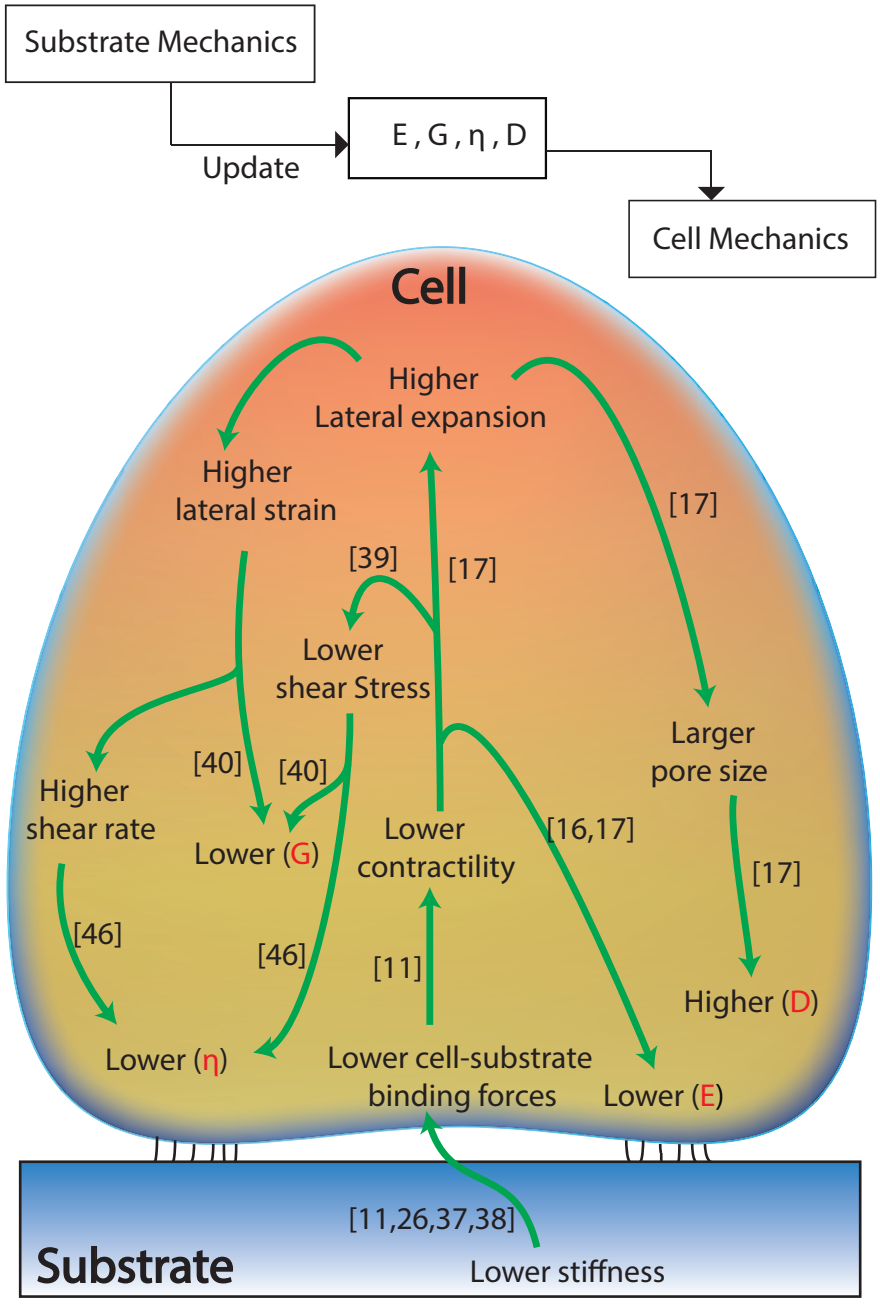

Figure 3.3 Schematic sketch of the cell biomechanical behavior change in response to substrate mechanics.

the poroelasticity scale law, $D \sim E\xi^2/\mu$ (where μ is the viscosity of the cytosol), instead it concurs with the previous findings that the pore radius is more dominant than E in affecting the cell poroelasticity Mollaeian et al. (2018a); Moeendarbary et al. (2013). However, the nonlinearity of cell poroelasticity did not show a unanimous relation with the substrate stiffness nonlinearity. Specifically, when the indentation depth was doubled from 650 nm (see Fig. 3.1), D increased by 20%, 33%, 91%, and 103% for NIH/3T3 cells seeded on the cell culture dish, 10:3, 10:1, and 10:0.5 PDMSs, respectively, and 12%, 60%, 70%, and 125% for MDCK cells, respectively. However, the stiffness vs. indentation relation of the substrates were divided: monotonic for dish and 10:3 PDMS and opposite for 10:1 and 10:0.5 PDMSs, as shown in Fig. 3.2. Note that the stiffness of 10:0.5 PDMS decreased the most (69%) compare to the other three as the indentation depth increased (see Fig. 3.2). Therefore, the nonlinearity of the cell poroelasticity is more significant on the softer substrates, especially the one whose stiffness is the most negatively correlated with the indentation depth. When the indentation increases, the increase of ξ is more significant on the softer substrate because the weaker cell-substrate bonding can cause further cytoskeleton expansion Burridge et al. (1988); Chen et al. (2004); Geiger et al. (2009); Yim et al. (2010). In this case, even if the cells are softer (i.e., with lower E), D still increases—ξ is more dominant than E in affecting D Mollaeian et al. (2018a); Moeendarbary et al. (2013). As a result, the monotonic D vs. indentation relation for cells is more pronounced on the substrates with inversely correlated stiffness vs. indentation, and the more dramatic this inverse correlation is, the more significant cell poroelasticity nonlinearity is. Therefore, the cellular poroelasticity and its nonlinearity are also directly affected by the substrate stiffness and its nonlinearity. Note that the differences of E, G, η, and D, respectively, of the MDCK cells on the four substrates are less significant at the indentation depth of 650 nm compare to the other two depths and the results for NIH/3T3 cells. One possible explanation is the cell morphology difference: MDCK cells are in general much taller than NIH/3T3 cells (8 μm vs 6 μm) and have thicker plasma membrane as epithelial cells Sorce et al. (2015), thus the substrate effect on the MDCK cell behavior at the low indentation (e.g., 650 nm) was not as significant as that on the NIH/3T3 cell. Once the MDCK cells are indented deep enough (i.e., deeper layers

of cells are probed), the effect of substrate mechanics becomes more pronounced and both the Young's modulus and the shear modulus follow the same trend compare to the substrate stiffness. To further understand how the cells sense the substrate mechanics, we also investigated the F-actin cytoskeleton for the MDCK and NIH/3T3 cells seeded on the four different substrates.

3.3.3 Substrate mechanics affects cell biomechanical behavior by regulating the cell morphology

In this study, the effect of the substrate mechanics on F-actin distribution as a sensory mechanism of the cell was investigated Gupta et al. (2015). The differences of F-actin structure were clearly observed on the four substrates, as shown in Fig. 3.4. Comparing the F-actin alignment deviation for cells on each substrate, it is clear that stiffer substrate led to more uniform F-actin organization (i.e., more uniformly distributed F-actin alignment angles) of both MDCK and NIH/3T3 cells; however, F-actin was disoriented on soft PDMSs, and the softer the substrate was, the less uniform the F-actin alignment was. This observation is consistent with previous findings that stronger actin-myosin cross bridging on harder substrates can lead to more stabilized and enhanced F-actin cytoskeleton alignment Discher et al. (2005).

Combine with the significant biomechanical behavior differences of the cells on the four substrates, it is clear that the substrate mechanics affects the cellular biomechanical behavior through regulating the inner structure, such as F-actin cytoskeleton. Specifically, our previous work Mollaeian et al. (2018a) has shown that depolymerization of F-actin would cause significant reduction of the cell stiffness and increase of the cell diffusion coefficient, and the nonlinearities of cell stiffness and poroelasticity became more significant as well. Also, it has been reported that depolymerization of F-actin contributes to the reduction of cytoskeleton stiffness and the increase of the cytoplasmic pore size Mollaeian et al. (2018a); Moeendarbary et al. (2013); Schillers et al. (2010). Thus, the measured cell mechanical behavior on different substrates, which caused F-actin structure change, associated to depolymerized F-actin. Moreover, as previously reported, living cells respond to the substrate stiffness by reformation of the cytoskeleton components and adhesion molecules activities

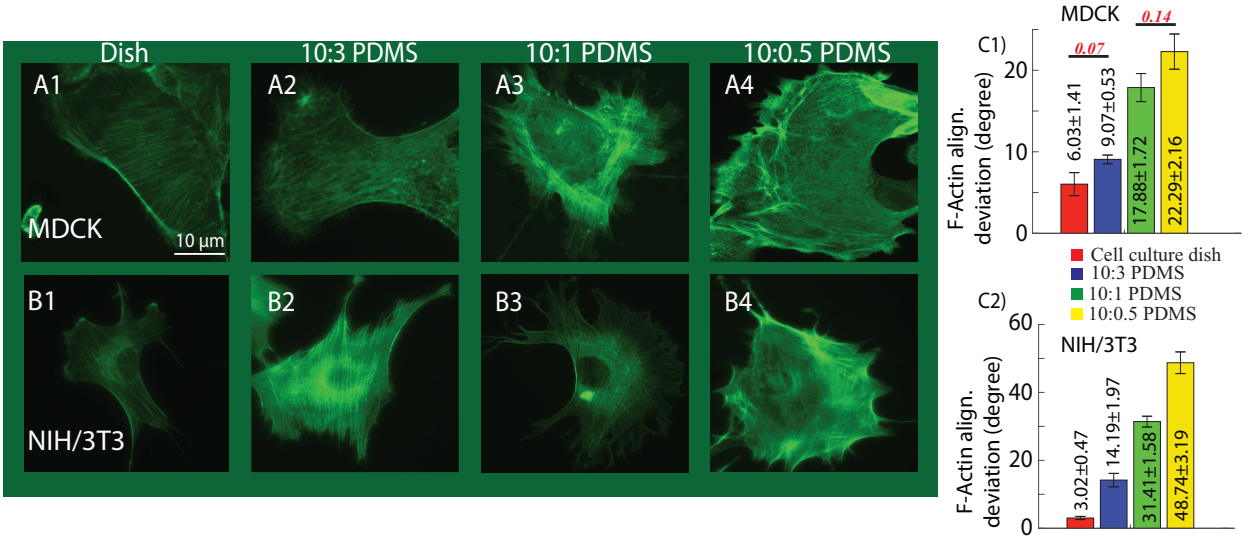

Figure 3.4 Examples of F-actin cytoskeleton images of (A1-A4) MDCK and (B1-B4) NIH/3T3 cells seeded on the four substrates, respectively. The cells were fixed and stained 24 hours after being seeded. Scale bar: 10 μm. The F-actin alignment deviations for (C1) MDCK and (C2) NIH/3T3 cells seeded on each substrate. n=6. Student's t-test was performed to analyze the statistical difference: data for all substrates were compared to each other for each cell type. A p <0.005 was yielded for each comparison unless otherwise denoted in the figure (with p values in red bold italic font).

Jin et al. (2004); Hinz et al. (2001). Particularly, the stimulation of cytoskeleton effectors including Ras superfamily proteins leads to enhanced stress fibers and increases cell growth on stiffer substrates Chrzanowska-Wodnicka and Burridge (1996); Beningo and Wang (2002). Tyrosine phosphorylation, calmodulin- and vinculin activated myosin, and enhanced Rho and Rac proteins activity along with stronger actin-myosin cross-bridging on the harder substrates lead to more stabilized local adhesion and enhanced F-actin cytoskeleton alignment Chrzanowska-Wodnicka and Burridge (1996); Beningo and Wang (2002); Pelham and Wang (1997); Doyle et al. (2004); Fillingham et al. (2005). Therefore, the cell-substrate bonding strength —a direct result of substrate stiffness— modifies the cytoskeleton integrity and thus regulates the cell mechanical behavior. Specifically, weaker cell-exerted forces to the softer substrate in response to mechanics of the substrate leads to

cytoskeleton and stress fibers deformation, lower tyrosine phosphorylation, calmodulin and vinculin activities, which further causes lower contractility of the cell and weaker cross-bridging of the actin-myosin Chrzanowska-Wodnicka and Burridge (1996); Beningo and Wang (2002); Pelham and Wang (1997); Doyle et al. (2004); Fillingham et al. (2005). Thus, lower Young's modulus was quantified. Also, the lower cell-substrate interaction and instability of the focal adhesion on the soft polymers causes weakened (less uniformly aligned) cell cytoskeleton, resulting in increased intracellular fluid flow and thus higher diffusion coefficient. This enhanced intracellular fluid flow also contributes to the reduction of apparent viscosity of the cells on the softer substrates.

Therefore, the results confirmed that substrate mechanics regulates cellular biomechanical behavior by modifying the cytoskeleton structure. These findings on the adaptation of the biomechanical behavior of the adherent cells to the substrate mechanics may be further used to control and regulate the cellular mechanical behavior to manipulate the mechanotransduction process. To fully understand and model the cell-substrate mechanical sensing, more in-depth investigations are needed to explain the physiological and biomechanical behavior of the cells caused by different extracellular environment. As for the future work, it is of importance to study the cell morphology variation (e.g., cell shape) caused by substrate mechanics. As the lower stiffness regime (i.e., <100kPa) of substrate stiffness is more relevant to cell differentiation and organization of the cytoskeleton, the proposed work will be extended to this regime as well. Furthermore, as 3D cell culture environment is more close to the actual cell existing condition in living bodies and the cell mechanical behavior is quite different from 2D culture cases Alapan et al. (2016); Marelli et al. (2014); Sniadecki et al. (2007), the study of cell mechanical behavior change due to culture environment change will be further extended to 3D cases in the future.

3.4 Conclusion

In this study, the effect of substrate mechanics on biomechanical behavior of the cells was investigated using AFM indentation approach. The elastic, viscoelastic, and poroelastic nonlinearity of MDCK and NIH/3T3 cells on substrates with different mechanics (i.e., 10:0.5, 10:1, 10:3 PDMSs,

and polystyrene cell culture dish) were quantified at different indentation depths. It was found that the cell elasticity, viscoelasticity, and their nonlinearities were synchronized with the substrate stiffness and its nonlinearity, respectively. The diffusion coefficient of the cells increased, monotonically, with the increase of the indentation depth on all substrates. Particularly, this poroelasticity nonlinearity was more pronounced for the cells cultured on the softer substrates due to larger lateral expansion of the cell and larger cytoskeletal pore size. Moreover, the cell F-actin cytoskeleton images suggested that the stiffer the substrate was, the more uniform the F-actin alignment was. Thus, combine the results together, it is clear that the substrate mechanics affects the cellular mechanics by regulating the inner structure of the cells.

3.5 Materials and methods

3.5.1 Chemicals

Sylgard 184 silicone elastomer and elastomer base were purchased from Ellsworth (Germantown, WI, USA). Dulbecco's Modified Eagles Medium (DMEM) was purchased from Sigma Aldrich (St. Louis, MO, USA). Minimum Essential Medium Eagle (MEM) and Phosphate-Buffered Saline (PBS) were purchased from Corning cellgro (Manassas, VA, USA). Fetal bovine Serum (FBS) and penicillin-streptomycin (pen-strep) were obtained from Gibco (Grand Island, New York, USA). Paraformaldehyde (PFA, 4 % in PBS) was purchased from Alfa Aesar (Ward Hill, MA, USA). Bovine Calf Serum (BCS) was purchased from VWR (Radnor, PA, USA). Triton X-100 was purchased from Fisher Scientific (Fair Lawn, NJ, USA). Acti-stain^{TM} 488 Phalloidin was purchased from Cytoskeleton, Inc. (Denver, CO, USA).

3.5.2 Polymer substrate preparation

To prepare PDMS substrates with different stiffness, Sylgard 184 silicone elastomer base and the curing agent with the base-to-curing agent ratios of 10:0.5, 10:1, and 10:3 were mixed for around 10 min. The mixtures were degassed under vacuum until air bubbles disappeared (around 30 min) and poured onto flat polystyrene Petri dishes. The thickness of the prepolymers was kept constant

as 2 mm. Then, the prepolymers were cured at 70 °C for 10 hours following cooling to the room temperature (25 °C).

3.5.3 Cell culture and treatment

NIH/3T3 cells were cultured in DMEM containing 10% BCS and 1% pen-strep. MDCK cells were cultured in MEM containing 10% FBS and 1% pen-strep. The cells were subcultured at a density of 1.0×10^4 cells/ml on the three PDMS substrates and polystyrene cell culture dishes (35 mm Falcon, Durham, NC, USA) and maintained at 37 °C in 5% CO_2 incubator for 24 hours prior to the AFM measurement. For the AFM nanomechanical measurements, the existing medium in the dishes was replaced by fresh growth medium to remove dead and loosely attached cells.

3.5.4 Immunofluorescence and F-actin quantification

To capture the F-actin cytoskeleton images, cell growth medium was removed from the dish following washing the cells with PBS at 37 °C to remove the dead and loosely attached cells. Then, the cells were fixed using 4% PFA/PBS and kept at room temperature for 10 min. The cells were then permeabilized for 5 min at room temperature using 0.5 % Triton X-100 in PBS. Finally, after rinsing the cells with PBS three times, the actin cytoskeleton was stained using Actin-stain^{TM} 488 Phalloidin at a final concentration of 100 nM in PBS, and the cells were kept in dark for 30 min at room temperature. Then the fluorescent F-actin cytoskeleton images were obtained using an inverted optical microscope (Olympus, IX73, Japan) and equipped with a sola light engine (Lumencor, Beaverton, OR, UAS) offering access to solid state illumination. At least eight images were taken per substrate for each cell type.

The F-actin alignment deviation was quantified using MATLAB image processing tool. F-actin fibers were detected using Canny edge detection in this program. Then the F-actin alignment deviation was then quantified by calculating the variance in the fiber orientation angles, as determined using Hough transform.

3.5.5 Atomic Force Microscopy (AFM) measurement

All AFM measurements were performed at room temperature in cell growth medium with a Bruker BioScope Resolve AFM system (Santa Barbara, CA, USA), which is integrated with an inverted optical microscope (Olympus, IX73, Japan). Colloidal AFM probe (Novascan, IA, USA) with sphere radius of 2.5 μm was used. The cantilever spring constant of 0.02 N/m was acquired using thermal tune approach Hutter and Bechhoefer (1993). Drive voltage and sensor data of the AFM system were acquired using an NI PCIe-6353 DAQ board (National instrument, Austin, TX, USA) with Matlab Simulink Desktop Real-time platform (Mathworks, MA, USA). Cells were measured at a location away from the top to minimize the nucleus effect (see Fig. 3.5 (A)). The height of the measured NIH/3T3 and MDCK cells are 7$\pm$1 μm and 8.5$\pm$1.5 μm, respectively (mean$\pm$stadard deviation). To minimize the effect of the finite cell thickness and substrate effect Dimitriadis et al. (2002); Charras et al. (2001); Chan et al. (2012), the target indentation depths were chosen as 650, 1000, and 1300 nm which were less than a quarter of the minimum cell height. To investigate the effect of substrate mechanics on the biomechanical behavior of the MDCK and NIH/3T3 cells, the AFM indenting speed was kept at 20 μm/s until desired indentations were reached (i.e., the indenting process), and then the probe was kept resting on the cell at that position for five seconds (i.e., force-relaxation process) (see Fig. 3.5 (B) and (C)). The indenting velocity and indentation depths were chosen based on previous studies Mollaeian et al. (2018a); Schillers et al. (2010); Mollaeian et al. (2017) to observe the cellular poroelastic force relaxation by triggering different layers of the cells. For the two types of cells seeded on each substrate (three PDMS ones and polystyrene cell culture dish), the AFM measurement was performed on at least six different cells at each indentation depth.

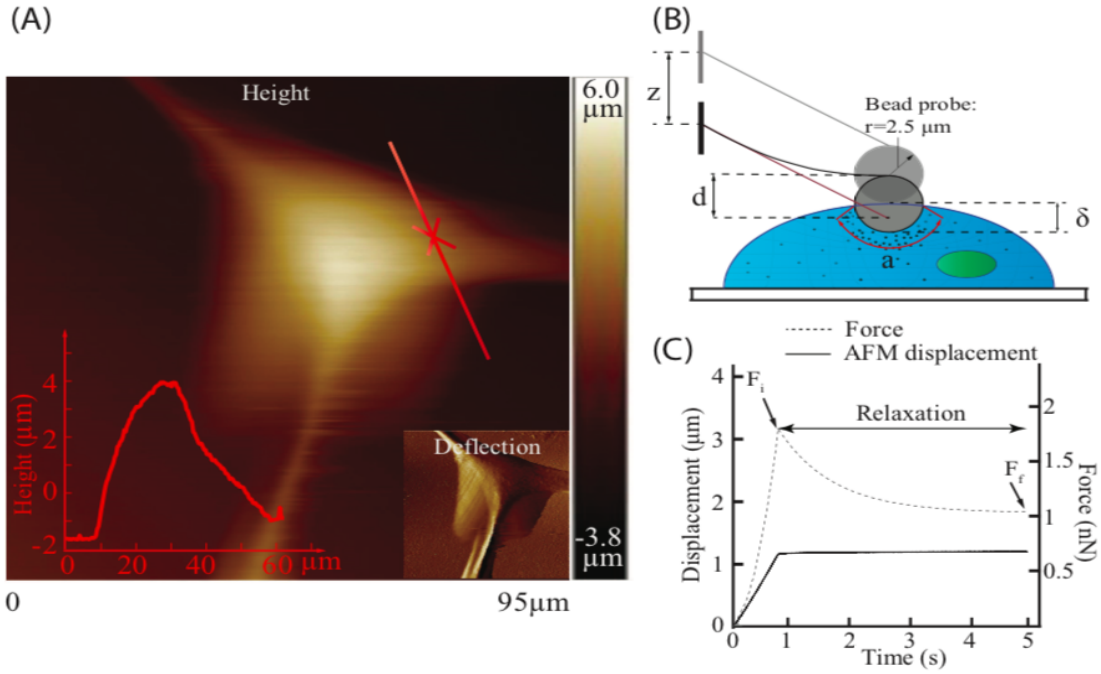

Figure 3.5 (A) AFM topography image of an MDCK cell, where the red cross represents the measurement site. (B) AFM measurement of the cells with a sphere probe (radius 2.5 μm). (C) The probe-cell interaction force and AFM displacement (z) profile during the force-relaxation process, where F_i is the probe-cell interaction force at the beginning of the relaxation process (i.e., the end of the indenting process), and F_f is the force at the end of the relaxation process.

3.5.6 Biomechanical quantification of the cells

3.5.6.1 Cell elasticity

Indentation depth, $\delta(t)$, was obtained using the cantilever deflection, $d(t)$, and the AFM displacement, $z(t)$, as Ren et al. (2015)

$$\delta(t) = z(t) - d(t). \tag{3.1}$$

Since the AFM probe used was spherical and the cells were indented at a speed (20 μm/s) that was faster than the intracellular fluid efflux rate (1.5-8.5μm/s) Mollaeian et al. (2018a); Moeendarbary et al. (2013), the cells could be treated as an incompressible material during the indenting process Kalcioglu et al. (2012); Moeendarbary et al. (2013) and the cell Young's Modulus was then

quantified using the Hertzian contact model Sneddon (1965); Ghaednia et al. (2016), i.e.,

$$F(t) = \frac{4}{3}\frac{E}{1-\bar{\nu}^2} r^{\frac{1}{2}} \delta^{\frac{3}{2}}(t), \tag{3.2}$$

where $F(t) = k \times d(t)$ is the probe-cell interaction force (k: spring constant of the cantilever), $r = 2.5$ μm is the sphere probe radius, and $\bar{\nu}$ =0.5 is the incompressible cell Poisson's ratio. The shear modulus of the undrained (i.e., incompressible during the fast indenting process) cell network, G, was then calculated through Sneddon (1965):

$$F_i = \frac{16}{3} G a \bar{\delta}, \tag{3.3}$$

where $\bar{\delta}$ and F_i are the indentation depth and probe-cell interaction force at the beginning of the force-relaxation process (i.e., the end of the fast indenting process), respectively. The probe-cell contact size, a, was quantified using the probe radius and the indentation depth as

$$a = \sqrt{r\bar{\delta}}. \tag{3.4}$$

During the force-relaxation process (i.e,. probe resting on the cells after fast indenting once the targeted indentation depth was reached), significant intracellular efflux occurs to equilibrate the unbalanced inner pressure of the cell (caused by fast indentation)—cell poroelasticity. As a result, the probe-cell interaction force decreases significantly even when the AFM displacement was kept unchanged. The fully relaxed force (i.e., the probe-cell interaction force at the end of the relaxation process (e.g., five seconds after fast indenting)), F_f, could be quantified as Moeendarbary et al. (2013):

$$F_f = \frac{8}{3(1-\nu)} G a \bar{\delta} \tag{3.5}$$

where ν denotes the cell Poisson's ratio during the force-relaxation process. Note that ν is different from $\bar{\nu}$ as the cells are compressible due to the intracellular fluid efflux during the relaxation process. Therefore, the Poisson's ratio of the solid cellular matrix during the relaxation process could then be quantified using Eqs. 3.3 and 3.5 as:

$$\nu = 1 - \frac{F_i}{2F_f} \tag{3.6}$$

3.5.6.2 Viscoelasticity

With the Poisson's ratio quantified using Eq. 3.6, the viscoelastic behavior of the cells was obtained following the method proposed by Dimitriadis et al. Ketene et al. (2012):

$$F(t) = \frac{4}{3}\frac{E_r}{1-\nu} r^{\frac{1}{2}} \bar{\delta}^{\frac{3}{2}} [\, 1 + (\, \frac{\tau_\sigma - \tau_\epsilon}{\tau_\epsilon}) \, e^{-\frac{t}{\tau_\epsilon}}]. \tag{3.7}$$

where τ_σ and τ_ϵ are the relaxation time constants for load and deformation, respectively. E_r is the relaxed modulus. The values of E_r, τ_σ, and τ_ϵ were obtained by fitting the force-time curve during the relaxation process using Eq. 3.7, and the apparent viscosity of the cell was then approximated as Ketene et al. (2012)

$$\eta = E_r (\, \tau_\sigma - \tau_\epsilon) \, . \tag{3.8}$$

3.5.6.3 Poroelasticity

Since the cell size (>30 μm) was more than ten times larger than the AFM tip radius (2.5 μm), the probe-cell interaction could be approximated as a poroelastic half-space indented by a spherical indenter, and the following empirical poroelastic model obtained by finite-element-analysis was used for analyzing the cell poroelasticity Hu et al. (2010):

$$\frac{F(t) - F_f}{F_i - F_f} = 0.491 e^{-0.908\sqrt{\frac{Dt}{a^2}}} + 0.509 e^{-1.679\frac{Dt}{a^2}} . \tag{3.9}$$

where D is the diffusion coefficient, and was obtained by fitting the force-time curve during the relaxation process using the above Eq. (3.9).

3.5.7 Stiffness quantification of the substrates

The Young's moduli of the cell culture dish and the PDMS substrates with different base to agent ratio (i.e., 10:0.5, 10:1, and 10:3) were measured in air using AFM. The AFM indenting speed was kept at 20 μm/s until the desired indentation depths (300, 400, and 500 nm) were reached and then the probe was returned to its original position. Since the substrates are much harder than living cells, a stiffer AFM cantilever—TAP150A (Santa Barbara, CA, USA) with the conical radius

and the spring constant of 8 nm and 5 N/m, respectively, was used for polymer characterization. The substrate stiffness was then quantified as following Sneddon (1965)

$$F_t = \frac{2}{\pi}\tan(\alpha)\frac{E_t}{1-\nu_t^2}\delta_t^2(t). \tag{3.10}$$

where α and ν_t are the tip opening angle and the Poisson ratio of the substrates, respectively. Additionally, the Poisson's ratio $\nu_t = 0.5$ Moeendarbary et al. (2013) was used for elasticity measurements. F_t is the tip-substrate interaction force, and E_t denotes the substrate stiffness.

3.5.8 Curve fitting and statistical analysis

Collected force-time relaxation curves from AFM were fitted by the poroelastic (Eq. (3.9)) and viscoelastic model (Eq. (3.7)) and the RMS fitting error was calculated to ensure the measurement consistency. Data in figures are presented as mean ± standard error. Student's t-test was performed to evaluate statistical significance, and the returned p values were reported in the figures.

3.6 References

Alapan, Y., Younesi, M., Akkus, O., and Gurkan, U. A. (2016). Anisotropically stiff 3d micropillar niche induces extraordinary cell alignment and elongation. *Advanced healthcare materials*, 5(15):1884–1892.

Alisafaei, F., Han, C.-S., and Sanei, S. H. R. (2013). On the time and indentation depth dependence of hardness, dissipation and stiffness in polydimethylsiloxane. *Polymer Testing*, 32(7):1220–1228.

Beningo, K. A. and Wang, Y.-l. (2002). Fc-receptor-mediated phagocytosis is regulated by mechanical properties of the target. *Journal of cell science*, 115(4):849–856.

Brandl, F., Sommer, F., and Goepferich, A. (2007). Rational design of hydrogels for tissue engineering: impact of physical factors on cell behavior. *Biomaterials*, 28(2):134–146.

Burridge, K., Fath, K., Kelly, T., Nuckolls, G., and Turner, C. (1988). Focal adhesions: transmembrane junctions between the extracellular matrix and the cytoskeleton. *Annual review of cell biology*, 4(1):487–525.

Carrillo, F., Gupta, S., Balooch, M., Marshall, S. J., Marshall, G. W., Pruitt, L., and Puttlitz, C. M. (2005). Nanoindentation of polydimethylsiloxane elastomers: Effect of crosslinking, work of adhesion, and fluid environment on elastic modulus. *Journal of materials research*, 20(10):2820–2830.

Chan, E. P., Hu, Y., Johnson, P. M., Suo, Z., and Stafford, C. M. (2012). Spherical indentation testing of poroelastic relaxations in thin hydrogel layers. *Soft Matter*, 8(5):1492–1498.

Charitidis, C. A. (2010). Nanoscale deformation and nanomechanical properties of polydimethylsiloxane (pdms). *Industrial & Engineering Chemistry Research*, 50(2):565–570.

Charras, G., Lehenkari, P. P., and Horton, M. (2001). Atomic force microscopy can be used to mechanically stimulate osteoblasts and evaluate cellular strain distributions. *Ultramicroscopy*, 86(1):85–95.

Charras, G. T., Coughlin, M., Mitchison, T. J., and Mahadevan, L. (2008). Life and times of a cellular bleb. *Biophysical journal*, 94(5):1836–1853.

Charras, G. T., Mitchison, T. J., and Mahadevan, L. (2009). Animal cell hydraulics. *Journal of Cell Science*, 122(18):3233–3241.

Charras, G. T., Yarrow, J. C., Horton, M. A., Mahadevan, L., and Mitchison, T. (2005). Non-equilibration of hydrostatic pressure in blebbing cells. *Nature*, 435(7040):365–369.

Chen, C. S., Tan, J., and Tien, J. (2004). Mechanotransduction at cell-matrix and cell-cell contacts. *Annu. Rev. Biomed. Eng.*, 6:275–302.

Chrzanowska-Wodnicka, M. and Burridge, K. (1996). Rho-stimulated contractility drives the formation of stress fibers and focal adhesions. *The Journal of cell biology*, 133(6):1403–1415.

Dembo, M. and Harlow, F. (1986). Cell motion, contractile networks, and the physics of interpenetrating reactive flow. *Biophysical journal*, 50(1):109–121.

Deuschle, J. K., de Souza, E. J., Arzt, E., and Enders, S. (2010). Nanoindentation studies on crosslinking and curing effects of pdms. *International Journal of Materials Research*, 101(8):1014–1023.

Dimitriadis, E. K., Horkay, F., Maresca, J., Kachar, B., and Chadwick, R. S. (2002). Determination of elastic moduli of thin layers of soft material using the atomic force microscope. *Biophysical journal*, 82(5):2798–2810.

Discher, D. E., Janmey, P., and Wang, Y.-l. (2005). Tissue cells feel and respond to the stiffness of their substrate. *Science*, 310(5751):1139–1143.

Doyle, A., Marganski, W., and Lee, J. (2004). Calcium transients induce spatially coordinated increases in traction force during the movement of fish keratocytes. *Journal of Cell Science*, 117(11):2203–2214.

Efremov, Y. M., Wang, W.-H., Hardy, S. D., Geahlen, R. L., and Raman, A. (2017). Measuring nanoscale viscoelastic parameters of cells directly from afm force-displacement curves. *Scientific Reports*, 7(1):1541.

Engler, A. J., Griffin, M. A., Sen, S., Bönnemann, C. G., Sweeney, H. L., and Discher, D. E. (2004). Myotubes differentiate optimally on substrates with tissue-like stiffness: pathological implications for soft or stiff microenvironments. *J Cell Biol*, 166(6):877–887.

Fillingham, I., Gingras, A. R., Papagrigoriou, E., Patel, B., Emsley, J., Critchley, D. R., Roberts, G. C., and Barsukov, I. L. (2005). A vinculin binding domain from the talin rod unfolds to form a complex with the vinculin head. *Structure*, 13(1):65–74.

Geiger, B., Spatz, J. P., and Bershadsky, A. D. (2009). Environmental sensing through focal adhesions. *Nature reviews Molecular cell biology*, 10(1):21.

Ghaednia, H., Pope, S. A., Jackson, R. L., and Marghitu, D. B. (2016). A comprehensive study of the elasto-plastic contact of a sphere and a flat. *Tribology International*, 93:78–90.

Ghaednia, H., Wang, X., Saha, S., Xu, Y., Sharma, A., and Jackson, R. L. (2017). A review of elastic–plastic contact mechanics. *Applied Mechanics Reviews*, 69(6):060804.

Ghibaudo, M., Saez, A., Trichet, L., Xayaphoummine, A., Browaeys, J., Silberzan, P., Buguin, A., and Ladoux, B. (2008). Traction forces and rigidity sensing regulate cell functions. *Soft Matter*, 4(9):1836–1843.

Giannone, G. and Sheetz, M. P. (2006). Substrate rigidity and force define form through tyrosine phosphatase and kinase pathways. *Trends in cell biology*, 16(4):213–223.

Guilak, F., Cohen, D. M., Estes, B. T., Gimble, J. M., Liedtke, W., and Chen, C. S. (2009). Control of stem cell fate by physical interactions with the extracellular matrix. *Cell stem cell*, 5(1):17–26.

Guo, W.-h., Frey, M. T., Burnham, N. A., and Wang, Y.-l. (2006). Substrate rigidity regulates the formation and maintenance of tissues. *Biophysical journal*, 90(6):2213–2220.

Gupta, M., Sarangi, B. R., Deschamps, J., Nematbakhsh, Y., Callan-Jones, A., Margadant, F., Mège, R.-M., Lim, C. T., Voituriez, R., and Ladoux, B. (2015). Adaptive rheology and ordering of cell cytoskeleton govern matrix rigidity sensing. *Nature communications*, 6:7525.

Hinz, B., Celetta, G., Tomasek, J. J., Gabbiani, G., and Chaponnier, C. (2001). Alpha-smooth muscle actin expression upregulates fibroblast contractile activity. *Molecular biology of the cell*, 12(9):2730–2741.

Hu, Y., Zhao, X., Vlassak, J. J., and Suo, Z. (2010). Using indentation to characterize the poroelasticity of gels. *Applied Physics Letters*, 96(12):121904.

Hutter, J. L. and Bechhoefer, J. (1993). Calibration of atomic-force microscope tips. *Review of Scientific Instruments*, 64(7):1868–1873.

Jiang, G., Huang, A. H., Cai, Y., Tanase, M., and Sheetz, M. P. (2006). Rigidity sensing at the leading edge through $\alpha v\beta 3$ integrins and rptpα. *Biophysical journal*, 90(5):1804–1809.

Jin, M., Andricioaei, I., and Springer, T. A. (2004). Conversion between three conformational states of integrin i domains with a c-terminal pull spring studied with molecular dynamics. *Structure*, 12(12):2137–2147.

Kalcioglu, Z. I., Mahmoodian, R., Hu, Y., Suo, Z., and Van Vliet, K. J. (2012). From macro- to microscale poroelastic characterization of polymeric hydrogels via indentation. *Soft Matter*, 8(12):3393–3398.

Ketene, A. N., Schmelz, E. M., Roberts, P. C., and Agah, M. (2012). The effects of cancer progression on the viscoelasticity of ovarian cell cytoskeleton structures. *Nanomedicine: Nanotechnology, Biology and Medicine*, 8(1):93–102.

Kilian, K. A., Bugarija, B., Lahn, B. T., and Mrksich, M. (2010). Geometric cues for directing the differentiation of mesenchymal stem cells. *Proceedings of the National Academy of Sciences*, 107(11):4872–4877.

Leipzig, N. D. and Shoichet, M. S. (2009). The effect of substrate stiffness on adult neural stem cell behavior. *Biomaterials*, 30(36):6867–6878.

Marelli, M., Gadhari, N., Boero, G., Chiquet, M., and Brugger, J. (2014). Cell force measurements in 3d microfabricated environments based on compliant cantilevers. *Lab on a Chip*, 14(2):286–293.

McNaught, A. D. and McNaught, A. D. (1997). *Compendium of chemical terminology*, volume 1669. Blackwell Science Oxford.

Moeendarbary, E., Valon, L., Fritzsche, M., Harris, A. R., Moulding, D. A., Thrasher, A. J., Stride, E., Mahadevan, L., and Charras, G. T. (2013). The cytoplasm of living cells behaves as a poroelastic material. *Nature materials*, 12(3):253–261.

Mollaeian, K., Liu, Y., Bi, S., and Ren, J. (2018). Atomic force microscopy study revealed velocity-dependence and nonlinearity of nanoscale poroelasticity of eukaryotic cells. *Journal of the mechanical behavior of biomedical materials*, 78:65–73.

Mollaeian, K., Liu, Y., and Ren, J. (2017). Investigation of nanoscale poroelasticity of eukaryotic cells using atomic force microscopy. In *ASME 2017 Dynamic Systems and Control Conference*, pages V001T08A005–V001T08A005. American Society of Mechanical Engineers.

Munson, B. R., Okiishi, T. H., Rothmayer, A. P., and Huebsch, W. W. (2014). *Fundamentals of fluid mechanics*. John Wiley & Sons.

Nia, H. T., Han, L., Li, Y., Ortiz, C., and Grodzinsky, A. (2011). Poroelasticity of cartilage at the nanoscale. *Biophysical journal*, 101(9):2304–2313.

Park, J. S., Chu, J. S., Tsou, A. D., Diop, R., Tang, Z., Wang, A., and Li, S. (2011). The effect of matrix stiffness on the differentiation of mesenchymal stem cells in response to tgf-β. *Biomaterials*, 32(16):3921–3930.

Pelham, R. J. and Wang, Y.-l. (1997). Cell locomotion and focal adhesions are regulated by substrate flexibility. *Proceedings of the National Academy of Sciences*, 94(25):13661–13665.

Pogoda, K., Jaczewska, J., Wiltowska-Zuber, J., Klymenko, O., Zuber, K., Fornal, M., and Lekka, M. (2012). Depth-sensing analysis of cytoskeleton organization based on afm data. *European Biophysics Journal*, 41(1):79–87.

Ren, J., Huang, H., Liu, Y., Zheng, X., and Zou, Q. (2015). An atomic force microscope study revealed two mechanisms in the effect of anticancer drugs on rate-dependent young's modulus of human prostate cancer cells. *PloS one*, 10(5):e0126107.

Rianna, C. and Radmacher, M. (2017). Influence of microenvironment topography and stiffness on the mechanics and motility of normal and cancer renal cells. *Nanoscale*, 9(31):11222–11230.

Saez, A., Buguin, A., Silberzan, P., and Ladoux, B. (2005). Is the mechanical activity of epithelial cells controlled by deformations or forces? *Biophysical journal*, 89(6):L52–L54.

Schillers, H., Wälte, M., Urbanova, K., and Oberleithner, H. (2010). Real-time monitoring of cell elasticity reveals oscillating myosin activity. *Biophysical journal*, 99(11):3639–3646.

Sirghi, L., Ponti, J., Broggi, F., and Rossi, F. (2008). Probing elasticity and adhesion of live cells by atomic force microscopy indentation. *European Biophysics Journal*, 37(6):935–945.

Sneddon, I. N. (1965). The relation between load and penetration in the axisymmetric boussinesq problem for a punch of arbitrary profile. *International journal of engineering science*, 3(1):47–57.

Sniadecki, N. J., Anguelouch, A., Yang, M. T., Lamb, C. M., Liu, Z., Kirschner, S. B., Liu, Y., Reich, D. H., and Chen, C. S. (2007). Magnetic microposts as an approach to apply forces to living cells. *Proceedings of the National Academy of Sciences*, 104(37):14553–14558.

Solon, J., Levental, I., Sengupta, K., Georges, P. C., and Janmey, P. A. (2007). Fibroblast adaptation and stiffness matching to soft elastic substrates. *Biophysical journal*, 93(12):4453–4461.

Sorce, B., Escobedo, C., Toyoda, Y., Stewart, M. P., Cattin, C. J., Newton, R., Banerjee, I., Stettler, A., Roska, B., Eaton, S., et al. (2015). Mitotic cells contract actomyosin cortex and

generate pressure to round against or escape epithelial confinement. *Nature communications*, 6:8872.

Takai, E., Costa, K. D., Shaheen, A., Hung, C. T., and Guo, X. E. (2005). Osteoblast elastic modulus measured by atomic force microscopy is substrate dependent. *Annals of biomedical engineering*, 33(7):963–971.

Tee, S.-Y., Fu, J., Chen, C. S., and Janmey, P. A. (2011). Cell shape and substrate rigidity both regulate cell stiffness. *Biophysical journal*, 100(5):L25–L27.

Ulrich, T. A., de Juan Pardo, E. M., and Kumar, S. (2009). The mechanical rigidity of the extracellular matrix regulates the structure, motility, and proliferation of glioma cells. *Cancer research*, 69(10):4167–4174.

Wang, H.-B., Dembo, M., Hanks, S. K., and Wang, Y.-l. (2001). Focal adhesion kinase is involved in mechanosensing during fibroblast migration. *Proceedings of the National Academy of Sciences*, 98(20):11295–11300.

Wang, H.-B., Dembo, M., and Wang, Y.-L. (2000). Substrate flexibility regulates growth and apoptosis of normal but not transformed cells. *American Journal of Physiology-Cell Physiology*, 279(5):C1345–C1350.

Wang, Z., Volinsky, A. A., and Gallant, N. D. (2014). Crosslinking effect on polydimethylsiloxane elastic modulus measured by custom-built compression instrument. *Journal of Applied Polymer Science*, 131(22).

Wells, R. E. and Merrill, E. W. (1961). Shear rate dependence of the viscosity of whole blood and plasma. *Science*, 133(3455):763–764.

Xie, S. and Ren, J. (2018). Note: Precision control of nano-positioning stage: An iterative learning-based model predictive control approach. *Review of Scientific Instruments*, 89(7):076103.

Yeung, T., Georges, P. C., Flanagan, L. A., Marg, B., Ortiz, M., Funaki, M., Zahir, N., Ming, W., Weaver, V., and Janmey, P. A. (2005). Effects of substrate stiffness on cell morphology, cytoskeletal structure, and adhesion. *Cell motility and the cytoskeleton*, 60(1):24–34.

Yim, E. K., Darling, E. M., Kulangara, K., Guilak, F., and Leong, K. W. (2010). Nanotopography-induced changes in focal adhesions, cytoskeletal organization, and mechanical properties of human mesenchymal stem cells. *Biomaterials*, 31(6):1299–1306.

CHAPTER 4. INVESTIGATION OF THE EFFECT OF SUBSTRATE MORPHOLOGY ON MDCK CELL MECHANICAL BEHAVIOR USING ATOMIC FORCE MICROSCOPY

This manuscript has been published by *Applied Physics Letters*

Keyvan Mollaeian [1], Yi Liu[1], Siyu Bi[1], and Juan Ren[1]*

[1] Department of Mechanical Engineering, Iowa State University, Ames, Iowa, 50011, USA

Correspondence: juanren@iastate.edu; Tel.: +1-515-294-1805

4.1 Abstract

Living cells sense and respond to their extracellular environment. Their contact guidance is affected by the underlying substrate morphology. Previous studies of the effect of substrate pattern on the mechanical behavior of living cells were only limited to the quantification of the cellular elasticity. However, how the length and time scales of the cellular mechanical properties are affected by the patterned substrates have yet to be studied. In this study, the effect of the substrate morphology on the biomechanical behavior of living cells was thoroughly investigated using indentation-based atomic force microscopy. The results showed that the cellular biomechanical behavior was affected by the substrate morphology significantly. The elasticity and viscosity of the cells on the patterned PDMS substrates were much lower compared to those cultured on flat PDMS. The poroelastic diffusion coefficient of the cells was higher on the patterned PDMS substrates, specifically on the substrate with 2D pitches. In addition, fluorescence images showed that the substrate topography directly affects the cell cytoskeleton morphology. Together, the results suggested that cell mechanical behavior and morphology can be controlled using substrates with properly designed topography.

4.2 Introduction

Anchorage-dependent cells sense and respond to the underlying substrate Discher et al. (2005). The cells tune their focal adhesions to adapt to their extracellular environment Abidine et al. (2018). Recent developments in micro- and nano-scale fabricated materials provide new prospects for the investigation of cell mechanics change affected by substrate topography Liu et al. (2018a); Shabaniverki et al. (2018a,b); Yadav et al. (2018). For instance, it has been reported that patterned substrate affects cell regulation such as migration Jiang et al. (2005), gene expression Park et al. (2006), cell signaling Giannone and Sheetz (2006), and cell polarization Chan and Yousaf (2008). However, the effect of the substrate's pattern on cellular mechanical properties at different time and length scales is poorly understood. Thus, to have an in-depth understanding of the substrate effect on cell mechanics, study of the length- and time-dependence of the cell mechanical behavior subject to different substrate patterns is necessary.

Currently, the effect of substrate texture on the cellular behavior has been mostly studied by quantification of the cell Young's modulus at a single measurement depth using atomic force microscopy (AFM) due to its high spatial and nanoscale resolution Xie and Ren (2019); McKee et al. (2011). For instance, McKee et al. (2011) investigated the biomechanical behavior of the HTCEpi cells on patterned substrates using AFM and found that increasing the pitch size of the substrate led to the Young's modulus increase of the cells in the area where the nucleus was present McKee et al. (2011). Rianna et al. (2017) investigated the Hertzian elastic modulus of the cancer cells on PDMSs with nanogroove patterns using AFM and reported that the textures led to a decrease in Young's modulus of the cancer cells compared to the control Rianna et al. (2018). However, these methodologies do not account for the biphasic nature of living cells, in which the porous solid cytoskeletal network is bathed in liquid cytosol Moeendarbary et al. (2013). Therefore, poroelastic behavior should be quantified as well to investigate living cell mechanical behavior Mollaeian et al. (2018a). Poroelasticity of living cells describes the cells' ability to equilibrate the intracellular pressure when external force stimuli exist, and is represented by the diffusion coefficient, D, which is related to the pore size of the cytoskeleton, ξ, the elastic modulus, E, and the viscosity of

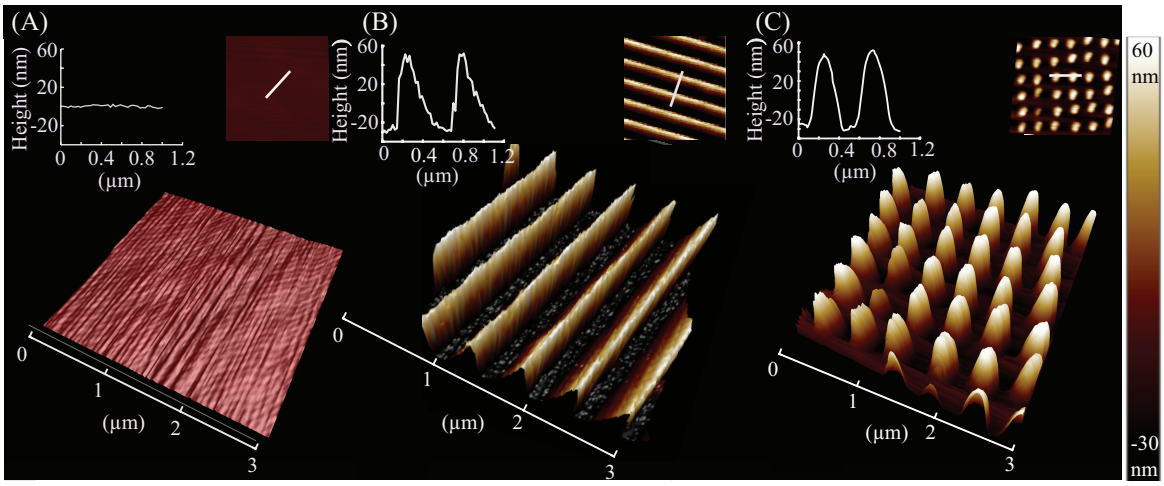

Figure 4.1 AFM topography images of (A) flat PDMS, (B) 1D PDMS, and (C) 2D PDMS substrates.

the cytosol, μ Charras et al. (2009). Thus, the quantification of the poroelasticity along with viscoelasticity (i.e., apparent viscosity) and elasticity can provide a complete picture of the cell biomechanics' variation caused by substrate texture. Moreover, since it is well known that the cell mechanical response is length (i.e., indentation depth) dependent Mollaeian et al. (2018a); Liu et al. (2019); Mollaeian et al. (2018b) due to heterogeneity of cell structure, it is also necessary to study the cell mechanical behavior under various stimulation depths to understand the effect of substrate's pattern on the length-dependence of cell mechanics.

Polydimethylsiloxane (PDMS) materials have been widely used as common cell culture substrate. Despite the drawbacks of the PDMS such as hydrophobicity, its flexibility, optical tranparency, gas permeability, and non-toxicity make it as an appealing substrate for cell studies Halldorsson et al. (2015); Lee et al. (2004). For instance, PDMS substrates with different rigidities have been used to manipulate the signaling pathway of the neuronal differentiation of the human embryonic stem cells Willerth (2017), and it was reported that the primary mouse cortical neurons co-cultured with neurons derived from mouse neural stem cells inside PDMS microconduits generate electrical signal interactions Takayama et al. (2012). Therefore, the effect of PDMS substrate topography on mechanical behavior of MDCK cells using AFM force-indentation mea-

surement technique has been investigated in this study. Specifically, mechanical characterization is performed on Madin-Darby canine kidney (MDCK) cells cultured on PDMS substrates of the same base/curing agent ratio with different patterns (flat, ridges (1D) and elevated disks (2D) with 80 nm height and 0.5 μm pitch size, see Fig. 4.1), and the relation between the substrate's texture and cell mechanical behavior (elasticity E, shear modulus G, viscoelasticity η, and poroelasticity D) at different indentation depths is presented. To investigate the effect of substrates' pattern on the biomechanical behavior of the cells, the cells were indented with the indenting velocity of 20 μm/s until the desired indentation depths were reached (i.e., the indenting process) and the probe was then rested on the cells for one second (the force-relaxation process). The cell poroelasticity (i.e., D) was quantified through fitting the force-time relaxation curve (i.e., force vs. time response during the force-relaxation process) using the following empirical poroelastic model Moeendarbary et al. (2013):

$$\frac{F(t)-F_f}{F_i-F_f} = 0.493e^{-0.822\sqrt{\frac{Dt}{a^2}}} + 0.507e^{-1.348\frac{Dt}{a^2}}. \tag{4.1}$$

where a is the probe-cell contact size during the time force relaxes from F_i to F_f. Complete details of AFM mechanical characterization procedure are given in Supplementary Information. Furthermore, the actin filament (F-actin) morphology change caused by different substrate patterns is also investigated. Details on the cell preparation and AFM measurement procedure are presented in the supplementary material.

4.3 Results and discussion

As shown in Fig. 4.2, the synthetic structured substrates affect the cellular mechanical behavior significantly. Agreeing with previous studies, the nonlinearity (mechanical property vs. indentation relation) of E, G, and η of the cells seeded on the all PDMS substrates are synchronized with the substrates': all decreased monotonically with the increase of the indentation depth Mollaeian et al. (2018b); Gupta et al. (2015). Specifically, the stiffness of the PDMS substrates is decreased by almost 45% when the indentation depth is increased from 300 nm to 500 nm. As a result, E of the cells cultured on the flat, 1D, and 2D PDMS substrates decreased by 69%, 54%, and

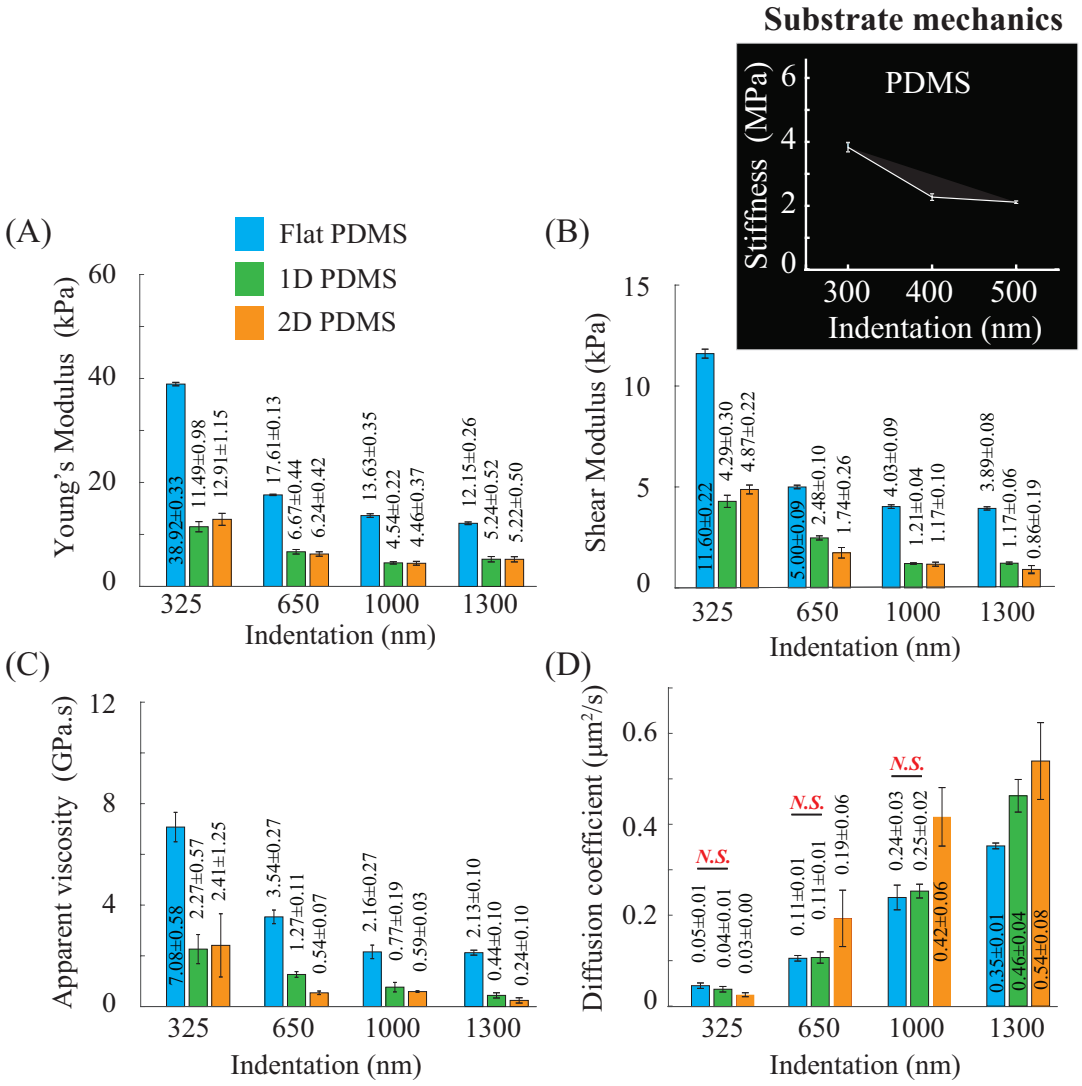

Figure 4.2 (A) Young's modulus, (B) shear modulus, (C) apparent viscosity, and (D) diffusion coefficient of MDCK cells seeded on different substrates, respectively, measured at four indentation depths (325, 650, 1000, and 1300 nm) and the indenting velocity of 20μm/s. n=6. Student's t-test was performed to analyze the statistical difference: for each indentation, data were compared with respect to the ones measured on the flat PDMS at the same indentation; and for each substrate, the data measured at the minimum indentation (325 nm) for that substrate were chosen as control. A p <0.05 was yielded for each comparison unless otherwise denoted in the figure (N.S.: not significant.).

60% when the indentation depth was increased from 325 to 1300 nm, respectively, and similar trend of nonlinearity of G and η were observed for all measured cells on the three substrates as well. This observed similarity in mechanical nonlinearity between cells and substrates is caused by mechanical adaptation of the living cells to the substrate's nonlinear mechanics Mollaeian et al. (2018b). However, the diffusion coefficient, D, was monotonically increasing: D increased by 600%, 1050%, and 1700% for the cells seeded on the flat, 1D and 2D PDMS substrates, respectively, when the indentation was quadrupled from 325 nm. This result is consistent with the poroelastic scale law, $D \sim E\xi^2/\mu$ (where μ is the viscosity of the cytosol), that the pore size is more dominant than E in affecting the poroelastic behavior of the cells Moeendarbary et al. (2013); Mollaeian et al. (2018a). As the cells are subject to local cytoskeleton stretching at bigger indentations, larger lateral expansion is resulted, which directly leads to larger pore size, ξ, of the cytoskeleton meshwork. Therefore, the diffusion coefficient increases at higher indentation depth, regardless of the substrate mechanical nonlinearity.

Besides the cell adaptation to substrate mechanical property, the experiment results show that the cell mechanical behavior can be directly altered by the substrate topography. Compared to the values measured from the the control (i.e., cells on the flat PDMS), the Young's modulus of the cells on the 1D PDMS at the indentation depths of 325, 650, 1000, and 1300 nm decreased by 71%, 62%, 67%, and 57% , and the decrease was 67%, 65%, 67%, and 57%, respectively, for the cells cultured on the 2D PDMS. In addition, G and η of the cells on the 1D and 2D PDMSs at each indentation depth reduced by at least 50% and 64%, respectively, with respect to the ones of the control. These reductions are caused by the reduced cell-substrate contact area on the patterned substrates. Previous studies have shown that the smaller contact area on the structured substrates (e.g., 1D and 2D PDMS substrates) results in lower focal adhesion and contractility compared to the flat PDMS substrate Teixeira et al. (2003). Then as a result, lower cellular Young's modulus were observed Teixeira et al. (2003). Note that the Young's modulus of MDCK cells measured in this study 4-40 kPa is in agreement with previously reported values Sorba et al. (2019). Furthermore, the lower contractility of the cells on the structured substrates leads to lower shear stress of the

cells Mollaeian et al. (2018b); Engler et al. (2004). Thus, the shear modulus (G=shear stress/shear strain) of the cells seeded on the 1D and 2D PDMSs is lower than that of the control at each indentation depth. Note that E and G values measured for the cells on the 1D and 2D PDMSs are similar indicating that the pattern shape (with the same height and pitch size) does not affect the stiffness of the cells much. Meanwhile, the high degree lateral expansion of the cells seeded on the patterned PDMSs leads to higher intracellular fluid flow rate (i.e., shear rate). Therefore, the cell apparent viscosity (η = shear stress/shear rate Wells and Merrill (1961)) measured for the cells on the 1D and 2D PDMSs decreases at each indentation depth compared to that of the cells on the flat PDMS (i.e., control).

However, the diffusion coefficient was higher for the cells on the patterned PDMSs at each indentation depth compared to the values measured on the flat PDMS. Specifically, at the higher indentation depths: with respect to the values measured from the control, D of the cells on the 1D PDMS at the indentation depths of 1000 and 1300 nm increased by 4% and 31%, respectively, and the increase was 75% and 54%, respectively, for the cells seeded on the 2D PDMS. The MDCK cells seeded on the 2D PDMS behave more poroelastic at the measured indentation depths due to the lower contractility and larger expansion of the cells which further result in larger pore size, and thus, bigger diffusion coefficient. It is noticed that the difference of D is not significant at the indentation of 325 nm as the substrate morphology effect is not significant at low measurement depth due to the thick plasma membrane of MDCK cells Sorce et al. (2015). Moreover, for the cells seeded on the 1D PDMS, D was not much different compared to that measured on the flat PDMS. We suspect this might be due to the constrained cell morphology on the 1D PDMS. Therefore, we investigated the F-actin cytoskeleton morphology for an in-depth understanding of the biomechanical behavior of the cells.

As can be seen in Fig. 4.3, the F-actin alignment and the cell shape were guided by the substrate patterns. The alignment angles of F-actin of the cells seeded on the 1D PDMS substrate is more uniform than the other two cases. This is because the F-actin alignment follows the substrate topography patterns Rianna et al. (2018); Teixeira et al. (2003); Flemming et al. (1999). Specifically,

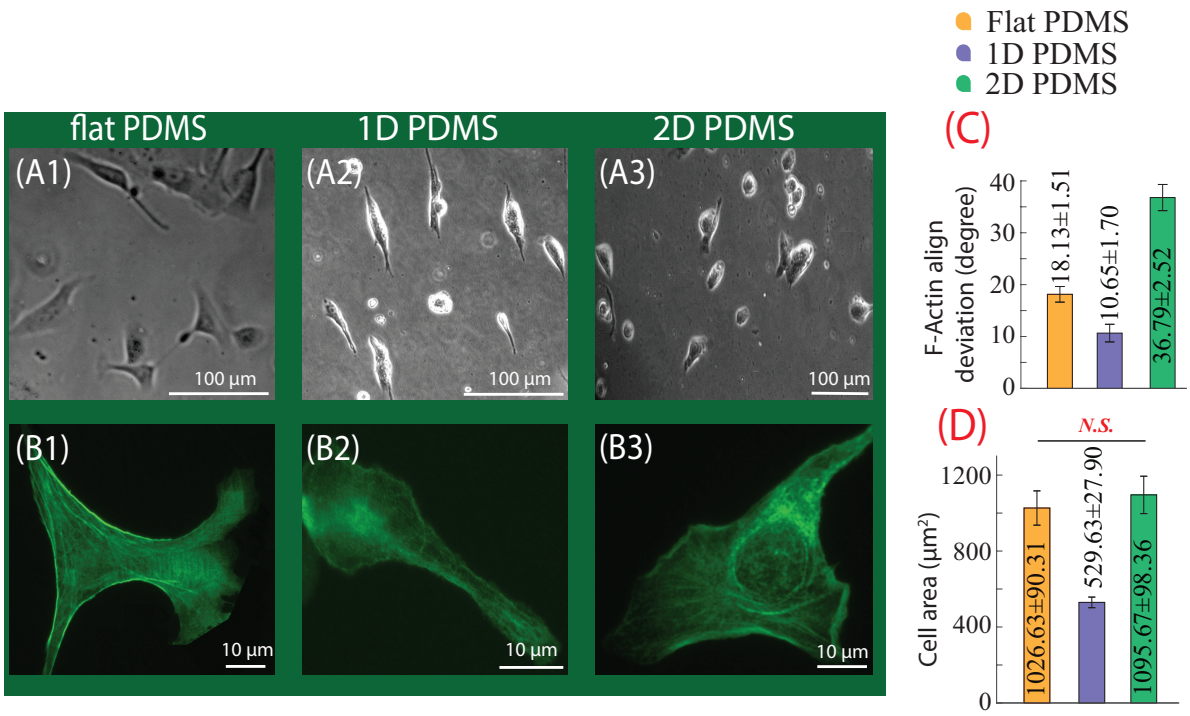

Figure 4.3 Example of optical images ((A1)-(A3)) and F-actin cytoskeleton images ((B1)-(B3)) of MDCK cells seeded on the three substrates, respectively. (C) and (D) show the comparison of the F-actin alignment angle deviations and the cell area quantified from the F-actin cytoskeleton on each substrate, respectively. n=10. Student's t-test was performed to analyze the statistical difference: data were compared with respect to the ones measured on the flat PDMS. A p <0.05 was yielded for each comparison unless otherwise denoted in the figure (N.S.: not significant.).

on the 1D substrate, focal adhesions are mostly located on the top surface of the ridges Teixeira et al. (2003); Matsuzaka et al. (2000), therefore, the cell shape and the F-actin alignment directly follow the direction of the 1D ridges Flemming et al. (1999); Ohara and Buck (1979). Thus, the cells are stretched along one direction, i.e., the cells are thin and long, and the cell area is smaller compared to the other two cases. Similarly, the cells on the 2D PDMS are stretched along multiple directions (i.e., with square or round shapes) due to the pitches on the substrate. As a result, the larger F-actin alignment deviation and cell area are yielded Teixeira et al. (2003); Sunami et al. (2014); Yeung et al. (2005). Different from the patterned substrates, the flat PDMS allows the cell

membrane and cytoskeleton to expand freely, i.e., the cell shape is more random. Thus, the F-actin alignment deviation is between the values for the other two cases, and the cell area is relatively large. As a result, the difference in F-actin cytoskeleton morphology directly reflected the cell mechanical behavior difference during the biomechanical measurement since the cytoskeleton morphology has been shown to play a fundamental role in cellular mechanics Mollaeian et al. (2018b).

The cell morphology images and the quantified F-actin cytoskeleton data together with the cell biomechanical characterization results indicate that the substrate topography affects the cell biomechanical behavior and the cell morphology, simultaneously. Therefore, the results of this study suggest that it is possible to achieve cell mechanical behavior and morphology control using substrates with properly designed topography patterns. For further studies, It would be interesting to investigate the effect of substrate topography on cytoskeleton morphology in details, and quantify the relation between the cytoskeleton morphology and cell mechanical properties to provide more information on cell mechanical behavior control through extracellular environment.

See supplementary material for the details of materials, PDMS and cell preparation, and AFM mechanical characterization procedure.

This work was supported by the National Science Foundation (NSF) [CMMI-1634592], [CMMI-1751503], and Iowa State University. We also thank Dr. Meng Lu from Iowa State University for generously providing the PDMS substrates.

4.4 Supplementary material

4.4.1 Chemicals

Sylgard 184 silicone elastomer and elastomer base were purchased from Ellsworth (Germantown, WI, USA). Dulbecco's Modified Eagles Medium (DMEM) was purchased from Sigma Aldrich (St. Louis, MO, USA). Minimum Essential Medium Eagle (MEM) and Phosphate-Buffered Saline (PBS) were purchased from Corning cellgro (Manassas, VA, USA). Fetal Bovine Serum (FBS) and penicillin-streptomycin (pen-strep) were obtained from Gibco (Grand Island, New York, USA). Paraformaldehyde (PFA, 4% in PBS) was purchased from Alfa Aesar (Ward Hill, MA, USA).

Bovine Calf Serum (BCS) was purchased from VWR (Radnor, PA, USA). Triton X-100 was purchased from Fisher Scientific (Fair Lawn, NJ, USA). Acti-stain^{TM} 488 Phalloidin was purchased from Cytoskeleton, Inc. (Denver, CO, USA).

4.4.2 Polymer substrate preparation

PDMS substrates were prepared by mixing the Sylgard 184 silicone elastomer base and the curing agent with the base to curing agent ratio of 10:1 for 10 min followed by the vacuum degasification process for 30 min to remove air bubbles. The PDMS with no pattern (i.e., flat PDMS) was then made by pouring the slurry material into a polystyrene Petri dish and curing at 70 °C for 10 h followed by cooling to the room temperature. The 1D and 2D PDMS substrates were prepared in two steps (Wang et al. (2016); Monshat et al. (2019)): first, a silicone master mold with nanopost patterns was used for creating a PDMS mold with opposite surface profile. Then, the PDMS mold was used to create the PDMS nanopost with the desired features as the silicone stamp one. The PDMS substrates were then directly used for cell culturing without additional coating with any adhesion protein. The PDMSs with nano ridges and elevated disks are called 1D and 2D, respectively (see Fig. 4.4).

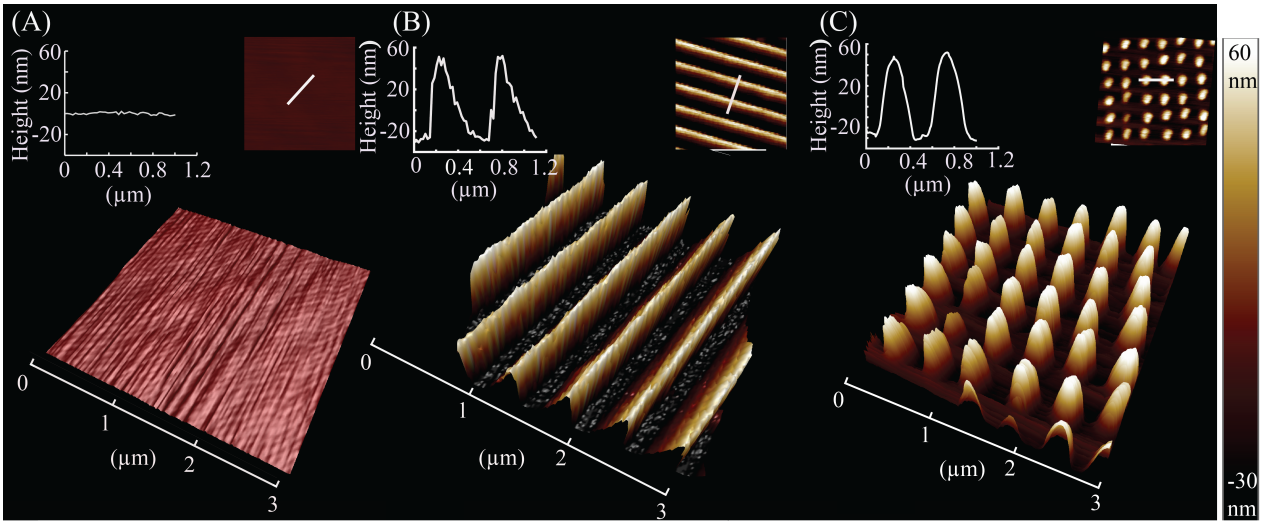

Figure 4.4 AFM topography images of (A) flat PDMS, (B) 1D PDMS, and (C) 2D PDMS substrates.

4.4.3 Cell culture and treatment

The MDCK cells were cultured in MEM containing 10% FBS and 1% pen-strep at a density of 1.0×10^4 cells/ml on the three PDMS substrates and maintained at 37 °C in 5% CO_2 incubator for 24 h prior to the AFM measurement. The existing medium was replaced with the fresh medium to remove dead and loosely attached cells prior to AFM measurement.

4.4.4 Immunofluorescence

The actin filaments (F-actin) cytoskeleton of the cells on each substrate was fluorescently stained to capture the cell morphology. The cells were washed with PBS at 37 °C to remove the dead and loosely cells. Then they were fixed with 4% PFA/PBS and kept at room temperature for around 10 min. The cells were permeabilized with 0.5% Triton X-100 in PBS at room temperature for 5 min and rinsed with PBS afterward. Then, the F-actin cytoskeleton was stained using 100 nM Actin-stain ^{TM} 488 Phalloidin in PBS. The cells were kept in a dark room at 4 °C for 30 min. The fluorescent F-actin cytoskeleton images were obtained using an inverted optical microscope (Olympus IX73, Japan) integrated with a sola light engine (Lumencor, Beaverton, OR, USA). At least 10 images were taken for each substrate.

The F-actin alignment deviation was quantified using the recently developed IRAQ approach (Liu et al. (2018b)).

4.4.5 Atomic Force Microscopy (AFM) measurement

All AFM measurements were performed at room temperature in the aforementioned cell growth medium using a Bruker BioScope Resolve AFM system (Santa Barbara, CA, USA), which is integrated with an inverted fluorescent microscope (Olympus, IX73, Japan). AFM probe (DNP, Bruker, Camarillo, CA, USA) with a nominal conical radius and opening angle of 20 nm and 20°, respectively, was used. For each used probe, the AFM probe radius was calibrated using the polycrystalline titanium roughness sample (Bruker Inc., Santa Barbara, CA, USA) for accurate quantification. The cantilever spring constant of 0.03 N/m was acquired using thermal tune ap-

proach (Hutter and Bechhoefer (1993)). During the experiment, the AFM probe was in contact with the cells at the location away from the top to minimize the nucleus effect (see Fig. 4.5 (A)) for the AFM measurement location). The height of the measured MDCK cells were 8.5±1.5 μm (mean± SD). The chosen target indentations (325, 650, 1000, 1300 nm) were much less than a quarter of the cell height to minimize the measurement error arising from the finite cell thickness (Dimitriadis et al. (2002); Moeendarbary et al. (2013)). Also, as the AFM tip radius is three orders of magnitude smaller than the cell width, it is valid to consider the cell surface as semi-infinite during the cell-probe interaction. To investigate the effect of substrates' pattern on the biomechanical behavior of the cells, the cells were indented with the indenting velocity of 20 μm/s until the desired indentations were reached (i.e., the indenting process) and the probe was then rested on the cells for one second (the force-relaxation process). The AFM measurement at each indentation depth was performed on at least six different cells cultured per substrate. In addition, the PDMS substrates were imaged in PeakForce mode (Bruker Inc., Santa Barbara, CA, USA) with the PeakForce amplitude and setpoint of 150 nm and 438 nN, respectively (see Fig. 4.4).

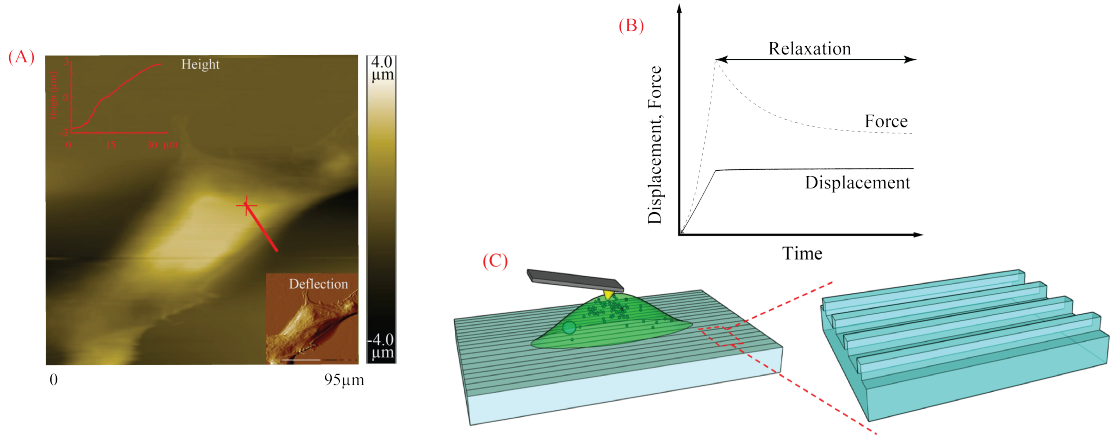

Figure 4.5 (A) AFM topography image of an MDCK cell (the red cross represents the measurement site.), (B) the probe-cell interaction force and AFM displacement profile during force-relaxation process, and (C) illustration of the indenting process on the cell cultured on the patterned substrate

4.4.6 Nanomechanical quantification of the cells

- Cell elasticity

  Indentation depth, $\delta(t)$, was quantified by subtracting the cantilever deflection, $d(t)$, from the AFM displacement, $z(t)$:

$$\delta(t) = z(t) - d(t) \tag{4.2}$$

  Since the indenting velocity, 20μm/s, was faster than the intracellular fluid efflux rate, the cells could be considered as incompressible during the indenting process (Mollaeian et al. (2018b)), then the Young's modulus can be quantified using the following Sneddon model (Sneddon (1965)):

$$F(t) = \frac{2}{\pi}\frac{E}{(1-\nu^2)}tan(\alpha)\delta^2(t) \tag{4.3}$$

  where $F(t) = kd(t)$ is the probe-cell interaction force, α is the tip opening angle, and ν=0.5 is the incompressible cell Poisson's ratio. Since the Young's modulus is linearly related to shear modulus ($E = 2G_u(1+\nu)$), Eq. (4.3) could be rewritten as:

$$F(t) = \frac{4}{\pi}\frac{G_u}{(1-\nu)}tan(\alpha)\delta^2(t) \tag{4.4}$$

  where the shear modulus of the undrained (i.e., incompressible during the fast indenting process, ν=0.5) cell meshwork is given as:

$$G_u = \frac{F_i}{4a\overline{\delta}} \tag{4.5}$$

  where the probe-cell contact size, a, can be quantified as $a = \frac{2}{\pi}\overline{\delta}tan(\alpha)$. F_i and $\overline{\delta}$ are the cell-probe interaction force and the indentation depth at the beginning of the force-relaxation process, respectively.

  The intracellular fluid does not have sufficient time to redistribute during the fast indenting process. Therefore, the intracellular pressure equilibrates by the fluid efflux and force reduction. The fully relaxed force at the end of the relaxation process (i.e., one second after fast indentation), F_f, was then quantified as:

$$F_f = \frac{2}{1-\nu}G_d a\overline{\delta} \tag{4.6}$$

where ν and G_d are the cell Poisson's ratio and drained shear modulus during the force-relaxation process, respectively. The Poisson's ratio of the solid cellular matrix during the relaxation process can be then quantified using Eqs. (4.5) and (4.6) as (Kalcioglu et al. (2012)):

$$\nu = 1 - \frac{F_i}{2F_f} \tag{4.7}$$

- Apparent viscosity

  The viscoelastic behavior of the cells was quantified following the method proposed by Darling et al. (2007):

$$F(t) = \frac{2}{\pi}\frac{E}{(1-\nu)}tan(\alpha)\bar{\delta}^2(t)[1 + (\frac{\tau_\sigma - \tau_\epsilon}{\tau_\epsilon})e^{-\frac{t}{\tau_\epsilon}}] \tag{4.8}$$

  Where E_r is the relaxed modulus, and τ_σ and τ_ϵ are the relaxation time constants for load and deformation, respectively. To quantify E_r, τ_σ, and τ_ϵ values, the force-time relaxation curve was fitted by Eq. (4.8) and apparent viscosity, η, was estimated as (Ketene et al. (2012)):

$$\eta = E_r(\tau_\sigma - \tau_\epsilon) \tag{4.9}$$

- Poroelastic diffusion coefficient

  As the cells size (>30 μm) was much larger than the AFM tip radius (20 nm), the probe-cell interaction could be approximated as a poroelastic half-space indented by a conical indenter, and the cell poroelastic diffusion coefficient, D, could be quantified through fitting the force-time relaxation curve by empirical poroelastic model (Moeendarbary et al. (2013)):

$$\frac{F(t) - F_t}{F_i - F_f} = 0.493e^{-0.822\sqrt{\frac{DT}{a^2}}} + 0.507e^{-1.348\frac{DT}{a^2}} \tag{4.10}$$

  Fig. 4.6 represents examples of the force relaxation curve fitted by poroelastic and viscoelastic models.

- Statistical analysis

  The RMS fitting error was calculated to ensure the viscoelastic and poroelastic measurement accuracy. Student t-test was performed to evaluate the statistical significance, and the returned p values were reported in the figures.

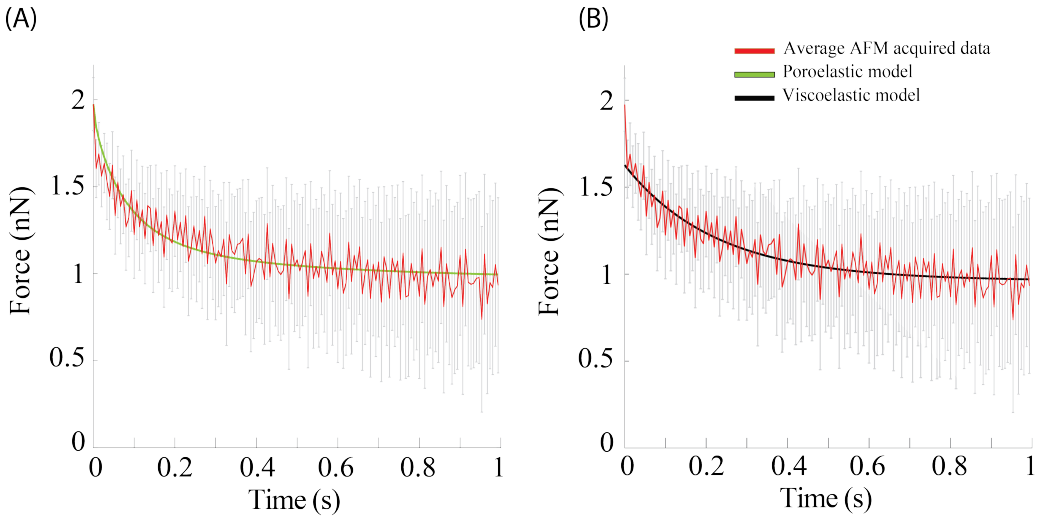

Figure 4.6 Force-relaxation curve (at the indenting velocity of 20 μ m/s and indentation depth of 1000 nm for the cells cultured on 2D PDMS substrate) fitted by (A) the poroelastic model (Eq.(4.10)) and (B) the viscoelastic model (Eq.(4.8)).The error bars are the raw force data of the all six force-relaxation measurements. (Fitting results: $E = 4.46$ kPa, $G = 1.17$, $\eta = 0.59$, GPa $= 0.42$ $\mu m^2/s$, $\nu = -0.06$, $E_R = 3.47$ GPa/s, τ_ϵ =0.23 s, and $\tau_\sigma = 0.4$ s.)

4.5 References

Abidine, Y., Constantinescu, A., Laurent, V. M., Rajan, V. S., Michel, R., Laplaud, V., Duperray, A., and Verdier, C. (2018). Mechanosensitivity of cancer cells in contact with soft substrates using afm. *Biophysical journal*, 114(5):1165–1175.

Chan, E. W. and Yousaf, M. N. (2008). A photo-electroactive surface strategy for immobilizing ligands in patterns and gradients for studies of cell polarization. *Molecular BioSystems*, 4(7):746–753.

Charras, G. T., Mitchison, T. J., and Mahadevan, L. (2009). Animal cell hydraulics. *Journal of Cell Science*, 122(18):3233–3241.

Darling, E. M., Zauscher, S., Block, J. A., and Guilak, F. (2007). A thin-layer model for viscoelastic, stress-relaxation testing of cells using atomic force microscopy: do cell properties reflect metastatic potential? *Biophysical journal*, 92(5):1784–1791.

Dimitriadis, E. K., Horkay, F., Maresca, J., Kachar, B., and Chadwick, R. S. (2002). Determination of elastic moduli of thin layers of soft material using the atomic force microscope. *Biophysical journal*, 82(5):2798–2810.

Discher, D. E., Janmey, P., and Wang, Y.-l. (2005). Tissue cells feel and respond to the stiffness of their substrate. *Science*, 310(5751):1139–1143.

Engler, A. J., Griffin, M. A., Sen, S., Bönnemann, C. G., Sweeney, H. L., and Discher, D. E. (2004). Myotubes differentiate optimally on substrates with tissue-like stiffness: pathological implications for soft or stiff microenvironments. *J Cell Biol*, 166(6):877–887.

Flemming, R., Murphy, C. J., Abrams, G., Goodman, S., and Nealey, P. (1999). Effects of synthetic micro-and nano-structured surfaces on cell behavior. *Biomaterials*, 20(6):573–588.

Giannone, G. and Sheetz, M. P. (2006). Substrate rigidity and force define form through tyrosine phosphatase and kinase pathways. *Trends in cell biology*, 16(4):213–223.

Gupta, M., Sarangi, B. R., Deschamps, J., Nematbakhsh, Y., Callan-Jones, A., Margadant, F., Mège, R.-M., Lim, C. T., Voituriez, R., and Ladoux, B. (2015). Adaptive rheology and ordering of cell cytoskeleton govern matrix rigidity sensing. *Nature communications*, 6:7525.

Halldorsson, S., Lucumi, E., Gómez-Sjöberg, R., and Fleming, R. M. (2015). Advantages and challenges of microfluidic cell culture in polydimethylsiloxane devices. *Biosensors and Bioelectronics*, 63:218–231.

Hutter, J. L. and Bechhoefer, J. (1993). Calibration of atomic-force microscope tips. *Review of Scientific Instruments*, 64(7):1868–1873.

Jiang, X., Bruzewicz, D. A., Wong, A. P., Piel, M., and Whitesides, G. M. (2005). Directing cell migration with asymmetric micropatterns. *Proceedings of the National Academy of Sciences*, 102(4):975–978.

Kalcioglu, Z. I., Mahmoodian, R., Hu, Y., Suo, Z., and Van Vliet, K. J. (2012). From macro- to microscale poroelastic characterization of polymeric hydrogels via indentation. *Soft Matter*, 8(12):3393–3398.

Ketene, A. N., Schmelz, E. M., Roberts, P. C., and Agah, M. (2012). The effects of cancer progression on the viscoelasticity of ovarian cell cytoskeleton structures. *Nanomedicine: Nanotechnology, Biology and Medicine*, 8(1):93–102.

Lee, J. N., Jiang, X., Ryan, D., and Whitesides, G. M. (2004). Compatibility of mammalian cells on surfaces of poly (dimethylsiloxane). *Langmuir*, 20(26):11684–11691.

Liu, B., Monshat, H., Gu, Z., Lu, M., and Zhao, X. (2018a). Recent advances in merging photonic crystals and plasmonics for bioanalytical applications. *Analyst*, 143(11):2448–2458.

Liu, Y., Mollaeian, K., and Ren, J. (2018b). An image recognition-based approach to actin cytoskeleton quantification. *Electronics*, 7(12):443.

Liu, Y., Mollaeian, K., and Ren, J. (2019). Finite element modeling of living cells for afm indentation-based biomechanical characterization. *Micron*, 116:108–115.

Matsuzaka, K., Walboomers, F., De Ruijter, A., and Jansen, J. A. (2000). Effect of microgrooved poly-l-lactic (pla) surfaces on proliferation, cytoskeletal organization, and mineralized matrix formation of rat bone marrow cells. *Clinical oral implants research*, 11(4):325–333.

McKee, C. T., Raghunathan, V. K., Russell, P., and Murphy, C. J. (2011). Probing effect of biophysical cues on cell behavior with atomic force microscopy. *Microscopy and Analysis-UK*, (148):25.

Moeendarbary, E., Valon, L., Fritzsche, M., Harris, A. R., Moulding, D. A., Thrasher, A. J., Stride, E., Mahadevan, L., and Charras, G. T. (2013). The cytoplasm of living cells behaves as a poroelastic material. *Nature materials*, 12(3):253–261.

Mollaeian, K., Liu, Y., Bi, S., and Ren, J. (2018a). Atomic force microscopy study revealed velocity-dependence and nonlinearity of nanoscale poroelasticity of eukaryotic cells. *Journal of the mechanical behavior of biomedical materials*, 78:65–73.

Mollaeian, K., Liu, Y., Bi, S., Wang, Y., Ren, J., and Lu, M. (2018b). Nonlinear cellular mechanical behavior adaptation to substrate mechanics identified by atomic force microscope. *International journal of molecular sciences*, 19(11):3461.

Monshat, H., Liu, L., and Lu, M. (2019). A narrowband photo-thermoelectric detector using photonic crystal. *Advanced Optical Materials*, 7(3):1801248.

Ohara, P. T. and Buck, R. C. (1979). Contact guidance in vitro: a light, transmission, and scanning electron microscopic study. *Experimental cell research*, 121(2):235–249.

Park, S. A., Kim, I. A., Lee, Y. J., Shin, J. W., Kim, C.-R., Kim, J. K., Yang, Y.-I., and Shin, J.-W. (2006). Biological responses of ligament fibroblasts and gene expression profiling on micropatterned silicone substrates subjected to mechanical stimuli. *Journal of bioscience and bioengineering*, 102(5):402–412.

Rianna, C., Kumar, P., and Radmacher, M. (2018). The role of the microenvironment in the biophysics of cancer. In *Seminars in cell & developmental biology*, volume 73, pages 107–114. Elsevier.

Shabaniverki, S., Thorud, S., and Juárez, J. J. (2018a). Protocol for assembling micro-and nanoparticles in a viscous liquid above a vibrating plate. *MethodsX*, 5:1156–1165.

Shabaniverki, S., Thorud, S., and Juarez, J. J. (2018b). Vibrationally directed assembly of micro- and nanoparticle-polymer composites. *Chemical Engineering Science*, 192:1209–1217.

Sneddon, I. N. (1965). The relation between load and penetration in the axisymmetric boussinesq problem for a punch of arbitrary profile. *International journal of engineering science*, 3(1):47–57.

Sorba, F., Poulin, A., Ischer, R., Shea, H., and Martin-Olmos, C. (2019). Integrated elastomer-based device for measuring the mechanics of adherent cell monolayers. *Lab on a Chip*.

Sorce, B., Escobedo, C., Toyoda, Y., Stewart, M. P., Cattin, C. J., Newton, R., Banerjee, I., Stettler, A., Roska, B., Eaton, S., et al. (2015). Mitotic cells contract actomyosin cortex and generate pressure to round against or escape epithelial confinement. *Nature communications*, 6:8872.

Sunami, H., Yokota, I., and Igarashi, Y. (2014). Influence of the pattern size of micropatterned scaffolds on cell morphology, proliferation, migration and f-actin expression. *Biomaterials science*, 2(3):399–409.

Takayama, Y., Moriguchi, H., Kotani, K., Suzuki, T., Mabuchi, K., and Jimbo, Y. (2012). Network-wide integration of stem cell-derived neurons and mouse cortical neurons using microfabricated co-culture devices. *Biosystems*, 107(1):1–8.

Teixeira, A. I., Abrams, G. A., Bertics, P. J., Murphy, C. J., and Nealey, P. F. (2003). Epithelial contact guidance on well-defined micro-and nanostructured substrates. *Journal of cell science*, 116(10):1881–1892.

Wang, Y., Liu, L., Wang, Q., Han, W., Lu, M., and Dong, L. (2016). Strain-tunable plasmonic crystal using elevated nanodisks with polarization-dependent characteristics. *Applied Physics Letters*, 108(7):071110.

Wells, R. E. and Merrill, E. W. (1961). Shear rate dependence of the viscosity of whole blood and plasma. *Science*, 133(3455):763–764.

Willerth, S. (2017). Synthetic biomaterials for engineering neural tissue from stem cells. In *Engineering Neural Tissue from Stem Cells*, pages 127–158. Elsevier.

Xie, S. and Ren, J. (2019). High-speed afm imaging via iterative learning-based model predictive control. *Mechatronics*, 57:86–94.

Yadav, P. S., Gulec, S., Jena, A., Tang, S., Yadav, S., Katoshevski, D., and Tadmor, R. (2018). Interfacial modulus and surfactant coated surfaces. *Surface Topography: Metrology and Properties*, 6(4):045007.

Yeung, T., Georges, P. C., Flanagan, L. A., Marg, B., Ortiz, M., Funaki, M., Zahir, N., Ming, W., Weaver, V., and Janmey, P. A. (2005). Effects of substrate stiffness on cell morphology, cytoskeletal structure, and adhesion. *Cell motility and the cytoskeleton*, 60(1):24–34.

CHAPTER 5. A DYNAMIC CELL CULTURE SUBSTRATE FOR IMPROVED CELLULAR UPTAKE OF NANOPARTICLES

Keyvan Mollaeian [1], Yi Liu[1], and Juan Ren[1]*

[1] Department of Mechanical Engineering, Iowa State University, Ames, Iowa, 50011, USA

Correspondence: juanren@iastate.edu; Tel.: +1-515-294-1805

5.1 Abstract

In the past dacade, extensive efforts have been taken on delivery of nanoparticles (NPs) for detection, diagnosis, and treatment of diseases. previous studies were mostly focused on the effect of NPs' and substrates' morphology on the efficacy of cellular uptake. However, creating a system which can mimic the extracellular environment and improve the drug delivery has not yet been reported. In this study, to investigate the cell uptake of NPs, a dynamic cell culture substrate was designed in two steps: 1. the polyaniline polymer (PANI) was deposited on the cell culture petri dish, and 2. the PANI substrate was coated by PDMS with base to curing agent ratio of 10:3 (PDMS/PANI). The substrates were characterized using Fourier Transform Infrared (FTIR) and Atomic Force Microscopy (AFM). It was found that the PDMS/PANI substrate expansion was positively correlated with the applied voltage to the PANI. In addition, the PDMS/PANI substrate was implemented for NPs delivery. Our results showed that the uptake of NPs by the cells cultured on PDMS/PANI substrate increases by expansion of the substrates. Moreover, our results suggest that the PDMS/PANI substrate is a promising device that can be used for controlling intra- and extracellular behavior of the cells.

5.2 Introduction

Nanoparticles (NPs) are widely used in a variety of biomedical applications due to their biocompatibility and functionalization (Ferrari (2005); Davis et al. (2010)). For instance, NPs have been used for Drug delivery, tissue engineering, cancer treatment, and diagnostic imaging (Wei et al. (2018); Davis et al. (2010)). Recent development in the fabrication of NPs provided new insights for drug delivery to specific intracellular compartment (Zhu et al. (2013); Li and Gu (2010); Li et al. (2008)). In addition, delivery of NPs into cell interior regulates different extra- and intracellular processes such as cytoskeleton reformation, migration, cell fate, and cell-cell interaction (Huang et al. (2016); Wei et al. (2018)). Although extensive research has been performed on the effect of NPs characteristics, such as size, shape, and surface modification, on the cell uptake, the role of surrounding environment of the cells in NP's delivery is poorly understood. Therefore, study of the effect of microenvironment on cellular uptake is crucial in achieving an efficient and well-controlled delivery of NPs.

Previously, studies of cellular uptake of NPs has been mostly focused on physiochemical properties of NPs (Behzadi et al. (2017)). Studies have shown that the efficacy of cellular uptake has positive correlation with the NPs' size (Shan et al. (2011)). Shapero et al. (2011) found that the efficacy of NPs internalization by the A549 lung epithelial cells decreased by size (Shapero et al. (2011)). Chithrani et al (2007) reported that the cellular uptake of NPs is shape dependent (Chithrani and Chan (2007)). Qiu et al. (2010) demonstrated that coating the gold nanorods (AuNR) with Diallyldimethyl ammonium chloride increases the cellular uptake (Qiu et al. (2010)). However, since the cell response adapts to extracellular environment, the substrate mechanics should also be considered when studying the cellular uptake of NPs (Mollaeian et al. (2018b)). Furthermore, studies have shown that substrate mechanics modulate cell regulation, such as signaling pathways, gene expression, cell polarization, and cytoskeleton components, which changes the intracellular trafficking of NPs (Mollaeian et al. (2018b); Park et al. (2006); Giannone and Sheetz (2006); Chan and Yousaf (2008)).

To date, there has been few studies reported the effect of substrate mechanics on cellular uptake of NPs. Kong e al. (2005) found that substrate rigidity regulates the gene expression and delivery (Kong et al. (2005)). Huang et al. (2013) reported that bovine aortic endothelial cells (BAECs) uptake of fluorescent NPs decreased by increasing the substrate stiffness (Huang et al. (2013)). In addition, it has been noted that patterned substrate results in lower cellular uptake of NPs (Huang et al. (2016)). However, these studies were only focused on cellular uptake of NPs cultured on static substrates at single cell-level. In addition, in a variety of physiological conditions, mechanical stimulation is applied through connective tissues to the side of the cells (Svennersten et al. (2011)). Therefore, to investigate cell-NPs interaction, design of a technique that mimics in-vivo extracellular environment is pivotal. Although several studies on intracellular behavior have focused on development of such platforms to stretch the living cells, they were limited to small range of linear strains when stressed by several kV's driving voltage (Poulin et al. (2018)). Moreover, majority of these platforms allow stimulation on a single cell (Poulin et al. (2018); Svennersten et al. (2011)). Thus, the designed microengineered platform should be compatible with biological laboratory equipment and precisely simulates the dynamics of the extracellular environment of cells with different confluency level as well.

In this study, we designed a novel and biocompatible cell culture dish to modulate the cellular uptake of NPs. Specifically, the cell culture petri-dish was functionalized by depositing polyaniline (PANI) which was synthesized via in-situ polymerization. Then the functionalized petri-dish was coated by Polydimethylsiloxane (PDMS) with the base-to-curing agent ratio of 10:3. The relation between the electrical and mechanical properties of the substrates was investigated using Atomic Force Microscopy (AFM). To understand how the substrate affects the cellular uptake, the Fluorescent Silica NPs were injected to the medium containing Madin–Darby canine kidney (MDCK) to study the change of cellular uptake caused by substrate motion.

5.3 Materials and methods

5.3.1 Chemicals

The aniline monomer and ammonium persulfate (APS) were purchased from Acros (Fair Lawn, NJ, USA). Sulfuric acid (H_2SO_4), anhydrous ethanol (C_2H_5OH), methanol (CH_3OH), and Triton X-100 were purchased from Fisher Scientific (Fair Lawn, NJ, USA). Sylgard 184 silicone elastomer and elastomer base were purchased from Ellsworth (Germantown, WI, USA). Minimum Essential Medium Eagle (MEM) and Phosphate-Buffered Saline (PBS) were purchased from Corning cell-gro (Manassas, VA, USA). Fetal bovine Serum (FBS) and penicillin-streptomycin (pen-strep) were obtained from Gibco (Grand Island, NY, USA). Paraformaldehyde (PFA, 4% in PBS) was purchased from Alfa Aesar (Ward Hill, MA, USA). Acti-stain^{TM} 488 Phalloidin was purchased from Cytoskeleton, Inc. (Denver, CO, USA). Fluorescent silica beads (SiO_2 NPs) with 90 nm diameter were purchased from Sigma Aldrich (St. Louis, MO, USA).

5.3.2 Polyaniline (PANI) synthesis

PANI substrates were synthesized by in-situ polymerization (Fig. 5.1). In summary, 1.14 g of APS was added to 140 mL of 1 M H_2SO_4 followed by addition of 10 mL of ethanol to the solution in an ice bath. Then, 684 μL of aniline monomer was added to the solution and stirred for 24 hours while maintaining the temperature at 0-4 °C. The final product was washed with distilled water and methanol to remove residual oxidant and dried at room temperature.

5.3.3 PDMS/PANI substrate preparation

To prepare PANI substrates, PANI powder was dispersed in the petri-dish containing DI water followed by drying at room temperature for 48 hours. The obtained PANI substrate was then attached to copper films using conductive epoxy and treated with 70 °C temperature for 4 hours. To prepare PDMS and PDMS/PANI substrate, the mixture of Sylgard 184 silicone elastomer base and the curing agent with the base-to-curing agent ratio of 10:3 was poured onto polystyrene Petri dish and PANI substrate, respectively, and degassed under vacuum until air bubbles disappeared

(around one hour). The substrates were then cured at room temperature for 24 hours. The substrate thickness was measured as 1.08 mm using atomic force microscopy (AFM).

5.3.4 Characterization

5.3.4.1 Fourier transform infrared Measurement

Fourier transform infrared spectra of PANI were recorded using Perkin Elmer Attenuated total reflectance-Fourier transform infrared (ATR-FTIR) spectroscopy (Waltham, Massachusetts, USA) equipped with single reflection ATR attachment with diamond crystal. Ten scans with spectral resolution of 4 cm^{-1} were taken at room temperature. The baseline correction with respect to the position of 4000 cm^{-1} were applied to the spectra.

5.3.4.2 Atomic Force Microscopy (AFM) measurement

All AFM measurements were performed at room temperature with a Bruker BioScope Resolve AFM system (Santa Barbara, CA, USA), which is integrated with an inverted optical microscope (Olympus, IX73, Japan). AFM probe (DNP, Bruker, Camarillo, CA, USA) with conical radius of 20 nm was used. The cantilever spring constant of 0.37 N/m was acquired using thermal tune approach Hutter and Bechhoefer (1993). Drive voltage and sensor data of the AFM were acquired using an NI PCIe-6353 DAQ board (National instrument, Austin, TX, USA) with Matlab Simulink Desktop Real-time platform (Mathworks, MA, USA). The probe was in contact with the surface of PDMS/PANI substrate before experiments. To obtain the electrical/mechanical relation of the PANI/PDMS substrate, the substrate was stimulated with 0.4, 0.8, 1.2, and 1.6V using DC power source while recording the deflection of the cantilever and the displacement of the z piezo. The AFM measurement was performed on at least six different places on each substrate.

5.3.5 Cell culture treatment

MDCK cell were cultured in MEM containing 10% FBS and 1 % per-strep at a density of 2.0×10^4 cells/ml on the PDMS-PANI substrate and polystyrene cell culture dish (35 mm Falcon, Durham,

NC, USA). The cell were maintained at 37 °C in an incubator with humidified atmisphere of 5% CO_2 for 72 hours prior to the experiment to achieve 90% confluency level. For all the experiments, the existing medium in the dishes was replace by fresh medium to remove dead and loosly attached cells.

5.3.6 Cell uptake of silica nanoparticles (SiO_2 NPs)

The SiO_2 NPs were dispersed in serum-free medium using vortex for 6 hours. The cells cultured on the substrates were exposed to SiO_2 NP with the concentration of 100 μg/ml followed by stimulation of the PDMS/PANI substrate with 0.4 V for 10 S using DC power source. Then, the cells were mamintained at 37 °C and 5% CO_2 in the incubator for 6 hours. The cells were washed with PBS to remove the unbounded nanoparticles prior to Immunofluorescence.

5.3.7 Immunofluorescence

Inverted optical microscope (Olympus, IX73, Japan) equipped with a sola light engine (Lumencor, Beaverton, OR, USA) was used for fluorescent imaging. To stain the cell cytoskeleton, the cell medium was replaced by 4% paraformaldehyde/PBS to fix the cells in the incubator for 10 mins. Then the cells were permeabilized using 0.5% Trinton X-100/PBS at room temperature for 5 mins. Finally, the F-actin cytoskeleton was stained using 100 nM Actin-stain^{TM} 488 phalloidin in PBS and the cells were kept in a dark room for 30 min. In addition, the cells were washed with PBS for 3 times before each step to remove the loosly attached cells and remaining residuals.

5.4 Results and discussion

5.4.1 Polymer characterization

The FTIR spectrum of the polyaniline (PANI) is shown in Fig. 5.1. Specifically, out-of-plane binding vibration of C-H bonds of PANI was recorded at ∼794 cm^{-1}. The band at 1048 cm^{-1} prescribes the $H_2SO_4^{-1}/SO_3^{-1}$ groups of sulfonated aromatic ring. The in-plane C-H bending vibration of aromatic rings was observed at 1140 cm^{-1}. In addition, the shoulder around 1253 cm^{-1} is

attributed to the C-N^+ stretching vibration in polaron lattice of PANI. 1300 cm^{-1} describes the vibration of the C-N bonds of the primary and secondary aromatic amines. Moreover, the peaks at 1482 cm^{-1} and 1565 cm^{-1} are ascribed to C=C stretching vibration of benzenoid rings and quinonoid ring, respectively. Table 5.1 summarizes the assignments of bands for FTIR spectrum of PANI and compares with literature (Tabrizi et al. (2018); Trchová and Stejskal (2011)).

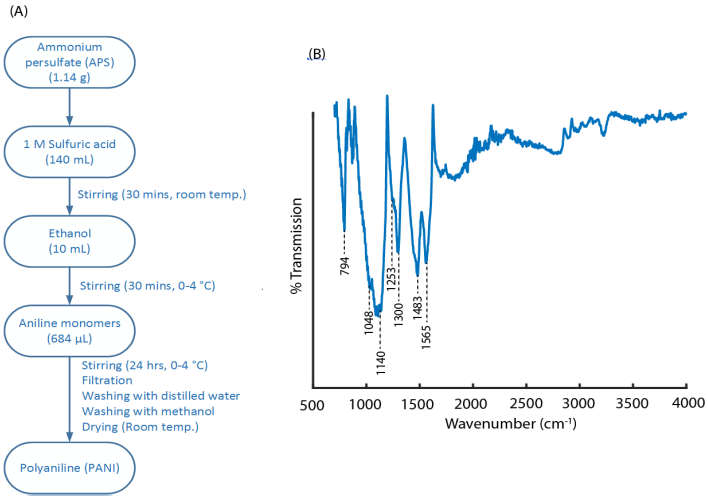

Figure 5.1 (A) Schematic representation of preparation procedure for Polyaniline (PANI) and (B) FTIR spectrum of PANI.

Table 5.1 FTIR assignments of polyaniline (vs:very strong, s:strong, m: medium, and sh: shoulder)

Wavenumber (cm^{-1})		
polyaniline	**Literature**	**Assignments**
1565 vs	1577, 1568 vs	C=C stretching vibration of quinonoid ring
1483 vs	1482, 1495 vs	C=C stretching vibration of benzenoid rings
1300 s	1307,1302 vs	vibration of the C-N bonds of the primary and secondary aromatic amines
1253 sh	1248, 1239 s	C-N^+ stretching vibration in polaron lattice of PANI
1140 vs	1148, 1149 vs	in-plane C-H bending vibration of aromatic rings
1048 sh	1145 sh	$H_2SO_4^{-1}/SO_3^{-1}$ groups of sulfonated aromatic ring
794 m	882, 815 m	out-of-plane binding vibration of C-H bonds

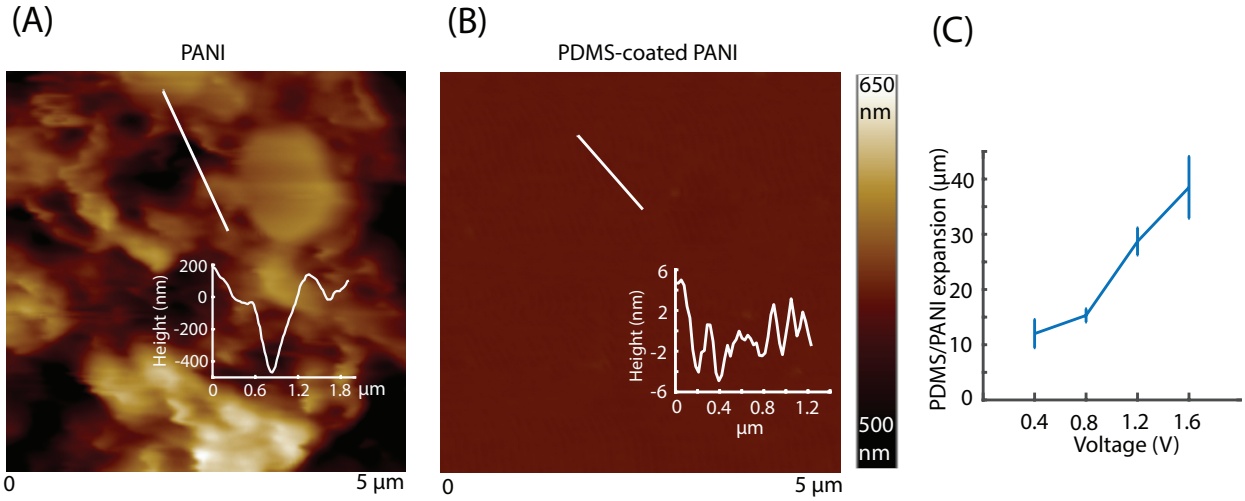

Figure 5.2 AFM topography of (A) PANI and (B) PDMS-coated PANI. (C) represents the PDMS/PANI expansion in response to applied voltage.

Fig. 5.2 represents the surface topography of PANI and PDMS/PANI substrates, and mechanical dynamics of the PDMS/PANI in response to DC voltage. In addition, the PDMS/PANI substrate was expanded when stressed by DC voltage. Particularly, the substrate expansion was 1.11%, 1.42%, 2.66%, and 3.56% when stressed by 0.4, 0.8, 1.2, and 1.6, respectively, comapared to the static substrtes.

5.4.2 Effect of PDMS/PANI substrate on the cellular uptake of nanoparticles

Previous studies have shown the effect of static substrate mechanics on the cellular uptake of nanoparticles (Huang et al. (2013, 2016). However, a design of a substrate that can control the dynamics of the cell uptake has not been reported yet. Thus, we designed and implemented a dynamic cell culture substrate (i.e., PDMS/PANI substrate) for MDCK cell uptake of silica beads. Specifically, we investigated the efficacy of the cell uptake by the expansion of the substrate when stressed by 0.4 V driving voltage.

As shown in Fig. 5.3, the substrates' dynamics affect the intracellular behavior, significantly. The amount of internalized nanoparticles by the cells cultured on the static PDMS/PANI substrate decreases compared to the cells on the cell culture petri-dish (i.e., control). Specifically, when

the substrates were indented by AFM until 300 nm indentation depth reached, the stiffness of PDMS/PANI substrate decreased by 58% compare to control. Consequently, the average intensity of the NPs/cell for the static PDMS/PANI substrate decreased by 10.7% when compared to the cells on the petri-dish which agrees with previous studies that stiffer substrates results in higher efficacy of the cellular uptake (Huang et al. (2013)). However, the average number of NPs uptake by the cells on the PDMS-PANI was increased significantly when stressed by 0.4 V. Particularly, the intensity of the NPs/cell on PDMS/PANI substrate was increased by 303% and 259.88 % when the substrate expanded by 1.11%, compared to static PDMS/PANI and cell culture petri-dish, respectively (see Fig. 5.4).

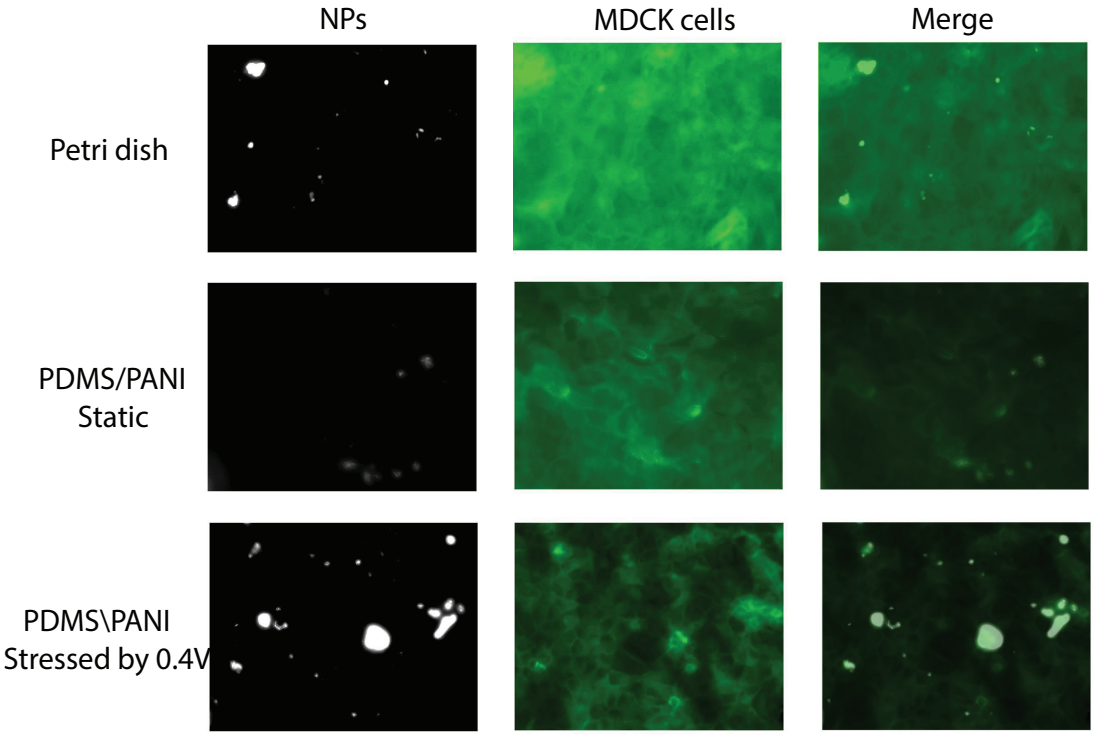

Figure 5.3 MDCK cell uptake of nanoparticles on petri dish, Static PDMS/PANI, and PDMS/PANI substrate when stressed by 0.4 V

The results clearly show that the substrate mechanics affects the cellular uptake of nanoparticles (Figs. 5.3 & 5.4). The stiffness of the substrate regulates the cell uptake of NPs (Huang et al. (2013); Kong et al. (2005)). Agreeing with previous studies, as the substrate stiffness increases,

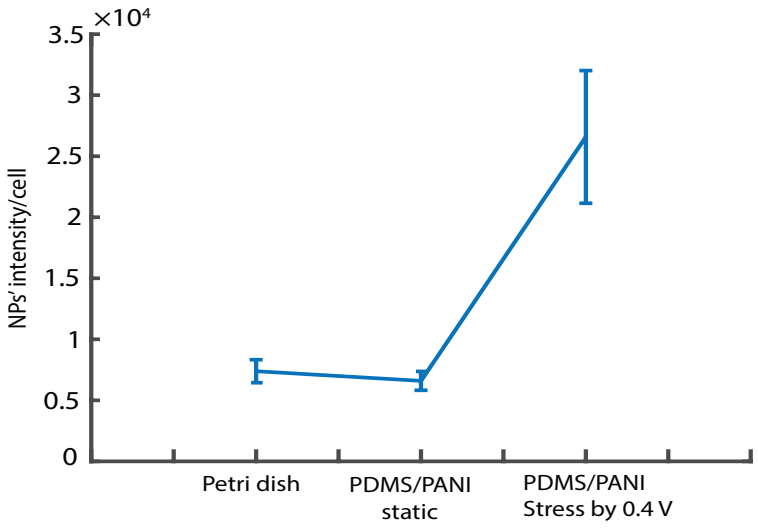

Figure 5.4 Comparison of NPs' intensity/cell for petri dish, static PDMS/PANI, and PDMS/PANI substrate when stressed by 0.4 V.

the cell-substrate binding increases due to enhanced focal adhesions and cytoskeleton reformation (Mollaeian et al. (2018b)). Consequently, the contractility and spreading area of the cell cultured on the stiffer substrate increases (Wei et al. (2018)). However, lower stiffness of the substrate leads to lower contractility and area of the cells (Mollaeian et al. (2018b); Wei et al. (2018)). As a result, the exposed surface area of the cells to NPs on the static PDMS/PANI substrate decreases compare to cells on petri-dish, which further leads to lower cellular uptake of NPs. Moreover, the uptake of NPs by cells increases when stretched via expansion of the PDMS/PANI substrates compared to others. The stretching of the cells in multiple direction, results in decreased cell-cell junction boundaries and increased cell area. Therefore, the accessible cell surface for NPs increases during the substrate expansion, which further increases the efficacy of the cell uptake (Wei et al. (2018); Huang et al. (2013); Kong et al. (2005)). Therefore, for the first time, our results demonstrated that the NPs delivery can be controlled by the dynamic behavior of the PDMS/PANI substrate.

5.5 Conclusion

A dynamic cell culture substrate was developed to investigate the cellular uptake of nanoparticles. Specifically, the cell culture dish was functionalized using polyaniline, and then coated with PDMS with base to curing agent ratio of 10:3 (PDMS/PANI substrate). It was shown that the electrical and mechanical properties of the PDMS/PANI substrate are positively corrolated. The effect of the dynamics of the PDMS/PANI substrate on cellular uptake of nanoparticles was investigated. The fluorescent images of the nanoparticles and the cells showed that stretching the confluent cells cultured on the PDMS/PANI substrate increased the efficacy of the nanoparticle's internalization by the cells. The results suggested that the fabricated PDMS/PANI substrate is a promising tool for controlling the cell mechanical behavior and drug delivery.

5.6 References

Behzadi, S., Serpooshan, V., Tao, W., Hamaly, M. A., Alkawareek, M. Y., Dreaden, E. C., Brown, D., Alkilany, A. M., Farokhzad, O. C., and Mahmoudi, M. (2017). Cellular uptake of nanoparticles: journey inside the cell. *Chemical Society Reviews*, 46(14):4218–4244.

Chan, E. W. and Yousaf, M. N. (2008). A photo-electroactive surface strategy for immobilizing ligands in patterns and gradients for studies of cell polarization. *Molecular BioSystems*, 4(7):746–753.

Chithrani, B. D. and Chan, W. C. (2007). Elucidating the mechanism of cellular uptake and removal of protein-coated gold nanoparticles of different sizes and shapes. *Nano letters*, 7(6):1542–1550.

Davis, M. E., Chen, Z., and Shin, D. M. (2010). Nanoparticle therapeutics: an emerging treatment modality for cancer. In *Nanoscience and technology: A collection of reviews from nature journals*, pages 239–250. World Scientific.

Ferrari, M. (2005). Cancer nanotechnology: opportunities and challenges. *Nature reviews cancer*, 5(3):161–171.

Giannone, G. and Sheetz, M. P. (2006). Substrate rigidity and force define form through tyrosine phosphatase and kinase pathways. *Trends in cell biology*, 16(4):213–223.

Huang, C., Butler, P. J., Tong, S., Muddana, H. S., Bao, G., and Zhang, S. (2013). Substrate stiffness regulates cellular uptake of nanoparticles. *Nano letters*, 13(4):1611–1615.

Huang, C., Ozdemir, T., Xu, L.-C., Butler, P. J., Siedlecki, C. A., Brown, J. L., and Zhang, S. (2016). The role of substrate topography on the cellular uptake of nanoparticles. *Journal of Biomedical Materials Research Part B: Applied Biomaterials*, 104(3):488–495.

Hutter, J. L. and Bechhoefer, J. (1993). Calibration of atomic-force microscope tips. *Review of Scientific Instruments*, 64(7):1868–1873.

Kong, H. J., Liu, J., Riddle, K., Matsumoto, T., Leach, K., and Mooney, D. J. (2005). Non-viral gene delivery regulated by stiffness of cell adhesion substrates. *Nature materials*, 4(6):460–464.

Li, Y., Chen, X., and Gu, N. (2008). Computational investigation of interaction between nanoparticles and membranes: hydrophobic/hydrophilic effect. *The Journal of Physical Chemistry B*, 112(51):16647–16653.

Li, Y. and Gu, N. (2010). Thermodynamics of charged nanoparticle adsorption on charge-neutral membranes: a simulation study. *The Journal of Physical Chemistry B*, 114(8):2749–2754.

Mollaeian, K., Liu, Y., Bi, S., Wang, Y., Ren, J., and Lu, M. (2018). Nonlinear cellular mechanical behavior adaptation to substrate mechanics identified by atomic force microscope. *International journal of molecular sciences*, 19(11):3461.

Park, S. A., Kim, I. A., Lee, Y. J., Shin, J. W., Kim, C.-R., Kim, J. K., Yang, Y.-I., and Shin, J.-W. (2006). Biological responses of ligament fibroblasts and gene expression profiling on micropatterned silicone substrates subjected to mechanical stimuli. *Journal of bioscience and bioengineering*, 102(5):402–412.

Poulin, A., Imboden, M., Sorba, F., Grazioli, S., Martin-Olmos, C., Rosset, S., and Shea, H. (2018). An ultra-fast mechanically active cell culture substrate. *Scientific reports*, 8(1):1–10.

Qiu, Y., Liu, Y., Wang, L., Xu, L., Bai, R., Ji, Y., Wu, X., Zhao, Y., Li, Y., and Chen, C. (2010). Surface chemistry and aspect ratio mediated cellular uptake of au nanorods. *Biomaterials*, 31(30):7606–7619.

Shan, Y., Ma, S., Nie, L., Shang, X., Hao, X., Tang, Z., and Wang, H. (2011). Size-dependent endocytosis of single gold nanoparticles. *Chemical Communications*, 47(28):8091–8093.

Shapero, K., Fenaroli, F., Lynch, I., Cottell, D. C., Salvati, A., and Dawson, K. A. (2011). Time and space resolved uptake study of silica nanoparticles by human cells. *Molecular Biosystems*, 7(2):371–378.

Svennersten, K., Berggren, M., Richter-Dahlfors, A., and Jager, E. W. (2011). Mechanical stimulation of epithelial cells using polypyrrole microactuators. *Lab on a Chip*, 11(19):3287–3293.

Tabrizi, A. G., Arsalani, N., Mohammadi, A., Ghadimi, L. S., Ahadzadeh, I., and Namazi, H. (2018). A new route for the synthesis of polyaniline nanoarrays on graphene oxide for high-performance supercapacitors. *Electrochimica Acta*, 265:379–390.

Trchová, M. and Stejskal, J. (2011). Polyaniline: The infrared spectroscopy of conducting polymer nanotubes (iupac technical report). *Pure and Applied Chemistry*, 83(10):1803–1817.

Wei, Q., Huang, C., Zhang, Y., Zhao, T., Zhao, P., Butler, P., and Zhang, S. (2018). Mechanotargeting: Mechanics-dependent cellular uptake of nanoparticles. *Advanced Materials*, 30(27):1707464.

Zhu, M., Nie, G., Meng, H., Xia, T., Nel, A., and Zhao, Y. (2013). Physicochemical properties determine nanomaterial cellular uptake, transport, and fate. *Accounts of chemical research*, 46(3):622–631.

CHAPTER 6. CONCLUSION

In this dissertation, a suit of indentation-based Atomic Force Microscopy (AFM) approaches have been developed to investigate the mechanical behavior of the cells at different physiological conditions. In addition, novel biocompatible substrate was designed to improve the drug delivery.

1. An indentation-based AFM approach was developed to investigate the nanoscale cell poroelasticity and elasticity simultaneously. Velocity-dependence and the non-linearity of MDA-MB-231 cell poroelastic behavior was quantified by quantifying the diffusion coefficient through fitting the force-relaxation curves with the poroelastic model. Moreover, the effects of actin filaments, microtubules, and myosin II on the cell elastic and poroelastic behavior was studied. It was found that the cell had poor poroelastic behavior when the indenting velocity was lower than 10m/s due to intracellular fluid redistribution within the cell during indentation. Lower diffusion coefficient for faster indenting velocities confirmed poor poroelastic behavior of the cell due to local stiffening of the cell at faster velocity. Deeper indentation led to higher diffusion coefficient and more efficient poroelastic relaxation of the cell due to the increases of the cytoplasmic pore size and cell stiffness. Inhibition of the afore-mentioned cytoskeletal components resulted in significant increase of the diffusion coefficient and dramatic decrease of the Young's modulus compared with the control. Differences of the three cytoskeleton inhibition treatments in affecting the nonlinearity of cell poroelasticity revealed that F-actin and myosin II affects cytoskeleton structure at both the superficial and the deeper layers, while microtubule is mainly affects the cell mechanical behavior at the deeper layers of the cytoskeleton.

2. The effect of substrate mechanics on biomechanical behavior of the cells was investigated using AFM indentation approach. The elastic, viscoelastic, and poroelastic nonlinearity of MDCK and NIH/3T3 cells on substrates with different mechanics (i.e., 10:0.5, 10:1, 10:3

PDMSs, and polystyrene cell culture dish) were quantified at different indentation depths. It was found that the cell elasticity, viscoelasticity, and their nonlinearities were synchronized with the substrate stiffness and its nonlinearity, respectively. The diffusion coefficient of the cells increased, monotonically, with the increase of the indentation depth on all substrates. Particularly, this poroelasticity nonlinearity was more pronounced for the cells cultured on the softer substrates due to larger lateral expansion of the cell and larger cytoskeletal pore size. Moreover, the cell F-actin cytoskeleton images suggested that the stiffer the substrate was, the more uniform the F-actin alignment was. Thus, combining the results together, it is clear that the substrate mechanics affects the cellular mechanics by regulating the inner structure of the cells.

3. The effect of the substrate morphology on the biomechanical behavior of living cells was thoroughly investigated using indentation-based atomic force microscopy. The results showed that the cellular biomechanical behavior was affected by the substrate morphology significantly. The elasticity and viscosity of the cells on the patterned Polydimethylsiloxane (PDMS) substrates were much lower compared to those of the ones cultured on flat PDMS. The poroelastic diffusion coefficient of the cells was higher on the patterned PDMS substrates, specifically on the substrate with 2D pitches. In addition, fluorescence images showed that the substrate topography directly affects the cell cytoskeleton morphology. Together, the results suggested that cell mechanical behavior and morphology can be controlled using substrates with properly designed topography.

4. A dynamic cell culture substrate was developed to investigate the cellular uptake of nanoparticles. Specifically, the cell culture dish was functionalized using polyaniline, and then coated with PDMS with base to curing agent ratio of 10:3 (PDMS/PANI substrate). The electrical/mechanical of the substrates were acquired using AFM. The effect of the dynamics of the PDMS/PANI substrate on cellular uptake of nanoparticles was investigated. The fluorescent images of the nanoparticles and the cells showed that stretching the confluent cells cultured on the substrates increase the efficiency of the nanoparticle's internalization by the cells. The

results suggested that the fabricated PDMS/PANI substrate is promising tool for controlling the cell mechanical behavior and drug delivery.

Although extensive research has been performed on the mechanobiology of the cells, understanding of how the mechanical cues activate signaling pathways and how these intracellular biochemical processes result in induced-force by cells to their extracellular environment is challenging. The most promising direction of future research in mechanotrasduction of the cells is developing a model than can describe the cell behavior at different physiological conditions. Moreover, The modeling approach combined with the experimental approach which can mimic the cell environment in human body would give a right direction in understanding, diagnosis, and treatment of malignant diseases such as cancer.